To the Graduate Council:

I am submitted herewith a dissertation written by Tarab Jamil Ahmad entitled "The effect of mobile phase composition and temperature on the adsorption behavior of tryptophan." I have examined the final electronic copy of this dissertation from the content and recommend that it be accepted in partial fulfillment of the requirements for the degree of Doctor of Philosophy, with a major in Chemistry.

Georges Guiochon
Major Professor

We have read this dissertation
and recommend its acceptance:

Michael J. Sepaniak

Zilling Xue

Grozdena Todorova

Accepted for the Council:

Linda Painter
Interim Dean Of Graduate Students

(Original signatures are on file with official student records)

THE EFFECT OF MOBILE PHASE COMPOSITION AND TEMPERATURE ON THE ADSORPTION BEHAVIOR OF TRYPTOPHAN

A Dissertation Presented for the

Doctor of Philosophy Degree

The University of Tennessee,

Knoxville

Tarab Jamil Ahmad

December 2006

DEDICATION

This dissertation is dedicated to my mom whose behind my success in my whole life, and to my family in Jerusalem and Amman. Special dedication goes to my patient husband and lovely kids who were truly giving me the power and strength to finish this work.

ACKNOWLEDGMENTS

I want to take this opportunity to express my most sincere respect and gratitude to all the people who helped to make this work possible. First I want to thank God by whom all things are made possible. He was the only one who give me the encouragement, hope and strength at the most difficult times.

I would also want to express my gratitude to my husband Zeyad and my sons Tariq, Tahir, and Yasser, and my daughter Sadiqah Yafah for their patience, love, and encouragement through all the difficult times. I also want to give my special thanks to my mother who was behind my success through all of my life, my step father, my brothers Ashraf, Yousef and my sisters Jacklyn, Fatima, and Fidaa, and their families for their encouragement, support.

I also wish to express my most sincere gratitude to the past group members Krzysztof Kaczmarski, Attila Filnger, Alberto Cavazini, Hyunjung Kim, Leonid Asnin, and Wilmer Galinada for their assistance and advice. In addition, I wish to express my gratitude for the current group members Fabrice Gritti, Khalid Mriziq, Lance Riddle, and Nicola Marchitti for all their friendship, suggestions and for making this experience a more enjoyable one.

Thanks to the Chemistry Department's staff for their support and unconditional help during these years of study. Also I would like to express my appreciation and respect to Bill Gurley, and Gary Wynn in the electronic shop for the endless support.

Thanks and deep appreciation to all the analytical and physical chemistry faculty division who contributed into my education through my course work Dr. Charles Feigerle, Dr. Michael Sepaniak, Dr. Georges Guiochon, Dr. James Chambers, Dr. Zilling Xue, Dr. Robert Hinde, and special thanks for Dr. Douglas Gilman and Fred Schell who were the first faculty members who welcomed me in the Chemistry Department.

I also would like to express my deep appreciation to my great supervisor Dr. Georges Guiochon for his guidance, advice, help, and endless support throughout the research. It has been an honor to be part of your research group. I would like to thank Dr. Fabrice Gritti for many helpful discussions regarding my research, and to my committee members Dr. Michael Sepaniak, Dr. Ziling Xue, and for their fruitful comments and suggestions. Special thanks to my fourth committee member Dr. Grozdena Todorova who was giving me the encouragement and advice for the past two years.

Finally I want to express my gratitude to the University of Tennessee Knoxville for the economical support and funding to this work.

ABSTRACT

Single-component adsorption isotherm data were acquired by frontal analysis for tryptophan on a C_{18}-Kromasil packed column, using acetonitrile-water solutions of various compositions (2.5, 5, and 7.5% ACN + 1% ACOH). These isotherms have a complex behavior, exhibiting at least one clear inflection point at an intermediate concentration and, possibly, another such point, close to the origin. The isotherm for 2.5 % ACN has the strongest curvature. At high concentrations, all these isotherms tend toward a limit, showing that the adsorbent has a finite saturation capacity. At low concentrations, these isotherms seem to exhibit langmuirian behavior. The isotherm model accounting best for these data is the bi-Moreau model, showing that two types of adsorption sites coexist on the surface and that strong adsorbate–adsorbate interactions take place. Large concentration band profiles of tryptophan were obtained for the three mobile phase compositions, at five different temperatures and the best values of the isotherm coefficients were determined by the inverse method (IM) of chromatography. The retention time of tryptophan decreases rapidly with increasing acetonitrile concentration in the mobile phase and so do the saturation capacities of the two types of adsorption sites, with the highest values of the two saturation capacities being found for the lowest ACN content and the lowest temperature. The adsorption constant on the low energy sites decreases with increasing acetonitrile content and temperature. In contrast, the adsorption constant on the high energy sites increases with increasing ACN

content of the mobile phase but decreases with increasing temperature. The solute–solute interaction parameters for the low and the high energy adsorption sites increase rapidly with increasing ACN concentration in the mobile phase and with increasing temperature.

CONTENTS

Chapter1

Introduction.....1

1.1 The Goals of Separation 4

1.2 Types of Liquid Chromatography.....5

1.3 Adsorption Chromatography.....6

1.4 Theory of Chromatography.....7

1.4.1 The Transfer Phenomena and Sources of Band Broadening.....7

1.4.2 Mass Balance Equation.....11

1.4.3 Initial and Boundary Conditions.....15

1.4.3a The Initial Conditions.....15

1.4.3b The Boundary Conditions.....16

1.4.4 The Ideal model.....18

1.4.5 The Lumped Kinetic Models.....20

1.4.6.The Equilibrium Dispersive Model.....20

1.4.7 Numerical Solution for Equilibrium Dispersive Model and Single Component problems.....22

1.4.8 Determination of Single-Component Isotherms by Frontal Analysis...26

1.4.9 Models of Isotherm Used 26

1.4.10 The bi-Moreau Model.....27

1.4.11 The Quadratic Isotherm Model.....29

1.4.12 Isotherm Modeling.....29

1.4.13 The Inverse Method of Isotherm Determination.....30

1.4.14 Initial and Boundary Conditions for the ED Model.....31

1.4.15 Numerical Solution of the ED Model.....32

1.5 State of the Problem.....32

Chapter 2

Experimental.....39

2.1 Chemicals and Materials.....39

2.2 Column.....39

2.3 Apparatus.....40

2.3.1 Solvent Delivery System SDS.....40

2.3.2 Solvent Reservoir.....43

2.3.3 Solvent Degassing.....43

2.3.4 Metering Pump.....43

2.3.5 Rotary Valve.....45

2.3.6 Low Pressure Pump LPC.....45

2.3.7 High Pressure Pump.....46

2.3.8 Damping Unit.....46

2.3.9 Diode-Array Detector DAD.....48

2.3.10 Photodiode Array.....50

2.3.11 Auto Sampler Injector.....51

2.4 Temperature Control.....51

2.5 Frontal Analysis Measurement of Isotherm Data.....53

2.6 Acquisition of Overloaded Band Profiles of Tryptophan.....54

2.7 Detector Calibration 55

Chapter 3

Results and Discussion.....56

3.1 The Effect of the Nature and Concentration of the Organic Modifier on the Adsorption Behavior of L-Tryptophan.....56

3.1.1 Adsorption Behavior in Acetonitrile/Water Mobile Phases 56

3.1.2 Adsorption Behavior in Methanol/Water mobile phases.....67

3.2 The Effect of Temperature on the Adsorption Behavior of L-Tryptophan.....77

3.2.1 Influence of the Temperature on the Hold-up Volume.....77

3.2.2. Frontal Analysis and Breakthrough Curves.....87

3.2.3 Adsorption Isotherms.....91

3.2.4. Overloaded Band Profiles.....93

3.2.5. Parameters of the Isotherm 94

3.3. The Effect of Temperature at Different Mobile Phase Compositions.....98

3.3.1. Effect of the Temperature and the Mobile Phase Composition on the the Detector Calibration.....98

3.3.2. Effect of the Temperature and the Mobile Phase Composition on the Column Hold-up Volume.....110

3.3.3 Effect of the Temperature on the Breakthrough Curves.....110

3.3.3.1. Breakthrough Curves with 2.5% Acetonitrile in the Mobile Phase.....110

3.3.3.2. Breakthrough Curves with 5% Acetonitrile in the Mobile Phase.....112

3.3.3.3. Breakthrough Curves With 7.5% Acetonitrile in the Mobile Phase.....115

3.3.4. Effect of the Temperature on the Adsorption Isotherms.....116

3.3.5. Effect of the Temperature on the Overloaded Band Profiles.....119

3.3.6. Effect of the Temperature and the Mobile Phase Composition on the Parameters of the Isotherms.....121

3.3.6.1. Effect of the Mobile Phase Composition on the Isotherm Parameters.....122

3.3.6.2. Effect of the Temperature on the Isotherm Parameters.....123

Chapter 4

Conclusion.....126

References.....131

Vita.....140

LIST OF TABLES

Table 3.1 Best isotherm parameters and Fisher numbers for L-tryptophan on C_{18}-Kromasil with different aqueous solutions of ACN as the mobile phase.....62
Table 3.2 Best isotherm parameters and Fisher numbers for L-tryptophan on C_{18}-Kromasil with different aqueous solutions of MeOH as the mobile phase.....73
Table 3.3 Best isotherm parameters and Fisher numbers for L-tryptophan on C_{18}-Kromasil with aqueous solutions of 5% ACN and 1% acetic acid as the mobile phase at different temperatures.....86
Table 3.4 Best isotherm parameters obtained by frontal analysis method (FA) and by the inverse method(IM) for the low energy sites for L-tryptophan on C_{18}-Kromasil with aqueous solutions of 2.5%, 5%, 7.5% ACN and 1% acetic acid as the mobile phase at different temperatures 108
Table 3.5 Best isotherm parameters obtained by frontal analysis method (FA) and by the inverse method(IM) for the high energy sites for L-tryptophan on C_{18}-Kromasil with aqueous solutions of 2.5%, 5%, 7.5% ACN and 1% acetic acid as the mobile phase at different temperatures 109

LIST OF FIGURES

Figure 1.1 Gaussian Chromatogram showing the retention time and the adjusted retention time, the width and width at half height.....3
Figure 1.2 Differential mass balance in a column slice.....13
Figure 1.3 Relationship between the isotherms and their correspo.nding band profile.....19
Figure 2.1 Graphical representation of the HP1090 HPLC system from Agilent Technologies.....41
Figure 2.2 The main parts of the solvent delivery system.....42
Figure 2.3 A) Metering pump and valve; B) Low pressure compliance.....44
Figure 2.4 A) High pressure pump; B) High pressure damper parts..... 47
Figure 2.5 A) Absorption of light by a liquid in the detector cell; B) Elements of optical system of the Diode Array detector.....49
Figure 2.6 Top view of the main parts of the auto sampler injector..... 52
Figure 3.1 A) Experimental isotherm data (FA, symbols) of tryptophan on the C_{18} -Kromasil column obtained with three different ACN- water -acetic acid mixtures as the mobile phases..... 57
Figure 3.2 Selected breakthrough curves of tryptophan on the C_{18}-Kromasil column, at 1 ml/min, T = 296 K, 1% acetic acid..... 58
Figure 3.3 Comparison between calculated (solid lines) and experimental (dotted lines) large size band profiles on theC_{18} -Kromasil column, with concentration of tryptophan in the mother solution 0.5 g/L with the three mobile phases.....59
Figure3.4 Comparison between calculated (solid lines) and experimental (dotted lines) large size band profiles on theC_{18} -Kromasil column. with concentration of tryptophan in the mother solution 11 g/L.....60
Figure 3.5 Influence of the ACN concentration on the parameters of the isotherm.....61
Figure 3.6 A) Experimental isotherm data (symbols) of L-tryptophan on the C_{18} -Kromasil column obtained with four different MeOH-water- acetic acid mixtures as the mobile phases.....68
Figure 3.7 Overlaid selected breakthrough curves of tryptophan on C_{18} - Kromasil column, at 1 ml/min, T = 296 K, 1% acetic acid.....69
Figure 3.8 Comparison between calculated (solid lines) and experimental (short dots) band profiles on the C_{18} -Kromasil column with the four MeOH -water -acetic acid mixtures with tryptophan concentration in the sample equals to 2g/L.....70
Figure3.9 Comparison between calculated (solid lines) and experimental (short dots) band profiles on the C_{18} -Kromasil column with the four MeOH -water -acetic acid mixtures with tryptophan concentration in the sample equals to 11 g/L..... 71
Figure 3.10 Influence of the MeOH concentration on (A) the saturation capacities of the low- (q_1), and the high-energy sites (q_2).....72
Figure 3.11 A) Overlay of the chromatograms of thiourea at different

temperatures.....78
Figure 3.12 Breakthrough curves for the adsorption of tryptophan on C_{18}- Kromsil, using aqueous mobile phase containing 5% acetonitrile and 1% acetic acid. The concentration of tryptophan in the mother solution is 0.5 g/L.....79
Figure 3.13 Breakthrough curves for the adsorption of tryptophan on C_{18} - Kromsil, using aqueous mobile phase containing 5% acetonitrile and 1% acetic acid. The concentration of tryptophan in the mother solution is 1-5 g/L.....80
Figure 3.14 Breakthrough curves for the adsorption of tryptophan on C_{18}- Kromsil, using aqueous mobile phase containing 5% acetonitrile and 1% acetic acid. The concentration of tryptophan in the mother solution is 8 g/L..... 81
Figure 3.15 Experimental isotherm data (FA, symbols) of tryptophan on the C_{18} - Kromasil column obtained with an aqueous mobile phase containing 5% acetonitrile and 1% acetic acid. 82
Figure 3.16 Comparison between calculated (solid lines in black) and experimental (dotted lines in red) band profiles overlaid, on C_{18}-Kromasil with a mobile phase containing 5% acetonitrile and1% acetic acid at different temperatures. Injection of a solution of 8g/L tryptophan during 30 s.....83
Figure 3.17 Comparison between the calculated (solid lines in black) and the experimental (dotted lines in red) band profiles overlaid, on C_{18}-Kromasil with a mobile phase containing 5% acetonitrile and1% acetic acid at different temperatures. Injection of a solution of 0.5 g/L tryptophan during 30 s.....84
Figure 3.18 Evolution of the best values of the isotherm parameters obtained from IM, squares for low energy sites, and triangles for high energy sites.....85
Figure 3.19 Calibration of the detector.....99
Figure 3.20 Breakthrough curves for the adsorption of tryptophan on C_{18}-Kromasil. All the aqueous mobile phases contain 1% acetic acid with the concentration of tryptophan in the mother solution is 0.5 g/L.....100
Figure 3.21 Breakthrough curves for the adsorption of tryptophan on C_{18}- Kromasil All the aqueous mobile phases contain 1% acetic acid with the concentration of tryptophan in the mother solution is 2-5 g/L.....101
Figure 3.22 Breakthrough curves for the adsorption of tryptophan on C_{18}- Kromasil. All the aqueous mobile phase contain 1% acetic acid with the concentration of tryptophan in the mother solution is 8-11 g/L.....102
Figure 3.23 A) Experimental isotherm data (FA, symbols) of tryptophan on C_{18} - Kromasil with an aqueous mobile phase containing 2.5% acetonitrile and 1% acetic acid.....103
Figure 3.24 Experimental isotherm data (FA, symbols) of tryptophan on C_{18} - Kromasil with an aqueous mobile phase containing 5% acetonitrile and 1% acetic acid.....104
Figure 3.25 Experimental isotherm data (FA, symbols) of tryptophan on C_{18} - Kromasil with an aqueous mobile phase containing 7.5% acetonitrile and 1% acetic acid.....105
Figure 3.26 Comparison between calculated (solid lines in black) and experimental(dotted lines in red) band profiles overlaid. Conditions: C_{18-} Kromasil with a mobile phase containing 1% acetic acid. Data at 5 different temperatures

overlaid.....106
Figure 3.27 Effect of temperature on the parameters of the isotherm obtained by the IM method for three mobile phase compositions.....107

CHAPTER 1

INTRODUCTION

Chromatography was invented and developed in 1902-1906 by the Russian botanist Tswett [1] who employed this technique to separate various plant pigments such as chlorophylls and xanthophylls by passing solutions of these compound through glass column packed with finely divided calcium carbonate. The separated species appeared as colored bands on the column, which accounts for the name he chose for the method (Greek chroma meaning “color” and graphia meaning to “write”). His separation method was forgotten for thirty years until it was reborn in the mid 1930's when Kuhn and Lederer [2] rediscovered Tswett work through a German translation of his Dissertation. Following the pioneering work of A. J. P. Martin and his associates [3,4] in liquid, paper, and gas chromatography, and who were awarded the Nobel Prize in 1952, this method rapidly became the preferred method of separation. The growing needs by the scientists for better methods of separation and the following discoveries has led to several Nobel Prizes between the years 1937 and 1972 based upon work in which chromatography played a vital role [5].

In any chromatographic separation the process is based on the difference between the migration velocities of the different components of a mixture when they are carried by a stream of fluid percolating through a bed of solid particles called the column. The fluid and the solid phases constitute the chromatography system [2].

There are a very large number of phase combinations that have been and are used in the different applications of the method.

One of these phases must be a fluid to permit the differential migration needed in chromatography. Gases, liquids, or supercritical fluids can be used as the mobile phase (the fluid moving through the column). The second phase is solid or liquid and is almost always stationary (it is the one that stays in place inside the column). Therefore, chromatography can be classified into three main forms (Gas, liquid, supercritical chromatography) and all three have been used for analytical and preparative separations. Fluid entering the column is called eluent, and fluid emerging from the column is called eluate, and the process is called elution.

The retention time for the component t_R is the time needed after injection of the mixture onto the column until the component reaches the detector.

A chromatogram (Figure1.1) is a graph which shows the detector response as a function of time. The related quantity, retention volume is the volume of mobile phase required to eluate particular solute from the column. The dead time t_M is the time required for an average molecule of the mobile phase to pass through the column. The adjusted retention time t_R`and the capacity factor k`are defined by equations 1.1 and 1.2 respectively,

$$t_R' = t_R - t_m \qquad (Eq.1.1)$$

$$k' = \frac{t_R - t_m}{t_m} \qquad (Eq.1.2)$$

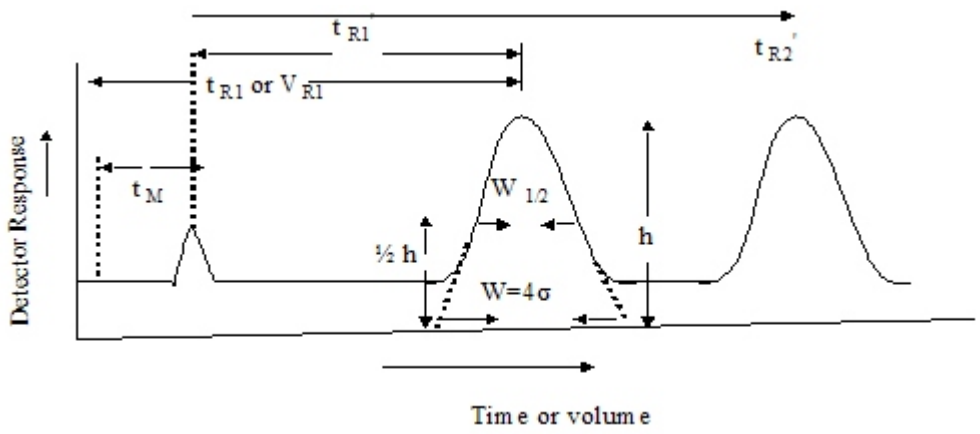

Figure1.1 Gaussian Chromatogram showing the retention time and the adjusted retention time, the width and width at half height

the partition coefficient or distribution coefficient [5] is defined by equation 1.3

$$K = C_S / C_M \qquad (Eq. 1.3)$$

where C_S is the molar concentration of the solute in the stationary phase, and C_M is the molar concentration in the mobile phase.

1.1 The Goals of Separations

The general goals of separation can be divided into two broad categories: preparative and analytical [6]. According to Giddings [6] analytical separations are based on the information generated in the process of separation, or realized by subsequent measurement made possible by separation. Most of the complex mixtures like environmental, and biochemical contain so many components that make it impossible to quantify them by spectroscopic or chemical methods unless separation is used to remove components that interfere with measurement.

Preparative separations on the other hand are used to purify components like drugs, fuels, metals, or products for industrial or human consumption. Preparative separations can be classified according to the amount of product separated into three groups [6]. The first group is large scale separations and they can produce tons of separated products in a day like plant scale industrial processes such as distillation, extraction, and smelting. The second group is reduced scale of production which include adsorption, crystallization, zone refining, filtration and electrolysis and it is used for industry to obtain grams to kilograms per day. And finally small scale (milligrams to grams) preparative work is important for the

recovery of valuable products like recombinant proteins from complex mixtures (e.g insulin and human growth hormone).

For a long time, the analytical applications of chromatography were dominant in this field. Little attention was paid to preparative chromatography and its applications. Recently however, the traditional separation tools available for chemical engineer proved to be unable to satisfy the needs of the laboratories and the production plants of the biotechnology companies and even the traditional pharmaceutical industries. Preparative liquid chromatography is recognized now as the most promising general process available for sufficiently large production rates of the high purity compounds required in the pharmaceutical industry.

1.2 Types of Liquid Chromatography

Among the many possible combinations between the two phases, the solid-liquid equilibria have many practical applications. In solid -liquid adsorption, ion exchange, size exclusion, and liquid-liquid partition are the most popular methods in liquid chromatography [7]. In solid-liquid adsorption, a solid stationary phase is used. Solute is adsorbed on the surface of the solid particles. The more strongly a solute is adsorbed, the slower it travels through the column. In ion exchange, the stationary phase is a resin in which anions such as ($-SO_3^-$)or cations such as($-N(CH_3)_3^+$) are covalently attached to the skeleton of the resin which can exchange counter ions with the stream of the mobile phase, while in size exclusion it is a solid with bores having sizes of the order of the dimensions of the molecules of the feed components and in which larger solutes pass through most quickly. Finally in liquid-liquid partitions, the stationary phase is liquid coated on solid support, and solutes

equilibrate between the phases [8].

1.3 Adsorption Chromatography

Adsorption chromatography can be divided into several important subgroups [7]:

1) Normal-phase liquid chromatography (NPLC) in which a polar solid adsorbent (e.g., porous alumina, silica, or zirconia) and an apolar solvent (e.g., pentane, dichloromethane, or THF) is used.

2) If the adsorbent is nonpolar (e.g., porous cross-linked polystyrene) or the adsorbent is covered with chemically-bonded groups (e.g., octadecyle groups bonded to silica), and the solvent is polar (e.g., water, methanol, or their mixtures), it is reversed-phase liquid chromatography (RPLC) system. However, if the liquid-solid interface becomes thicker than a conventional monolayer, the retention mechanism may become partition chromatography.

3) If the adsorbent is nonpolar (e.g., bonded octadecyle groups, alkyl 1,2 diols or polyglycol chains) and the solvent is a polar, dry organic solvent (e.g., diethyl ether) it is non-aqueous reversed-phase chromatography (NARP).

4) If both the adsorbent and the solvent are polar it is hydrophobic interaction chromatography (HIC).

5) If the surface of the adsorbent contains atoms or groups which can form rather strong complexes with the component of the feed or a few of them, and if any of these complexes can be dissociated in a different mobile phase to recover them we have bioaffinity chromatography.

1.4 Theory of Chromatography

1.4.1 The Transfer Phenomena and Sources of Band Broadening

The separation power of the column is a function of the mass transfer kinetics and of the axial dispersion coefficient. The thermodynamics of phase equilibria is the main factor that affect the shape of the individual band profiles in non-linear liquid chromatography using moderate columns with excellent packing material that allows a large number of equilibrium stages in the column. The effect of finite column efficiency on the band profiles can be accounted for by lumping all the band broadening effects into apparent axial dispersion coefficient.

Diffusion, mass transfer resistance, the kinetics of adsorption-desorption, and the viscosity of the mobile phase all contribute to the transfer phenomena. Diffusion is one main source of band spreading. The diffusion coefficient measures the rate at which a substance move randomly from a region of high concentration to a region with low concentration. The flux J(x) is defined by the number of moles crossing each square meter per second and this is the classical Fick's first law of diffusion [9].

$$J = -\frac{RT}{f}\frac{dC}{dz} = -D_{A,B}\frac{dC}{dz} \qquad (Eq.\ 1.4)$$

where $\partial C/\partial z$ is the concentration gradient Along the column, $D_{A,B}$ the diffusitivity or diffusion concentration of solute A, in solvent B, and f is the friction factor. However because it is difficult to measure J, Fick's second law

of diffusion (equation 1.5) is most widely used [9].

$$\frac{\partial C}{\partial t} = D_m \frac{\partial^2 C}{\partial z^2} \qquad (Eq.\ 1.5)$$

The diffusion coefficient is affected by several experimental conditions like the temperature, pressure, concentration of the solute, nature of the solvent and its composition, and the chemical structure of the solute. For example the diffusion of gases is 10^4 times faster than liquids, and macromolecules like proteins is much slower than the small molecules.

In a packed bed, it is impossible to move very far along a straight line without hitting the surface of a particle. The channels follow tortuous paths around the particles. In modeling of chromatography, the contributions of all the phenomena that contribute to the axial mixing are lumped into single axial dispersion coefficient. Two main mechanisms contribute to axial dispersion:
molecular diffusion and eddy diffusion [9]. The axial dispersion coefficient can be approximated by equation 1.6

$$D_L = \gamma_1 D_m + \gamma_2 d_p u \qquad (Eq.\ 1.6)$$

where d_p is the particle diameter and γ_1 and γ_2 are geometrical constants which have values of 0.7 and 0.5 respectively.

The eddy diffusion can be offset by the ordinary diffusion which result from the transfer of the molecules from one stream to another stream which has different pathway. The velocity of the flow affect this transfer, for example at low velocity there is sufficient time for this transfer to occur, while for high velocities the time is not sufficient for the diffusion to occur, therefore the eddy diffusion averaging does not occur which results in band broadening.

Another type of diffusion that occurs in column chromatography is longitudinal [5,6] diffusion. This diffusion is a band broadening process in which solutes diffuse from the concentrated center of a zone to the more dilute regions ahead of and behind the zone center or with and against the direction of the flow. This diffusion is directly proportional to the mobile phase molecular diffusion coefficient D_m and to the constant γ_1 the obstructive factor which has the value of 0.6 for packed column and unity for unpacked column. The longitudinal diffusion is inversely proportional to the mobile phase velocity. Thus for high velocities there is no sufficient time for the broadening from the center of the band to occur.

Another factor that affect band broadening is the mass transfer effect [5] which arises because of the many flowing streams of the mobile phase within a column and the layer making up the stationary phase both have finite widths. Therefore a time lag occurs when the solutes diffuse form the interior of these phase into their interfaces which results in the persistence of non-equilibrium conditions along the length of the column. This kind of broadening arise from diffusion that tends to be at right angles to the flow, in opposite to the longitudinal diffusion which arises from the tendency of the molecules to move parallel to the flow. Therefore

this diffusion is directly proportional to the mobile phase rate, and the faster the mobile phase moves the less time is available for equilibrium to be approached. If the rate of the mass transfer is infinite this kind of broadening will not occur.

The efficiency of the chromatographic column can be described by two terms the plate height H and the plate count N (N= L/H) where L is the column length. Martin and Synge [5] treated the column as if it is similar to a distillation column that is made up of several and continuos theoretical plates at which solute equilibrate between the stationary phase and the mobile phase. The plate height is defined as the variance per unit length and is given by equation 1.7

$$H = \frac{\sigma^2}{L} \qquad (Eq.1.7)$$

where it is assumed that the chromatographic peak has a Gaussian shape (Figure 1.1). To obtain the number of theoretical plates experimentally two methods can be used [5]. The first method is described by equation 1.8

$$N = 16 \left(\frac{t_R}{W}\right)^2 \qquad (Eq.1.8)$$

and it depends on the peak width W and the retention time t_R. The other method can be calculated using the width at half height (equation1.9)

$$N = 5.54\left(\frac{t_R}{W_{1/2}}\right) \qquad (Eq.1.9)$$

The relationship between the plate height and the column variables can be describe dy Van Deemter equation 1.10 [see ref 8]

$$H = A + B/u + Cu \qquad (Eq.\ 1.10)$$

where A is the contribution of the multipath term, B/u is the contribution of the longitudinal diffusion, and the Cu term is the contribution of the mass transfer. The HETP concept is strictly valid only when the rate of mass transfer kinetics is relatively fast and the profile of the elution peak is Gaussian. It is not valid in nonlinear chromatography [9].

1.4.2 Mass Balance Equation

The fluid and the solid constitute the chromatographic system, between the two phases of the system a phase equilibrium is reached for all component of the mixture. The separation may be successful only if the equilibrium constants of all these components have reasonable values. If they are too small for some components, these compounds travel at a velocity too close to that of the solvent and their complete separation cannot be achieved. If these constants are too large, the corresponding components do not leave the column or they leave it so late, and in bands that are so dilute that no useful purpose can be achieved [9].

There are many factors that control the equilibrium constants like temperature, the nature of the solid surface, and the nature and composition of the fluid used as the mobile phase. The specific surface area of the adsorbent and its pore volume are also important. All particles used in preparative separations are porous or penetrable by the molecules of the compounds investigated, in order to maximize the capacity of the corresponding column and to allow the handling and the separation of large samples. Fluid dynamics, mass transfer phenomena , and equilibrium thermodynamics play an important role in the outcome of the separation[9]. The relative importance of the thermodynamics of phase equilibria or the kinetics of mass transfer depend on the experimental conditions. However, in most of the cases, the mass of each of the components of the injected mixture is conserved. The mass balance equation was studied first by Wicke [10] and later by Wilson [11] and De Vault [12] independently under different forms.

The mass balance of a compound in a slice of chromatographic column for a single component may be written (equation 1.11):

$$\frac{\partial C_i}{\partial t} + F\frac{\partial q_i}{\partial t} + \frac{\partial C_i}{\partial z} = D_{L,i}\frac{\partial C_i^2}{\partial z^2} \qquad (Eq.1.11)$$

where C and q are the concentrations of the studied compound at time t and abscissa z (Figure 1.2) in the mobile phase and stationary phase respectively, u is the mobile phase velocity, and *F* the phase ratio of the column (with $F = (1-\epsilon)/\epsilon$ and

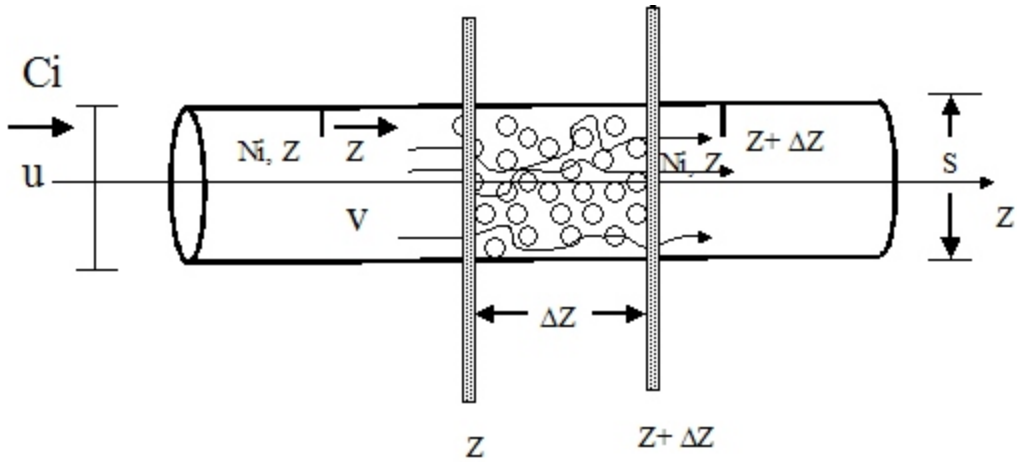

Figure 1.2 Differential mass balance in a column slice

ϵ is the total porosity, and D is the coefficient of axial dispersion, i.e, D accounts for band spreading by axial molecular diffusion in the tortuous packing and by eddy diffusion (lack of radial homogeneity of the mobile phase flow pattern. In liquid chromatography the mobile phase density is constant along the column, as the compressibility is negligible, [9] and the partial molar volumes of the solute in the stationary phases are nearly the same, and there is no sorption effect. The mobile phase velocity may be regarded as constant in equation (1.11) and there is no need for a mobile phase mass balance equation, as long as the mobile phase is pure and we can assume that it is not adsorbed [9]. In many cases, the mobile phase in liquid chromatography, is not pure and usually it is a mixture of a week solvent like H_2O and strong solvent or organic modifier like CH_3OH, or CH_3CN, or the mobile phase may contain some additives also like salts or buffers. In these case a mass balance equation must be written for each system component, i.e., for each component of the sample and the mobile phase if we want an accurate solution. However, the mass balance equation of the weak solvent may be omitted, assuming that it is not adsorbed on the stationary phase. Also it can be omitted for the organic modifier or some additives if they are much less strongly retained than the components of interest. The mass balance equations of each component of the sample and of the mobile phase without the weak solvent and of the appropriate relationships between the concentrations C_i of the components in the mobile phase and their concentrations in the stationary phase ,q_i constitutes the fundamental system of equations of chromatography. One of the approaches for the solution of this system is to assume that the two phase of the chromatographic system are always very

close to thermodynamic equilibrium, and that the transfer kinetics between and across the mobile and stationary phases in the column are very fast [9]. Thus there is arelationship between the concentrations, in both phase, of each component of the system. This relationship (equation 1.12), is the equilibrium isotherm:

$$C_{s,i} = q_i = f(C_1, C_2, \ldots, C_i, \ldots C_n) \qquad (Eq.1.12)$$

where $C_{s,i}$ is the instantaneous concentration of the component I in the stationary phase and q_i is its stationary phase concentration when in equilibrium with the concentrations C_j [j $\in$ (1,n)] in the mobile phase.

1.4.3 Initial and Boundary Conditions

These conditions are necessary for the solution of a system of partial differential equations. Such a system has an infinite number of solutions. The initial and boundary conditions define the exact solution needed. They are the mathematical translation of the experimental procedure followed.

1.4.3a. The Initial Conditions

The general initial condition [9] is

$$C_i(z, t=0) = 0 \qquad \text{for} \qquad 0 \leq z\ L \qquad (Eq.1.13)$$

where L is the column length. This initial condition describes the state of the column when the experimental begins, at t =0, and it works for conventional elution where

the column is filled with a weak mobile phase which does not participate in the equations [13]. In the cases where there is a mobile phase additive, gradient elution, staircase frontal analysis and displacement chromatography where the column contains a constant concentration C^0_a of a component interacting with the stationary phase at the beginning of the experiment, the initial condition is different from the above equation, and it has to be written for each case independently

1.4.3b. The Boundary Condition [9]

The most common boundary condition for elution is (eq1.14)

$$C_i(0,t) = C_i^0 \, \phi_s(t) \qquad (Eq.1.14)$$

where C^0_i is the concentration of the component I in the feed and $\varphi_s(t)$ is the injection profile assuming that the solubility of the components in the mobile phase exceeds C^0_i.

For linear or analytical chromatography the Dirac pulse injection or δ function is used as the conventional boundary condition. The concentration profile injected has a finite area, corresponding to a finite sample size, an infinite concentration, and a zero bandwidth. This condition might seem unrealistic, but it is successfully applied in analytical chromatography, and the actual injecting profile has usually a sharp front followed by a tailing decay. In analytical chromatography, the boundary conditions consist more often in the injection of a narrow pulse of sample or feed, after which a stream of mobile phase is again pumped through the column. The concentration of the pulse in theoretical studies is the Dirac function δ(t), while in

numerical calculations it is narrow rectangle.

The rectangular pulse injection has the following boundary conditions (equation 1.15)

$$
\begin{aligned}
C(0,t) &= 0 \quad \text{for } t < 0 \\
C(0,t) &= C_0 \quad \text{for } 0 < t \leq t_p \\
C(0,t) &= 0 \quad \text{for } t_p < t
\end{aligned}
\qquad \text{(Eq. 1.15)}
$$

where C_0 is the concentration of the pulse and t_p is its duration which is usually very small compared to the hold up volume. In the extreme case, it is narrow and it can be represented by the Dirac δ function [9]. The rectangular pulse injection applies for the preparative chromatography, where the column has finite length and efficiency.

Another boundary conditions which are most often used in chromatography is the Danckwerts Conditions [9], which is described by equation 1.16

$$
\begin{aligned}
&\left[uC - D\frac{\partial C}{\partial z} \right]_{z=0} = uC_0 \\
&\frac{\partial C}{\partial z}\Big|_{z=L} = 0
\end{aligned}
\qquad (Eq. 1.16)
$$

These conditions apply when the axial diffusion proceed at an infinite rate, and if vertical boundary conditions are applied. The left hand side (LHS) of the first equation is the flux in the column at the injection point, and it is equal to the injection

flux in the equivalent pipe (RHS).

The solution of the second order differential equations is very complex when there are two or more component in the sample or if the mobile phase has an additive, and only analytical solutions are available[9]. However, the problem may be solved by using different approaches for solving the problem, and different models like the ideal model, the equilibrium dispersive model, and the lumped kinetic models. The first two of these models will be explained briefly in the next sections.

The three major types of isotherm functions q = f (C) that are encountered in chromatographic systems are either linear, convex upward or Langmuirian, and convex downward or anti-Langmuirian (Figures 1.3a-c). The corresponding differential, band profiles for the ideal model and the equilibrium dispersive model are illustrated in Figures 1.3d-f , 1.3g-l and 1.3j-l respectively.

1.4.4 The Ideal Model

This model assumes that the two phases are in constant equilibrium, and that there are no sources of band broadening of kinetic origin or there is no axial dispersion and that the column has an infinite efficiency. It was studied by Wick [10], Wilson [11], and DeVault [12]. The mass balance equation for component I is simplified by equation1.17

$$\frac{\partial C_i}{\partial t} + F\frac{\partial q_i}{\partial t} + u\frac{\partial C_i}{\partial z} = 0 \qquad (Eq.\ 1.17)$$

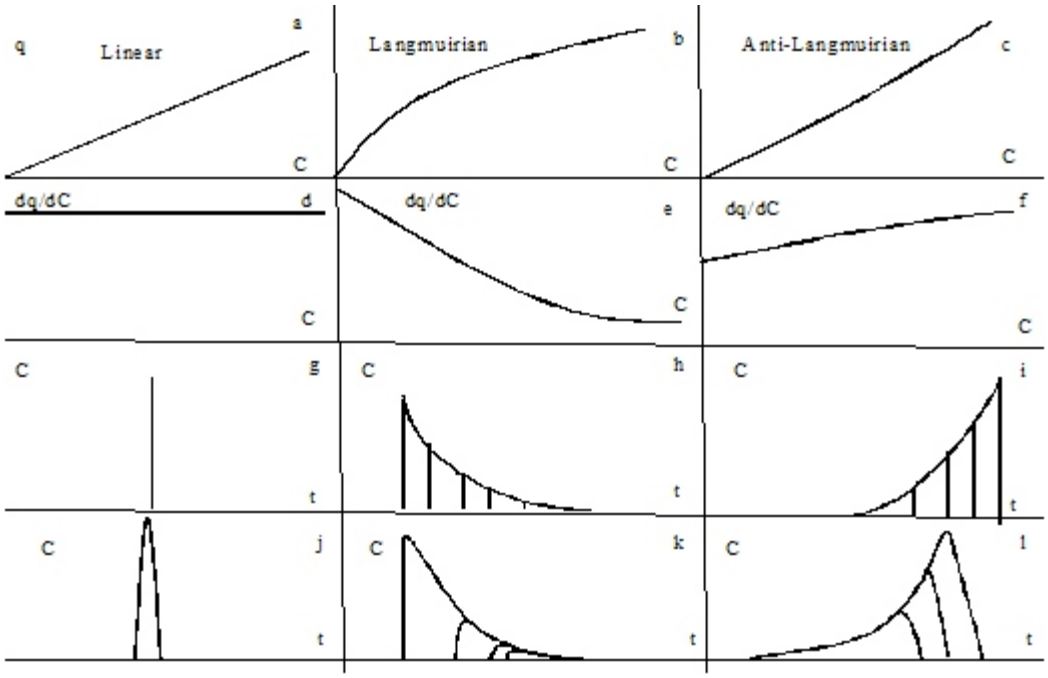

Figure 1.3 Relationship between the isotherms and their corresponding band profile. Single component isotherms A-C; their differentials D-F; and their band profiles using the ideal model G-I, and with axial dispersion J-L.

Since this model ignores axial mass kinetics and axial dispersion, it can propagate concentration discontinuities, or shocks. The mass balance equation for this model can be solved in a closed form for single component in overloaded elution chromatography for different kinds of isotherms, or for binary mixtures with competitive isotherms. For all other cases numerical solutions is used to solve the problem.

1.4.5 The Lumped Kinetic Models

In these models the mass balance equation is combined with a kinetic equation which relates the rate of variation of the concentration of each component in the stationary phase to its concentration in both phases and to the equilibrium concentration in the stationary phase. There are several models for the kinetic model, for example the linear kinetic model studied by Lapidus and Amundson [14] assumes first order kinetic model:

$$\frac{\partial C_{s,i}}{\partial t} = k_a\, C_i - K_d\, C_{s,i} \qquad (Eq.\ 1.18)$$

where $q_{s,i}$ is the column saturation capacity, k_a, and k_d are the rate constants and desorption of the component considered. Other models like the langmuir kinetic model and the general rate model are discussed in more details by Guiochon et al [9].

1.4.6 The Equilibrium Dispersive Model

This model assumes that all contributions due to the non-equilibrium can be lumped into apparent axial dispersion term. It further assumes that the apparent dispersion is constant, independent of the concentration of the sample component.

This model were studied by Giddings [15], Van Deemter et al. [16] and Haarhoff and Van der Linde [17]. They showed that when the mass transfer kinetics are fast but not infinitely fast, the mass balance equation can be written as (eq1.19)

$$\frac{\partial C_i}{\partial t} + F\frac{\partial q_i}{\partial t} + u\frac{\partial C_i}{\partial z} = Da,i\frac{\partial C_i^2}{\partial z^2} \qquad (Eq.\ 1.19)$$

where $D_{a,i}$ is the apparent dispersion coefficient which is given by equation 1.20

$$Da,i = \frac{HL}{2t_0} = \frac{Hu}{2} \qquad (Eq.1.20)$$

where H is the column height equivalent to a theoretical plate (HETP) for the component considered, and t_0 is the hold up volume of the column (t=L/u). This model is valid if mass transfer in the chromatographic column is controlled only by molecular diffusion across the mobile phase flowing around the particles and if the exchange between the two phases is fast. The diffusive term causes erosion of the discontinuity, therefore discontinuities cannot take place with a mass balance equation, and Instead of the sharp shock, there is a shock layer. The thickness of this layer is definite and it depends on the mass transfer and on the axial dispersion coefficient, and it has the same propagation as the shock.

1.4.7 Numerical Solutions for Equilibrium-Dispersive Model and Single Component Problems

There is no closed form solution for the equilibrium dispersive model equation, and the only available solution is either approximate analytical solutions [14-16] or a numerical solution using computation methods such as the finite differences, the finite elements, or collocation [17-19]. The approximate analytical solutions of this model, are valid only at low concentrations (loading factor is low and bC max is smaller than 0.05 to 0.1 [18]. These solutions were proposed by Houghton,[20], Harrhoff and Van der Linde [17], and Golshan-Shirazi and Guiochon [18]. The first original numerical solution of the equilibrium -dispersive model was developed and applied to the prediction of the band profiles in gas chromatography [21] and it was applied later for liquid chromatography [22-23]. It is used to predict the band profiles of large size samples. It requires knowledge of the HETP, column void volume, and extra-column volume, and the adsorption isotherm [24]. The mathematical basis of numerical solutions is the equation 1.21

$$\frac{\partial C}{\partial z} + \frac{\partial\left[\frac{1}{u}(C+Fq)\right]}{\partial t} = \frac{D_a}{u}\frac{\partial^2 C}{\partial z^2} \qquad (Eq.121)$$

by replacing (C + Fq)/u by G(C), we can write equation 1.21 as :

$$\frac{\partial C}{\partial z} + \frac{\partial G(C)}{\partial t} = \frac{D_a}{u}\frac{\partial^2 C}{\partial z^2} \qquad (Eq.1.22)$$

Several methods can be used to solve this equation numerically using fast computers like the finite difference methods, and the methods of orthogonal collocation on finite elements. A short description of the finite difference method will be presented here. Reference [9] have more details for this method and for other numerical methods.

The principle of the finite difference methods consists of replacing the continuous plane (z, t) by a grid. This grid consists of a number of small segments of space and time of size h for space and τ for time. Therefore, the first order terms

$$\frac{\partial C}{\partial z} \qquad and \qquad \frac{\partial C}{\partial t} \qquad (Eq.1.23)$$

can be replaced by one of the following finite differences [9]:

a forward finite difference: $\frac{C_{n+1}^{j} - C_{n}^{j}}{h}$ *and* $\frac{C_{n}^{j+1} - C_{n}^{j}}{\tau}$, *respectivly*

a backward finite difference: $\frac{C_{n}^{j} - C_{n-1}^{j}}{h}$ *and* $\frac{C_{n}^{j} - C_{n}^{j-1}}{\tau}$, *respectivly*

or a central finite difference: $\frac{C_{n+1}^{j} - C_{n-1}^{j}}{2h}$ *and* $\frac{C_{n}^{j+1} - C_{n}^{j-1}}{2\tau}$, *respectivly*

The second-order term $\partial^2 C/\partial z^2$ can be replaced similarly by a central finite difference

$$\frac{C^{j}_{n+1} - 2C^{j}_{n} + C^{j}_{n-1}}{h^2}$$

There are many methods to use the finite difference method to approximate the mass balance equation, but in all cases the numerical solution need to be stable, and the numerical or truncation errors that can be made during the calculations need to be controlled and evaluated. Czok and Guiochon [24] have compared the profiles obtained with the three finite difference methods, the forward-backward, the backward-forward, and the forward-backward $_{n+1}$ schemes. They found significant differences between the band profiles obtained at low column efficiency (300), but no meaningful differences at high efficiencies.

Another two kinds of investigations were also carried out using the equilibrium dispersive method: the first is the behavior of chromatographic columns under various sets of experimental conditions, in a variety of computer experiments [23,25,26]. The influence of the nature of the equilibrium isotherm (e.g., Langmuir, bi-Langmuir, or anti-Langmuir), of the column efficiency, and of the sample size and volume were the main areas of study for single-component profiles.

The second kind of investigation is to compare the calculated band profiles with the experimental results in order to validate calculation methods, algorithms, programs, and the procedures of measurements of relative parameters [23].

The results of the first kind of investigations showed that the there is a

difference in the band profiles if the isotherm deviates from linear behavior. If the isotherm is linear the elution profiles have a Gaussian shape, but if it is convex upward, such as the langmuir isotherm, the band profiles have a steep front and a diffuse rear boundary, while an initial convex-upward isotherm with an inflection point gives a band with a front rear shock layer. For a sigmoidal isotherm the shape of the band profile is affected by increasing the sample size. The band profiles initially have a sharp rear boundary due to the convex-downward isotherm in the low concentration range. At higher concentrations the change in the curvature results in a self-sharpening front. Their results showed also that the higher sample size the higher the column saturation capacity, and hence the higher the production rate and the lower the cost of chromatographic purification. Therefore it is very important to find a chromatographic system which gives higher saturation capacity, to increase the amount of the feed loaded per unit weight of column packing and lower production rate.

The second kind of investigations (i.e the comparison between the calculated and the experimental band profiles) using the equilibrium dispersive method have mostly been carried out using programs implementing the finite difference methods. To calculate the band profiles and to compare it with the experimental results, some information is needed like the adsorption isotherm, the HETP under linear conditions, the sample size, the flow rate of the mobile phase, the hold-up volume, and the column dimensions. A very good agreement is found between the calculated and the experiment overloaded band profiles using normal and reversed phase chromatography [27]. In all the cases the frontal analysis method was used

to obtain the isotherms for single-component isotherms.

1.4.8 Determination of Single-Component Isotherms by Frontal Analysis

Single component isotherm data were acquired by frontal analysis (FA), the most accurate method [28-29]. This method consists in successively replacing the stream of mobile phase percolating through the column with streams of solutions of the studied compound in this mobile phase, at increasing concentrations, and in recording the breakthrough curves at the column outlet. Mass conservation of the solute between the times when the new solution enters the column and when the breakthrough curve is eluted allows the calculation of the adsorbed amount, q^*, of solute on the stationary phase at equilibrium with the mobile phase concentration, C. This amount is best measured by integrating the breakthrough curve, using the equal area method [30]. The adsorbed amount is given by

$$q^* = \frac{C(V_{eq} - V_0 - V_{ex})}{V_a} \qquad (Eq.124)$$

where V_{eq}, V_0 and V_{ex} are the elution volume of the equivalent area of the solute ,the extra column volume, and the hold-up volume, respectively, and V_a is the volume of the stationary phase in the column.

1.4.9 Models of Isotherm Used

We report here only on those isotherm models that we found to account best for the isotherm data measured. Many other models (*e.g.*, Langmuir and multi-Langmuir models) were tried but rejected. They are not mentioned here. All the isotherm models considered are single-component models, although the problem

studied here is actually a two-compound problem because of the competition between acetonitrile and tryptophan for adsorption. So, a binary isotherm model might seem more appropriate. It has been shown, however, that using a single component model is acceptable when one of the two compounds (here acetonitrile) is much less strongly adsorbed than the other one (here, tryptophan) [28]. Then, the coefficients of the model depend on the mobile phase composition but the model still accounts correctly for the adsorption behavior of the retained compound.

1.4.10 The bi-Moreau Model

This is the model that best accounts for the adsorption isotherm data of tryptophan in ACN/water mobile phases. The Moreau isotherm model is the simplest extension of the Langmuir isotherm model in the case of an homogeneous adsorbent on the surface of which significant adsorbate-adsorbate interactions take place [31]. The bi-Moreau isotherm is the corresponding extension of the bi-Langmuir model to a surface covered with two homogeneous types of sites, on each of which adsorbate-adsorbate interactions take place, following Moreau model behavior. The model is written:

$$q^* = q_{s,1}\frac{b_1 C + I_1 b_1^2 C^2}{1 + 2b_1 C + I_1 b_1^2 C^2} + q_{s,2}\frac{b_2 C + I_2 b_2^2 C^2}{1 + 2b_2 C + I_2 b_2^2 C^2} \qquad (Eq.1.25)$$

where q^* and C are the equilibrium concentration of the compound considered in the adsorbed and the liquid phase respectively, and $q_{s,1}$, $q_{s,2}$, b_1, b_2, I_1, and I_2 are the monolayer saturation capacities, the equilibrium constants, and the adsorbate-

adsorbate interaction parameters on the sites of types 1, and 2, respectively. Note that the bi-Moreau model morphs into the bi-Langmuir model [32] when $I_1 = I_2 = 0$, equation1.25 above reducing to that of the bi-Langmuir model:

$$q^* = q_{s,1}\frac{b_1 C}{1+b_1 C} + q_{s,2}\frac{b_2 C}{1+b_2 C} \qquad Eq.(1.26)$$

The equilibrium constants b_1 and b_2 are associated with the adsorbtion energy $\in_{a,1}$ and $\in_{a,2}$, respectively, through the following classical equation [33].

$$b_1 = b_0 e^{\frac{Ea,1}{RT}} \qquad (Eq.1.27)$$

where $\varepsilon a,i$ is the adsorption energy on sites I, R is the ideal gas constant, T is the absolute temperature, and b_0 is a pre-exponential factor that could be derived from the molecular partition functions in the bulk and the adsorbed phases. The factor b_0 is often considered to be independent of the adsorption energy [33]. The adsorbate-adsorbate interaction parameter, I, can be written as [31]

$$I = e^{\frac{\varepsilon AA}{RT}} \qquad (Eq.\ 1.28)$$

where ε_{AA} is the interaction energy between two molecules of A adsorbed on close adsorption sites.

1.4.11 The Quadratic Isotherm Model

$$q^* = q_s \frac{(b_1 + 2b_2 C)C}{1 + b_1 C + b_2 C^2} \qquad (Eq.129)$$

Statistical thermodynamical considerations lead to an isotherm equation which is the ratio of two polynomials of the same degree [28,29,34-31]. The Langmuir isotherm, obtained with a first-degree polynomial, is the first such model. The quadratic isotherm, obtained with a second-order polynomial, is the second one The saturation capacity is q_s; b_1 and b_2 are the equilibrium constants. When the numerical coefficients meet certain conditions, this isotherm has an inflection point.

1.4.12 Isotherm Modeling

To determine the best model for a certain set of data, the different adsorption models are compared, usually on the basis of the Fisher test. The best model selected for the experimental data is the one that gives the highest value of the Fisher parameter [37] .

$$Fcalc = \frac{(n-l)\sum_{i=1}^{n}(q_{ex,i} - \overline{q}_{ex})^2}{(n-1)\sum_{i=1}^{n}(q_{ex},i - q_{i,l})^2} \qquad (Eq.1.30)$$

where $\overline{q_{ex}}$ is the mean value of the experimental data, $q_{ex,i}$, are the experimental data, l is the number of adjusted parameters of the model, and n the number of data points.

1.4.13 The Inverse Method of Isotherm Determination

This method consists in adjusting the coefficients of a preselected isotherm model in order to minimize the difference between one or several experimental band profiles and the profiles calculated with the equilibrium dispersive (ED) model, using this isotherm model [28,29,38]. The main advantage of this method of isotherm determination is that it requires the measurement of one or a few overloaded band profiles only [39-42]. The measurements are fast and require only small amounts of chemicals. In practice, band profiles are recorded, each recorded profile (detector response) is converted into a concentration profile through the use of a calibration curve, and the coefficients of a selected isotherm model are adjusted to minimize the sum $\sum_i \left(C_i^{sim} - C_i^{meas} \right)^2$.

The equilibrium-dispersive model of chromatography is used to calculate the band profiles [28,43-46]. It is particularly suitable for low molecular weight compounds of moderate polarity. In this model, we assume constant equilibrium between the stationary and the mobile phases and use an apparent dispersion term to account for the band broadening effects of both axial dispersion and the finite rate

of the mass transfer kinetics. The following mass balance equation is written for the solute:

$$\frac{\partial C}{\partial t} + F\frac{\partial q}{\partial t} + u\frac{\partial C}{\partial z} = Da\frac{\partial C^2}{\partial z^2} \qquad (Eq.1.31)$$

Where *C* and *q* are the concentrations of the solute in the mobile and the stationary phases, respectively, *z* the length, *t* the time, *u* the superficial linear velocity of the mobile phase, and *F* the phase ratio of the column (with $F = (1-\epsilon)/\epsilon$ and ϵ the total column porosity). D_a is the apparent dispersion coefficient that can be calculated

$$D_a = \frac{uL}{2N} \qquad (Eq.1.32)$$

from the column efficiency or number of theoretical plates

where *L* is the column length, and *N*, number of theoretical plates of the column, is measured under linear conditions, *i.e.*, with a small sample size.

1.4.14 Initial and Boundary Conditions for the ED Model

At $t = 0$, the concentrations of the solute in the mobile and in the adsorbed phase in the column are uniformly equal to zero. The stationary phase is in equilibrium with a stream of the pure mobile phase. The boundary conditions used are the classical Danckwerts-type boundary conditions [28,43] at the inlet and the outlet of the column. In all the calculations, the inlet profiles were assimilated to

rectangular profiles.

1.4.15 Numerical Solutions of the ED Model

The ED model was solved using the Rouchon program based on the finite difference method[43-31]

1.5 State of the Problem

The production costs in preparative HPLC should be minimized. This requires the selection of a stationary phase with a high selectivity and a high loading capacity to ensure a high production rate. Since separations must be carried out at high concentrations, preparative chromatography is essentially nonlinear and separations are governed by the equilibrium isotherms. The parameters of these isotherms depend on the nature and concentration of the organic modifier in the mobile phase and, for ionizable compounds, on the pH and the ionic strength and we need to understand this dependence. The influence of the experimental conditions on the nature and on the parameters of the adsorption isotherm, on the shape of the overloaded band profiles, and, even in many cases, of that of peaks obtained for what is generally considered as analytical-size samples continues to attract much attention. The effects of the pressure [47-49], the temperature [50-52], the ionic strength of the mobile phase [53-56], the nature and the pH of the buffer [57-59], and those of the nature and the concentration of the organic modifier [60-63] have been studied extensively in the recent years but progress has left many areas of uncertainty.

Many studies were devoted to understand the retention of ionizable compounds at high concentrations [57,58]. It is uncommon to elute ionizable

compounds with a mobile phase containing neither a salt nor a buffer. Although this is not a common procedure in analytical applications, this approach can provide useful information on the mechanism of the retention of these compounds on C_{18} -bonded silica materials. Previous reports on the effects of the ionic strength, the nature of the buffer, or that of the organic modifier on the adsorption data, the nature and parameters of the equilibrium isotherm and the shape of overloaded band profiles of propranolol [59-60], nortriptyline, and amytriptyline [61-62] have contributed much to the understanding of the adsorption mechanism in RPLC. However, there is practically no available data in the literature which compares the adsorption data of a compound obtained in RPLC with methanol(MeOH)/water and acetonitrile(ACN)/water mobile phases. There is no complete study on the adsorption isotherms of an ionizable compound that takes into consideration the effect of the nature of the organic modifier and its concentration in the mobile phase in the absence of a buffer or a salt. Most previous publications [47-63] considered the influence of the concentration of the buffer or salt at constant organic modifier concentration or that of the type of buffer [57-59] or salt [53-56] used. When two organic modifiers were used (MeOH and ACN), their concentrations were kept constant and chosen to achieve similar retention. Therefore, the first goal of this work is to study the effect of the composition of the mobile phase , i.e., of the nature and concentration of the organic modifier on the adsorption isotherm.

Two organic modifiers with seven different aqueous mobile phase compositions (2.5%, 5%,and 7.5% acetonitrile) and(7%, 10%, 15%, 20% methanol) all with 1%acetic acid were used in this work to study the adsorption behavior of

tryptophan at 23°C.

Most optimization procedures for HPLC methods neglect the influence of temperature. There are several solid reasons for this lack of interest, like the lack of columns that can withstand an elevated temperature and the resulting harsh conditions over an extended period of time [64] and the difficulties in keeping the entire column isothermal. Any temperature gradient across the column will result in a significant radial variation of the viscosity of the mobile phase, hence in a wide radial distribution of the velocity, the warping of the elution bands and a possibly dramatic loss of efficiency. It is far easier in practice to change the retention of a compound by adjusting the composition of the mobile phase [65-66]. However, the study of analytical separations has demonstrated the usefulness of temperature improve the separation speed, the column efficiency, and the selectivity of solutes [67-73]. This new popularity of temperature adjustment arose from the development of new thermally stable columns [74-81]. The increase in the separation speed is mainly caused by the correlative increase of the diffusivity of solutes [77], requiring higher mobile phase velocities to achieve the same efficiency, and decrease of the viscosity of the mobile phase that allows the operation of columns at these higher velocities [82-83]. Another advantage of using high temperatures in HPLC is the reduced operation cost due to the lower consumption of organic solvent because the hydrophobicity of water decreases with increasing temperature. Water may, sometimes, be used as the sole eluent [84-86]. Most efforts made so far to develop the use of elevated temperatures in HPLC are devoted to the preparation of stationary phases that can withstand high temperatures and to analytical

applications of high temperature HPLC in the separation of molecules of biological importance like proteins [76,87]. There is little information available in the literature on the effect of temperature on the adsorption behavior and the adsorption isotherms of single components.

Previous publications have studied the effects of the mobile phase composition [88] and the temperature [89] on the adsorption isotherm of phenol, a neutral compound with a small molecular weight, onto a C_{18} Kromasil column, with an aqueous solution of methanol as the mobile phase. It was found that the adsorption isotherm of phenol is accounted for by a bi-Langmuir model, which indicates that there are two types of sites on the adsorbent surface, low energy sites which are related to the surface of the bonded chains and high energy sites, which are probably located in deep cavities within the alkyl layer, cavities that are easily accessible to small molecules. Both the column temperature and the methanol concentration in the mobile phase affect the parameters of the isotherm of phenol. However, it is difficult to generalize from data acquired with one compound and more investigations are needed, using solutes with a larger molecular size, other adsorbents, and other organic modifiers. It has been found [90] that the mechanism of adsorption is affected by the nature of the solvent and solutes used. for example, the non-linear behavior of Vant't Hoff plots [91-93] and the characterization of C_{18}-silicas by Raman and nuclear magnetic reasonance [93-95] spectroscopy demonstrated that the alkyl layer on C_{18}-bonded silicas may undergo a phase transition from a "solid-like" ordered state to a "liquid-like" disordered state when the column temperature is increased.

The second goal of this work is to study the effect of temperature at different mobile phase compositions on the retention and adsorption of L-tryptophan, and that of the experimental conditions on the adsorption parameters of this compound and on the shape of its overloaded band profiles, in order to develop a better understanding of the retention and adsorption of organic compounds on RPLC packing materials. Therefore, three mobile phase compositions which contain aqueous solutions of 2.5%, 5%, and 7.5% acetonitrile and 1% acetic acid at five different temperatures (25, 35, 45, 55, and 65°C) were used to carry out our investigation.

A third goal for our work is to use the inverse method IM which is a numerical method to obtain the parameters of the adsorption isotherm of tryptophan under the above conditions i.e. different mobile phase compositions and different temperatures, and to compare these results with the results of the frontal analysis.

Several methods are available to determine equilibrium isotherms by chromatography, to model the data, and to study the influence of the experimental conditions on the isotherm parameters [96-97]. Frontal analysis (FA) and the pulse methods [98] are the most accurate methods to determine isotherm data. Both give sets of data that can be modeled readily. One advantage of FA is that it does not require the calibration of the detector if the column efficiency is high, the mass transfer fast and the amount of solute adsorbed can be calculated from the inflection time of the breakthrough curve without requiring its integration. However, FA becomes less accurate if breakthrough curves do not exhibit a sharp shock layer but have a diffuse front. This may occur when the column efficiency is low, when the

breakthrough curves are recorded with streams of low concentrations (*i.e.*, under nearly linear conditions), or in the case of S-shaped isotherms. Also, the FA method requires the acquisition of at least thirty data points that cover a sufficiently wide concentration range, from the quasi-linear part of the isotherm at low concentrations to the region close to the saturation of the mobile phase, in order to reach amounts adsorbed that are significant compared to the saturation capacity of the adsorbent. Therefore, this method requires large amounts of sample and solvents and it is time consuming.

The isotherms of tryptophan were measured under RPLC conditions and as the results will show later in this study the breakthrough curves had to be recorded at three wavelengths, 280, 305, and 310 nm for concentrations lower than 0.05 g/L, between 0.05 and 2g/L, and larger than 2g/L, respectively, to avoid absorbances in excess of 1.30 AU and obtain an accurate calibration curve. When FA is used to determine the isotherms of tryptophan, some advantages of the method are lost because the shapes of the breakthrough curves at low and high concentrations are different. Therefore the breakthrough curves must be converted from absorbance into concentration units to obtain the amounts adsorbed, making necessary the determination of calibration curves at different wave lengths to calculate the adsorption data. When data at different temperatures and mobile phase compositions are needed, calibration curves are required at each temperature and mobile phase composition used, making the experimental work longer, more complex, tedious, and more expensive.

In contrast, the inverse method consists in (1) injecting a series of pulses of

increasing size; (2) assuming an isotherm model with tentative numerical estimates of the coefficients of this isotherm on the basis of the profiles of these pulses; (3) calculating the band profiles for different amounts of the compound; (4) comparing the calculated and the recorded experimental profiles; and (5) using an optimization program to minimize the differences between these two sets of profiles [13]. The inverse method gives best estimates of the parameters of the isotherm model selected. It requires far less amount of sample and solvents since only a few profiles, one at low concentration and one or two overloaded profiles are needed.

CHAPTER 2

EXPERIMENTAL

2.1. Chemicals and Materials

The mobile phases used in this work were aqueous solutions of acetonitrile (2.5, 5, and 7.5%) or methanol (7, 10, 15, and 20%) and 1% acetic acid. Water, acetonitrile, methanol and glacial acetic acid are all HPLC grade, purchased from Fisher Scientific (Fair Law, NJ, USA) The solutes used are L-tryptophan and thiourea, both purchased from Aldrich (Milwaukee, WI, USA). L-tryptophan was used because it is the common composition of this commercial product. Since the chromatographic system used is achiral, the results would have been the same with D- or rac-tryptophan. The solutions were filtered before use on an SFCA (surfactant free cellulose acetate) filter membrane, 0.2 µm pore size (Suwannee, GA, USA).

2.2. Column

A manufactured-packed, 250 X 4.6 mm Kromasil column was used (Eka Nobel, Bohus, Sweden). This column was packed with a C_{18}-bonded, end capped silica. This column (Column #E6019) was one of the lot of 10 columns previously used by Kele and Guiochon [99], Gritti and Guiochon [100], and Felinger and Guiochon [101] for study of the reproducibility of the chromatographic properties of RPLC columns under linear and non-linear conditions. The physiochemical properties of the Kromsil-C_{18} adsorbent material packed in Stainless Steel Tubes are as follows: Particle shape: Spherical; Particle size: 5.98µm; Pore Size: 112 Å;

Specific Surface Area (before derivitization): 314 m^2/g; Total Carbon: 20%; Surface Coverage: 3.6 μmol/m^2.

2.3. Apparatus

The isotherm data of tryptophan were acquired using a Hewlett-Packard (now Agilent Technologies, Palo Alto, CA, USA) HP 1090 liquid chromatograph. This instrument (Figure2.1) includes a multi-solvent delivery system (three tanks, volume 1 L each), an auto-sampler with a 250 μm loop, a column thermostat, a diode array UV detector, and a computer data acquisition station. Compressed nitrogen and helium bottles (National Welders, Charlotte, NC, USA) are connected to the instrument to allow the continuous operation of the pump and solvent sparging. The microcomputer of this system was used to program a series of breakthrough curves. The extra-column volumes are 0.033 and 0.60 ml, as measured from the auto-sampler and from the pump system, respectively, to the column inlet. All the retention data were corrected for these contributions. The flow rate accuracy was periodically controlled by pumping the pure mobile phase at 22 C and 1ml/min during 50 minutes from each pump head, successively, into a volumetric glass of 50 ml. The relative error was less than 0.4 %, so that we can estimate the long term accuracy of the flow rate at 4μL/min at flow rates around 1ml/min. The main parts of the HP1090 are illustrated in the following sections [102].

2.3.1 Solvent Delivery System SDS

The SDS have three solvent channels (A, B, C). Each solvent channel (Figure 2.2) comprises a solvent reservoir and a dual-syringe metering pump with rotary valve.

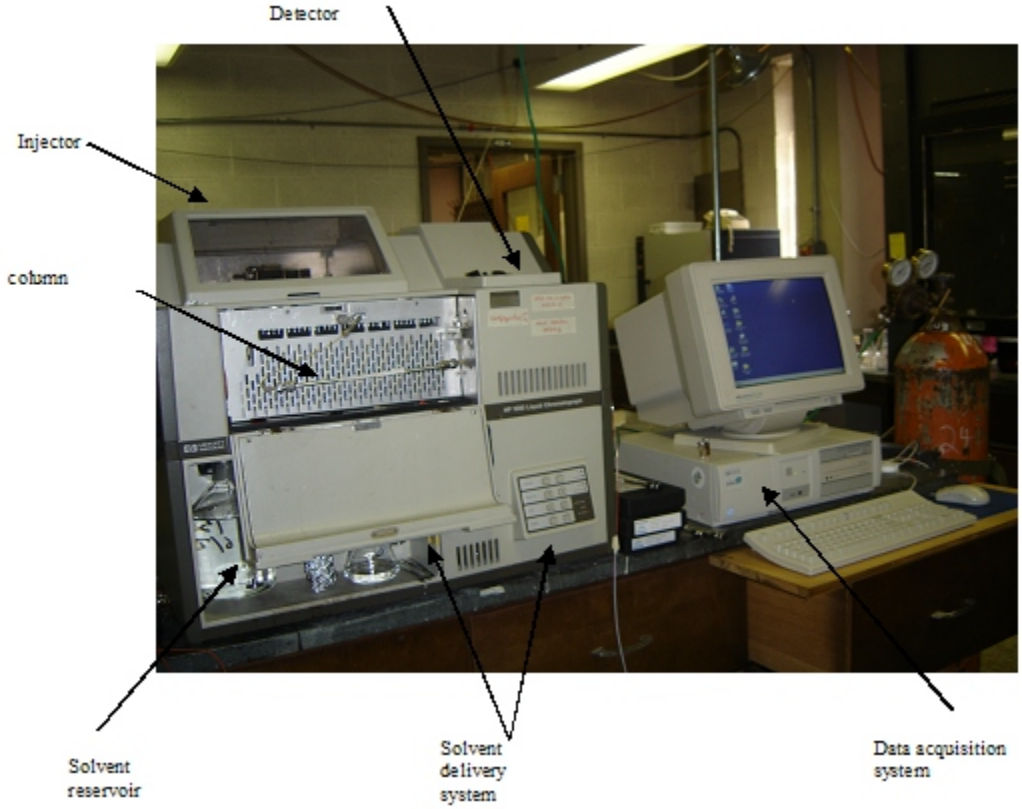

Figure 2.1 Graphical representation of the HP1090 HPLC system from Agilent Technologies.

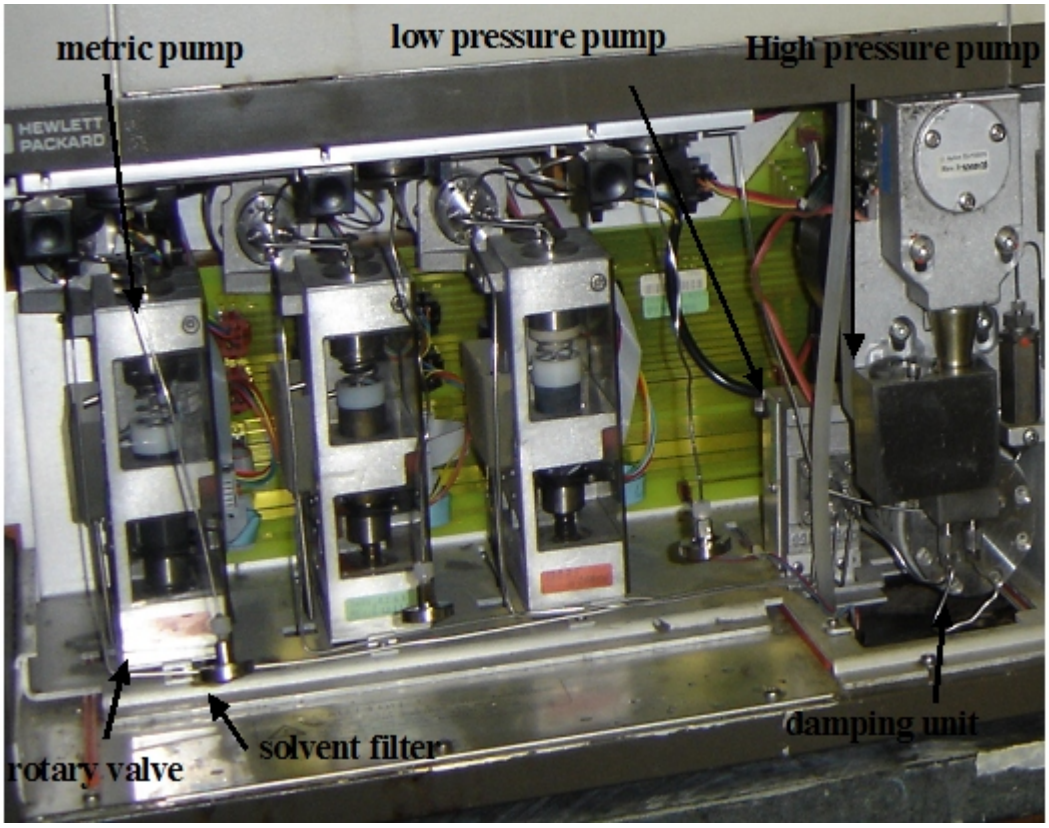

Figure 2.2 The main parts of the solvent delivery system

The channels are mixed at low pressure in the low pressure compliance before being pumped at high pressure, via a damping unit, through the injector and onto the column.

2.3.2 Solvent Reservoir

Each channel has a one liter capacity solvent reservoir. The solvent is drawn up through a solvent-inlet filter. 10mm pore size, suspended in the reservoir by a stailess-steel capillary.

2.3.3 Solvent Degassing

Hellium is divided equally between the solvent channels by a six-port manifold behind the HELIUM INLET union. Each solvent channel has a connection to one of the ports, leaving three free. The helium inlet line is attached to the solvent inlet filter inside the solvent reservoir. A frit of the upper surface disperses the helium in small bubbles. When the reservoir is saturated with helium, the bubbles remove other gases dissolved in the solvent. The gass flowing out of the solvent reservoirs are channelled to a three-port outlet, opening at the rear of the HP 1090 at the HELIUM VENT union for connection to a fume hood. A safety valve, opening into the cooling air circulation, prevents damage from overpressure conditions >0.2 bar.

2.3.4 Metering Pump

Metering is done at low pressure by a dual-syringe metering pump (Figures 2.2 and 2.3). During volume displacement the two syringes are used alternately, so that intake and delivery of the solvent are synchronous. The sapphire plungers in each syringe are driven by one stepper motor. An increment optical encoder,

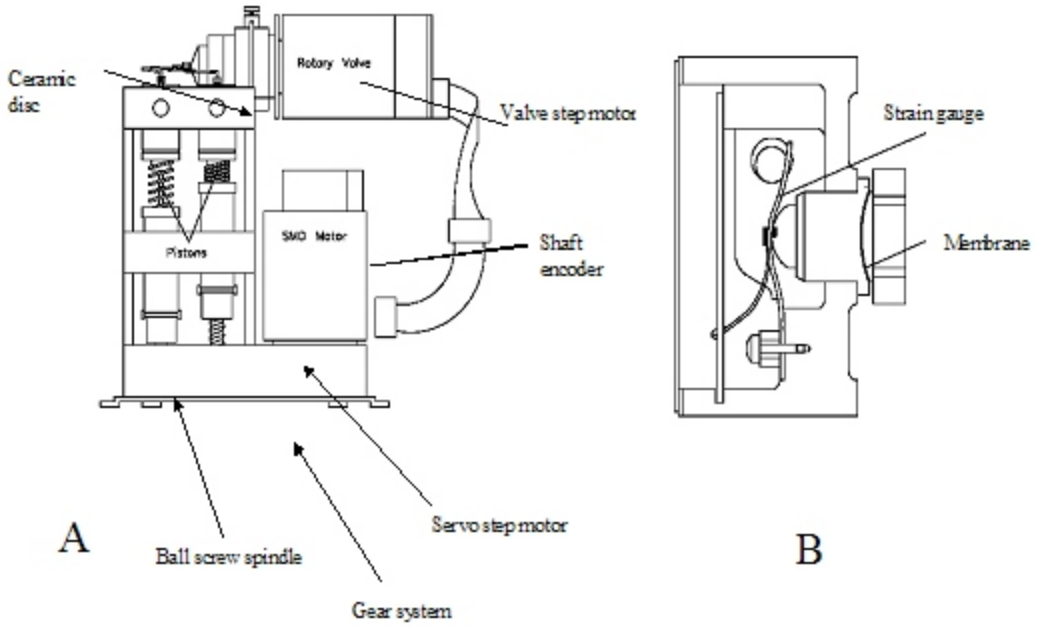

Figure 2.3 A) Metering pump and valve; B) Low pressure compliance.

mounted on top of the motor measures the position of the motor shaft with 0.25° angular resolution produced 1440 pulses per revolution. Gears transmit motor movement to a ball-screw spindle, which translates the circular movement of the gear into linear movement of the piston, with a volume resolution of 6.7 nl. The ball-screw spindle is spring-loaded to prevent backlash. A servo-loop system accurately controls the motion of the pump-motor shaft. When the plunger reaches the end of the cylinder on the forward stroke, the servo-control stops the motor drive and turns the rotary valve through 90°, receiving the connections of the plunger. The motor drive starts again, running in the opposite direction.

2.3.5 Rotary Valve

One four-port rotary valve, driven by another stepper motor, connects both syringes alternately with the solvent reservoir and solvent delivery. An absolute position encoder detects every 45° incremental position of the rotary valve, which itself moves in 15o increments. The sapphire rotor rotates against a ceramic-disc stator, sealed with a gasket. This gasket is made of KALREZ^{R}, a perfluoro elastomer, which is resistant to most chromatographic solvents.

2.3.6 Low Pressure Pump LPC

The contributions of each solvent to the total flow are mixed together in the chamber of the low-pressure compliance (LPC). The LPC (Figure2.2 and Figure 2.3) temporarily stores this solvent for the time the piston of the high pressure pump is on the pressure stroke: no flow can leave the LPC, allowing continuous metering-pump movement.

The solvent filling the chamber moves a metal cylinder which bends a spring.

An electrical circuit transforms the mechanical movement into an electrical signal, which the HP 1090 system controller uses to monitor low pressure. The LPC diaphragm is spring loaded: returning to the undeflected position when the high-pressure pump is filled, so that only the metering pump determines flow.

2.3.7 High Pressure Pump

The flow through the column is produced by the diaphragm pump operating at frequency of 10 Hz. The solvent enters a cavity in the pump head, separated from the oil slide of the pump by a diaphragm (Figure2.4a). When the piston starts to travel backwards, the solvent contained between the inlet and outlet valves expands and the pressure drops.

When this pressure has dropped to a value about 1 bar below the pressure in the LPC, the inlet valve opens and the solvent flows into the cavity, forcing the diaphragm to bend towards the oil side. As soon as the piston reverses, the inlet valve closes, and oil pressure builds-up. When system pressure is reached, the outlet valve opens, delivering solvent to the column. The oil pressure continues to increase until it is finally released via the override valve to the oil reservoir. Refill occurs as the piston travels back after reaching the lowest position. The balance between piston stroke volume and maximum volume of solvent delivered to the system per stroke is filled by oil taken from the oil reservoir through a check valve.

2.3.8 Damping Unit

The damping unit (Figure2.4b)is a simple cavity filled with a compressible liquid, separated from the solvent by a membrane. Pressure ripples from the high-pressure pump are reduced to < 2%. The back pressure from the column is

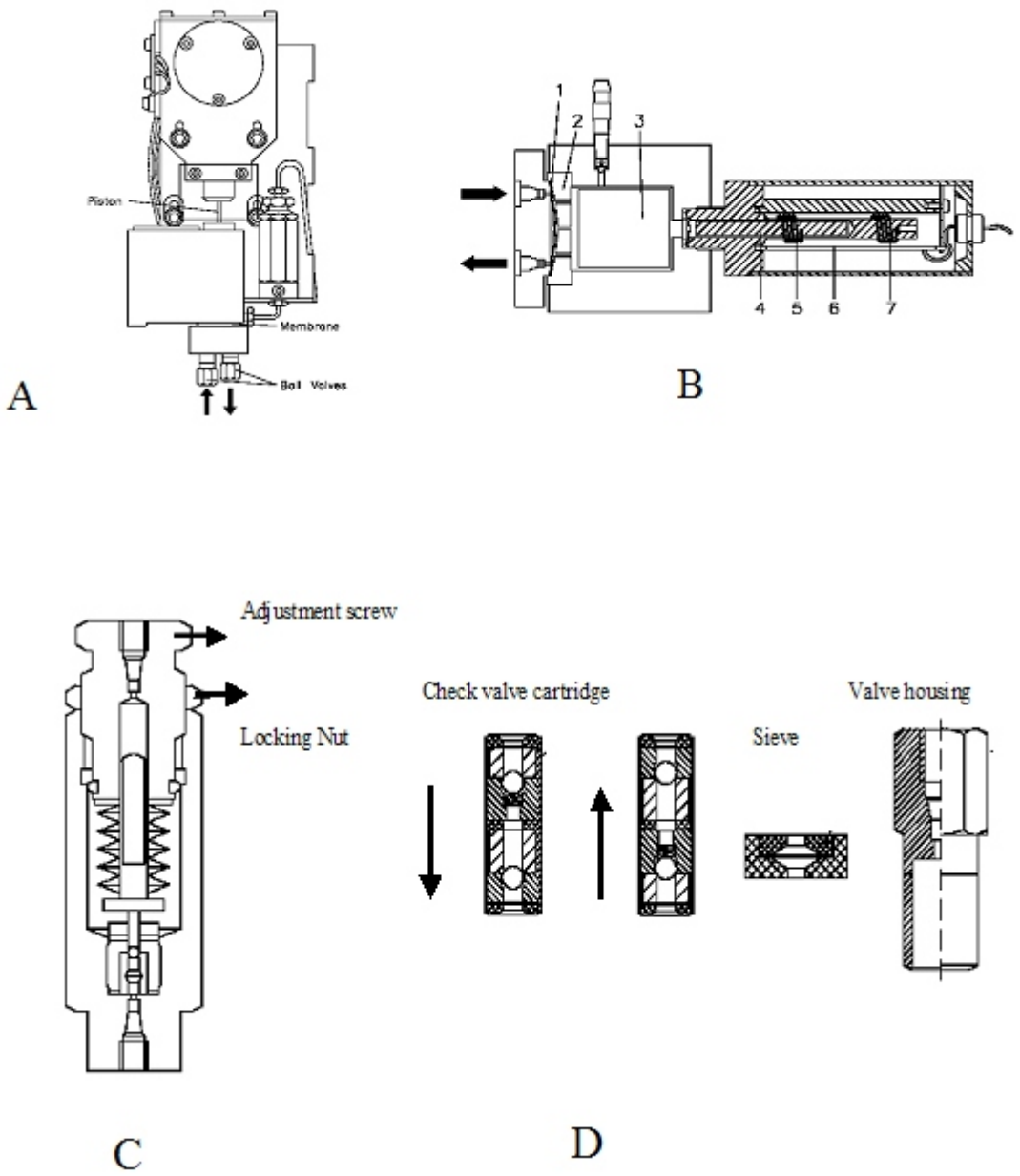

Figure 2.4. A) High pressure pump; B) High pressure damper parts.(1) membrane, (2) protection plate(3) steel block (4)steel rod (5)sample winding (6) transducer board (7) reference winding; C) override valve; D)solvent ball valves.

measured here.

2.3.9 Diode-Array Detector DAD

The DAD, like all UV/VIS detectors, measure the absorption of light by a liquid in the detector cell to determine the solute concentrations. Lambert-Beers' law defines the relationship between the absorbance A ($\log_{10}$ of the absorption), the length d of the cell (Figure 2.5a), the concentration of C of the absorbing coefficient for light of a certain wavelength. A UV/VIS detector can be used not only to detect a UV-absorbing compound eluting from a column (qualitative analysis) but also to determine the unknown concentration of a compound if, in a previous run, a calibration has been made with a known concentration of the compound of interest (quantitative analysis). Information about the chemical nature of a compound can be derived from its UV/VIS spectrum. A compound absorbs different amounts of light over the wavelength range- a function of its chemical structure.

The DAD takes spectra like a UV/VIS spectrophotometer: measuring the absorption of light of all wavelengths (scan). The DAD takes spectra at several points in time during the elution of a chromatographic peak and comparing them automatically, the DAD can indicate whether the composition of the peak is pure or not. The sensitivity of the chromatographic method can be increased by using the knowledge of the absorbance maxima of the components in the sample and automatic wavelength scanning. All the elements of the optical system (lamp, lens, shutter, flow cell, holographic grating and the photodiode array Figure 2.5b) are housed in the metal casting inside the detector compartment. The flow cell compartment is covered to prevent ambient light falling onto the photodiode array.

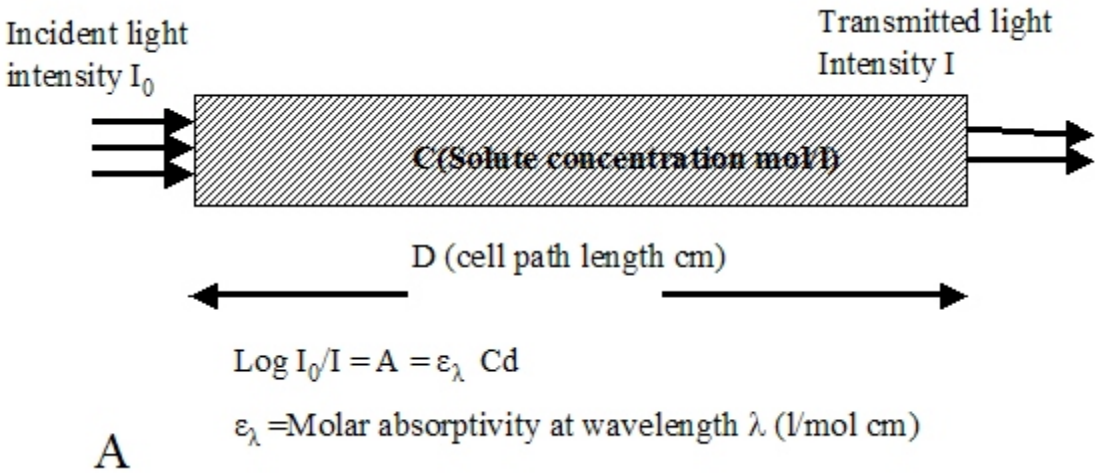

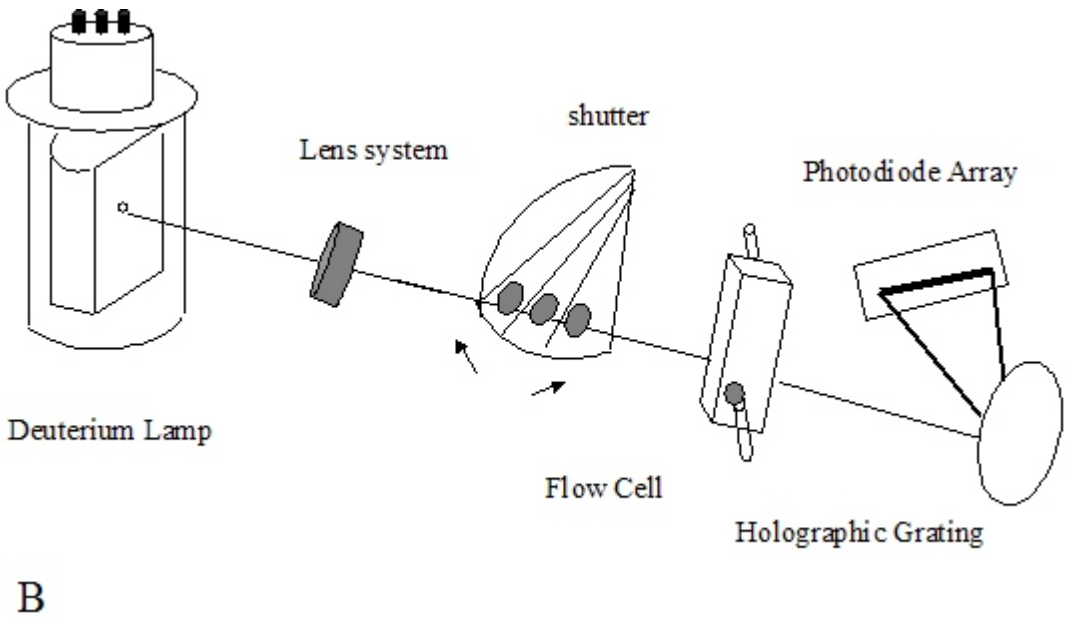

Figure 2.5. A) Absorption of light by a liquid in the detector cell; B) Elements of optical system of the Diode Array detector.

The lamp compartment is separate to allow for effective dissipation of heat. The radiation source is a deuterium gas discharge lamp. It generates a continuous spectrum of light with wavelengths that range from 190 nm to 600nm. The maximum emitted energy of a new lamp is at 240nm. The current supplied to the lamp can be switched from high(450nm) to low (300mA) if applications need full detectability. The light from the lamp is focused by an achromatic lens system onto the entrance of the flow cell. The transmitted radiation emerging from the flow cell is linearly dispersed by a holographic grating into a single wavelength, which are focused into the photodiode array. The photodiode array is a row of light sensitive cells, etched onto a silicon chip, which monitor all the wavelengths from 190 nm to 600 nm simultaneously. A three position shutter, located between the lens system and the flow cell, is the only moving part of the optical unit. Absorbance is measured when the shutter is in the open position. When closed, the shutter blocks the light path for measurement of dark current. In the third position, a holmium oxide filter is interposed. Holmium oxide has a characteristic spectrum which is used for wavelength calibration.

2.3.10 Photodiode Array

A row of more than 200 photodiodes and some control circuits are located on a silicon chip. When transmitted radiation falls on a photodiode, a photocurrent is generated. Each diode is connected in parallel to a capacitor, which is charged to a certain voltage. The photocurrent partially discharges the capacitor, which provides the basis for the measurement of absorbance. The external electronics measure the extent of the discharge when the capacitor is being recharged. To

recharge the capacitor, the transistor switch is closed and then re-opened. A shift register controls the transistor switches so that each photodiode is sequentially connected to the external electronics. This sequence is called the readout cycle. The time between two readout cycles is 10ms. The electronic signal is further processed by an analog-to-digital converter and a data -acquistion processor (DAP) to give absorbance data.

2.3.11 Auto Sampler Injector

The auto sampler (Figure 2.6) consists of ten magazines, numbered from 0 to 9, each holding ten vials, numbered 0 to 9, slot into the auto-sampler carriage. There are hundred possible positions numbered from 0 to 99. . During the injection cycle, the needle is raised up then the programmed vial is moved underneath the needle, then the sample is withdrawn by the needle which is connected to the syringe by microtubes. At the end of each cycle, the magazine is always returned to the starting position before moving the following vial into position beneath the needle. The auto sampler carriage and magazines are driven by two stepper motors.

2.2.4 Temperature Control

The adsorption data were obtained at five different temperatures, 25, 35, 45, 55, and 65°C. The temperature inside the instrument oven was kept constant to within +/- 1°C. If the temperature drifts above or below the assigned temperature by 1°C, the program stops the run. The temperature inside the column compartment was monitored by an external thermometer. It was found that its temperature was always different from the assigned temperature, by 3°C at 45 and 55°C, by 2°C at 65°C and by 0°C at 35°C.

Figure 2.6 Top view of the main parts of the autosampler injector

Control at 25°C was nearly impossible but it was found that by keeping open the column compartment all the time and setting the temperature at 25°C gave a column at a constant temperature of 23°C, at which the measurements were made. The temperature reported in the next section are those measured by the thermometer, not those assigned to the oven control function.

2.5. Frontal Analysis Measurements of Isotherm Data

In order to make accurate measurements of adsorption isotherm data, the retention factor should be neither too low nor too high. At low values of k', the accuracy of the adsorption data is poor. At high values, the number of data points that can be acquired within a reasonable period of time is low. Values of k' between 2 and 8 are ideal to achieve precise, accurate isotherm data determination. The mobile phase composition (2.5, 5, and 7.5% acetonitrile or 7, 10, 15,and 20% methanol) and the temperature selected for this work (23, 35, 42, 52, and 63°C) satisfy these conditions. One of the pumps of the instrument was used to deliver a stream of pure mobile phase (acetronitrile or methanol, water, acetic acid), the other to deliver a stream of a mother sample solution in the mobile phase, at a constant total flow rate of 1 mL/min. The column was washed and equilibrated with each one of the mobile phases used at the selected temperature for several hours depending on the mobile phase used [2]. The column was checked for equilibrium by injecting repeatedly thiourea samples, until the hold-up time stabilizes. Injections of thiourea were repeated before and between successive frontal analysis measurements. The hold-up volumes of each set of experiments made the same day were averaged and the result used for the calculations of both the FA and the IM methods.

Forty experimental adsorption data points were recorded successively at each temperature (23, 35, 42, 52, and 63°C), for each of the mobile phases used (2.5%, 5%, and 7.5% acetonitrile), and with tryptophan solutions containing between 0.005 and 11 g/L. The same data were recorded at one temperature 23°C for the mobile phases containing (7%, 10%, 15%, and 20% methanol). A sufficiently long interval (15-25 min) between successive breakthrough curves allowed re-equilibrium of the column with the pure mobile phase. In each case, the sample solution was pumped for 6 min, so that a plateau concentration was reached during each measurement and, at the end, the eluate composition was that of the solution pumped into the column. The flow rate was 1.0 ml/min for all the experiments. The detector signals were recorded at 280 nm at low concentrations (0.005- 0.5 g/L) and 305 or 310 nm at high concentrations (1- 11 g/L), respectively. The wavelength selected was chosen so that the UV signal did not exceed 1200 mAU

2.6 Acquisition of Overloaded Band Profiles of Tryptophan

The overloaded band profiles were acquired using two methods. First, a few injections of small samples were made on the plateaus recorded during the collection of the breakthrough curves needed for FA measurements. Overloaded band profiles were recorded for four sets of concentrations (0.05, 0.5, 2, and 8 or 11g/L). Later, the column having been equilibrated with one of the mobile phases, first at room temperature then at each other temperature considered, band profiles were acquired for small and large samples. The procedure was repeated for all the mobile phase compositions.

A computer program was used in both cases to acquire breakthrough curves

and overloaded band profiles at each set temperatures (23, 35, 42, 52, and 63 °C). This program includes equilibrating the column for two hours before injection of the sample and of thiourea. The overloaded band profiles of tryptophan were obtained by injecting solutions of tryptophan in the mobile phase. Injections of solutions at concentrations of 0.5-11g/L of tryptophan for 30 seconds were carried out by using the same pump as the one used to deliver the streams of tryptophan solutions in the FA measurements. The profiles were recorded at wavelengths of 280, 305, and 310 nm for the 0.05, 0.5, and 8 g/L solutions, respectively. The UV signal was transformed into concentration profile by using the calibration curve obtained from the plateau concentrations measured during the FA at the same wavelengths used. Segments of the elution profiles having between 500 and 1000 data points were used to perform the IM calculations and to derive estimates of the isotherm parameters. The number of theoretical plates used in the ED model was 2000.

2.7. Detector Calibration

The HP1090 instrument has a diode array UV detector. The detector was calibrated for each of the mobile phases used, at each temperatures set, and at the three wavelengths used, 280, 305, and 310 nm. The breakthrough curves obtained in each experiment were used for the calibration. The calibration data were fitted to a third degree polynomial and the calibration curves obtained were used to transform the absorbance signals into concentrations.

CHAPTER 3

RESULTS AND DISCUSSION

3.1 The Effect of the Nature and Concentration of the Organic Modifier on the Adsorption Behavior of L-Tryptophan

Tryptophan (pK_{a1} =2.3, pK_{a2} = 10.13) was dissolved in aqueous solutions of ACN or MeOH with 1% acetic acid. The pH of the solutions was between 5.10 and 5.20 for all the solutions prepared. At this pH, most molecules of tryptophan (pI = 5.89) are neutral zwitterions. This compound is poorly soluble and the addition of acetic acid improves its solubility. The effect of the nature and concentration of the organic modifier on the adsorption behavior of tryptophan was investigated by measuring its adsorption isotherm and deriving the parameters of this isotherm and their concentration dependence.

3.1.1 Adsorption Behavior in Acetonitrile/Water Mobile Phases

The adsorption isotherm data for tryptophan were measured with mobile phases containing 2.5, 5, and 7.5% ACN. Figure 3.1, and Figures 3.2, 3.3, 3.4 show the adsorption isotherms, the breakthrough curves of tryptophan respectively. The effect of the mobile phase composition on the parameters of the adsorption isotherm of tryptophan is illustrated in Figure 3.5 and in Table 3.1. The experimental adsorption data (symbols) and the curves (solid lines) resulting from the best fit of these three sets of experimental data to the bi-Moreau model, the model that gave

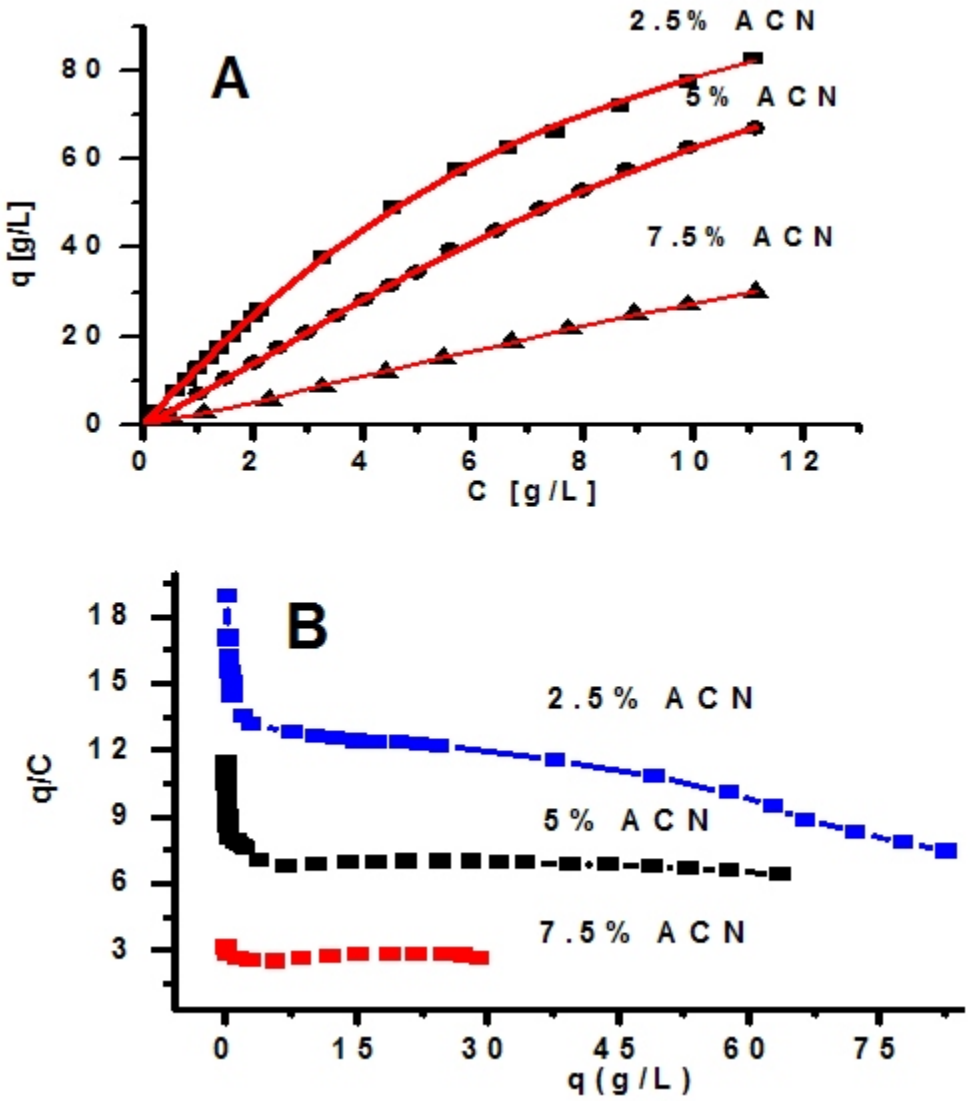

Figure 3.1 A) Experimental isotherm data (FA, symbols) of tryptophan on the C_{18} -Kromasil column obtained with three different ACN-water -acetic acid mixtures as the mobile phases. The solid line is the best fit of the data to a bi-Moreau model at T=296 K. Note that the curvature of the isotherm decreases from low to high ACN concentrations. Top to bottom; 2.5, 5, and 7.5% ACN. B)Scatchard plots for the adsorption of tryptophan on C_{18}-Kromasil with three different ACN-water-acetic acid mixtures as the mobile phases. Top to bottom; 2.5, 5, and 7.5% ACN.

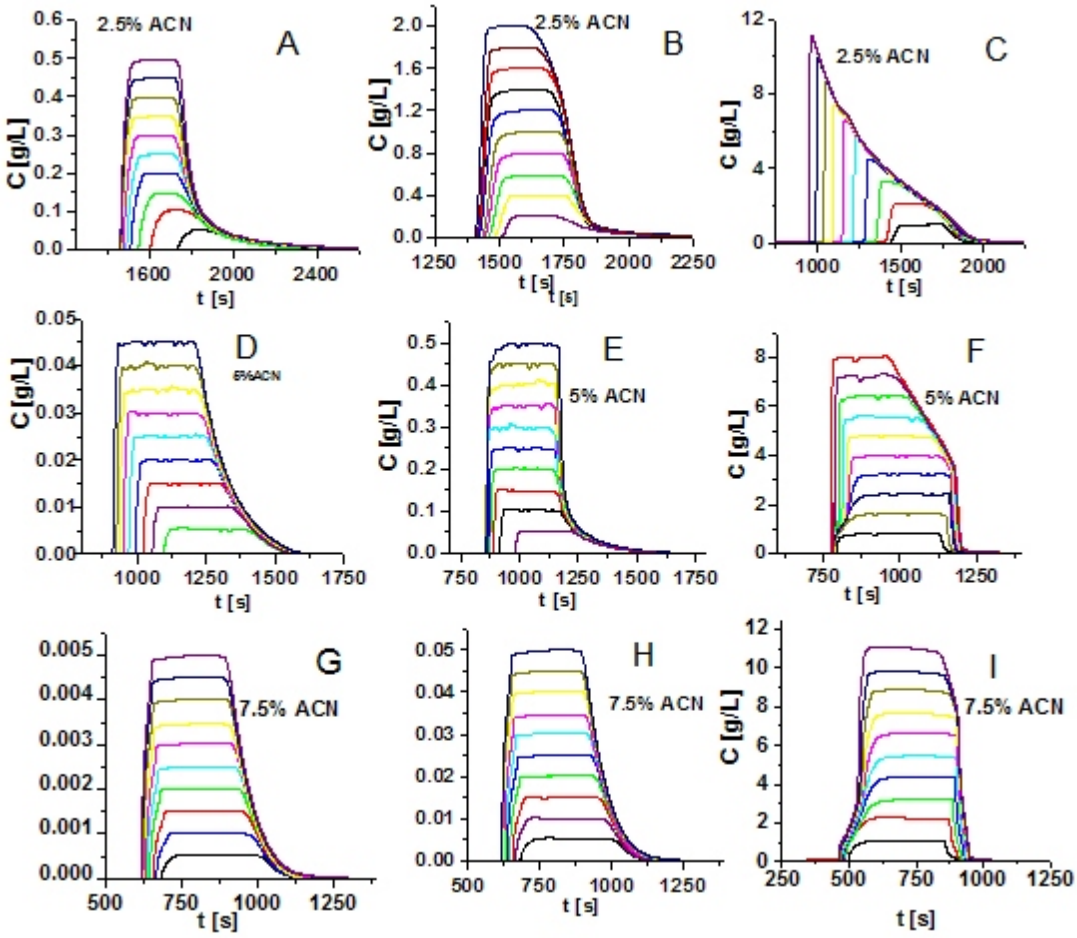

Figure 3.2 Selected breakthrough curves of tryptophan on the C_{18} -Kromasil column, at 1 ml/min, T = 296 K, 1% acetic acid. (A-C) 2.5 % aqueous mixture of ACN, 0.5 g/L at 305 nm, 2g/L at 305 nm, and 11 g/L at 310 nm; (D-F) 5 % ACN, 0.05 g/L at 280 nm; 0.5 g/L at 305 nm; 8 g/L at 310 nm; (G-I) 7.5 % ACN 0.05 g/L at 280 nm; 0.5 g/L, at 305 nm; and 11 g/L at 310 nm.

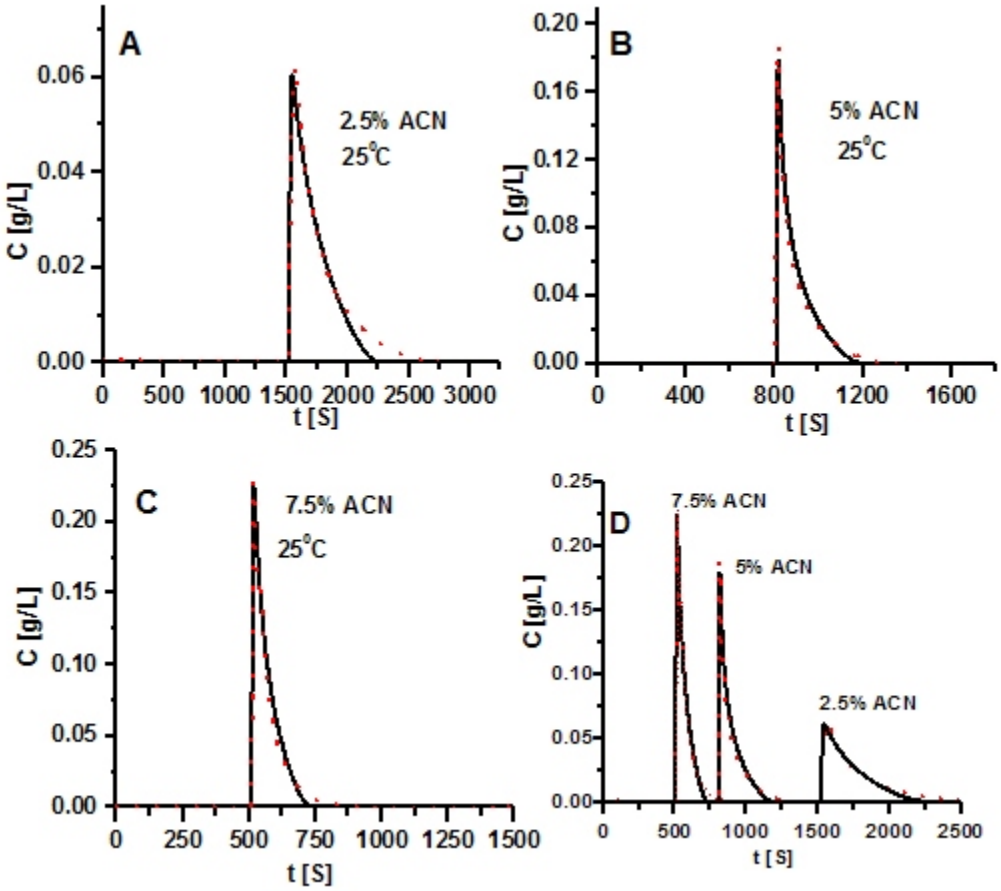

Figure 3.3Comparison between calculated (solid lines) and experimental (dotted lines) large size band profiles on theC_{18} -Kromasil column, with concentration of tryptophan in the mother solution 0.5 g/L. The three mobile phases. (A)2.5, (B) 5, (C)7.5% ACN, and (D) Overlay of band profiles for all three mobile phases. Injection of a solution of tryptophan during 30 s; wavelength 280 nm.

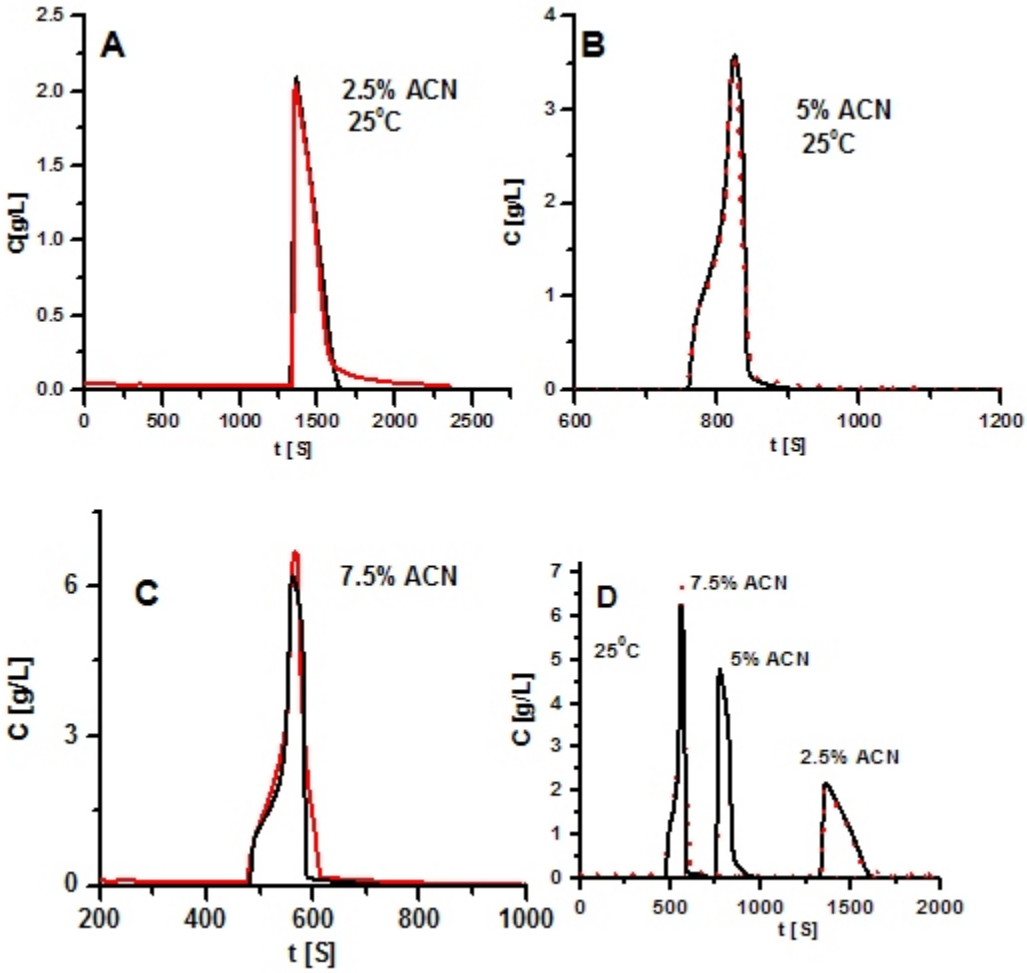

Figure 3.4 Comparison between calculated (solid lines) and experimental (dotted lines) large size band profiles on the Kromasil-C_{18} column with concentration of tryptophan in the mother solution 11 g/L. (A)2.5, (B) 5, C)7.5% ACN, and (D) Overlay of band profiles for all three mobile phases. Injection of a solution of tryptophan during 30 s; wavelength 310 nm.

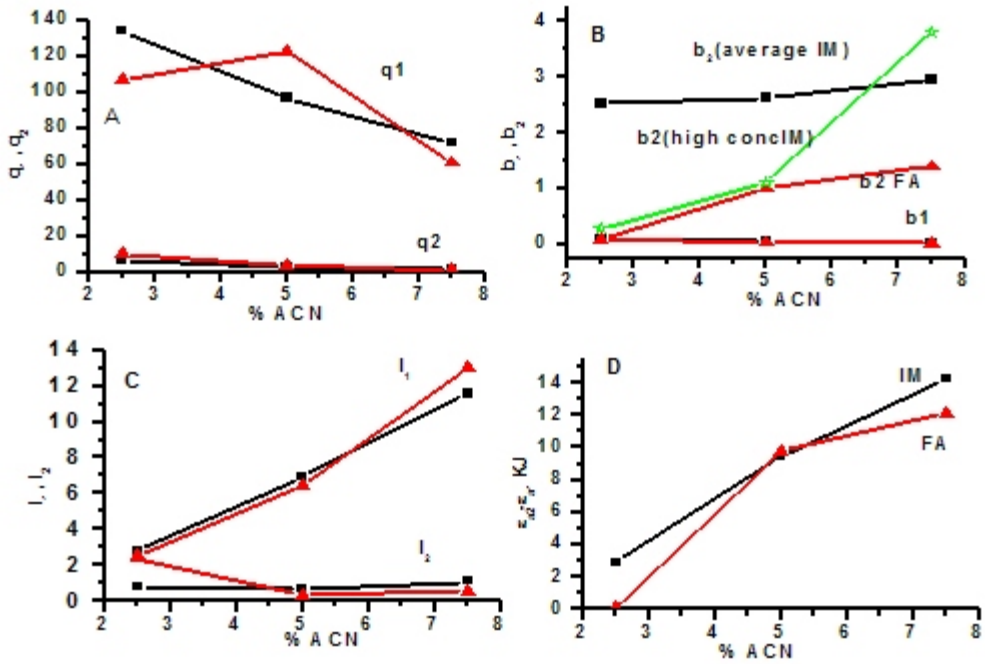

Figure 3.5 Influence of the ACN concentration on the parameters of the isotherm. (A) the saturation capacities of the low- (q_1) and the high-energy sites (q_2); (B) the adsorption constant on the low- (b_1) and the high-energy sites (b_2); C) the adsorbate-adsorbate interaction constant on the low- (I_1), and the high-energy sites (I_2). Each subfigure shows the corresponding isotherm parameter calculated by either non-linear fitting of the isotherm data to the bi-Moreau model (▲), or by the inverse method IM (■), using overloaded band profiles of tryptophan solutions injected for 30 s (IM averaged for all concentrations, see Table 1); (D) the difference between the adsorption energies on the high- and the low-energy sites versus the ACN concentration in the mobile phase.

Table 3.1 Best isotherm parameters and Fisher numbers for L-tryptophan on C_{18}-Kromasil with different aqueous solutions of ACN as the mobile phase.

[ACN]	Model	Method	q_1 (q_s)*	b_1 (a_1)*	I_1	q_2 (a_2)*	b_2	I_2	F
	bi-Moreau								
	a 11g/l	IM	131.10	0.1038	2.918	7.979	0.279	1.98	9900
	b 2g/l	IM	133.8	0.1018	2.573	7.943	0.278	0.185	
	c 0.5g/l	IM	137.7	0.0872	3.008	1.693	7.02	0.213	
2.5 %	Avg of a,b,c	IM	134.2	0.0976	2.833	5.87	2.52	0.792	
	=======	FA	106.8	0.0960	2.512	10.30	0.0989	2.38	
	Moreau	===	======	=====	=====	====	=====	=====	====
	=======	FA	128.3	0.0989	2.149				6900
	S-shaped	===	======	=====	=====	====	=====	=====	====
		FA	64.18	0.1977	0.0210				6900
	bi-Moreau								
	a 8g/l	IM	97.41	0.0458	7.89	3.436	1.110	0.630	14000
	b 5g/l	IM	97.18	0.0501	7.781	3.554	1.079	1.37	
	c 0.5g/l	IM	96.03	0.0600	5.00	0.800	5.700	6.979	
5%	Avg of a,b,c	IM	96.87	0.0520	6.89	2.597	2.630	0.665	
		FA	122.98	0.0378	6.466	4.071	1.021	0.331	
	=======	===	=======	=====	====	=====	====	== ==	== ==
	Moreau	FA	182.6	0.0369	2.745				13000
	=======	===	=== ==	=====	===	=====	====	===	== ==
	S-shaped	FA	91.30	0.0738	0.00374				13000
	bi-Moreau								
	a 11g/l	IM	84.19	0.0309	11.68	1.562	3.813	0.588	4400
	b 8g/l	IM	71.94	0.0285	13.31	1.251	2.434	2.434	
	c 0.5g/l	IM	60.5	0.0371	9.685	1.103	2.616	0.243	
7.5 %	Avg of a,b,c	IM	72.21	0.0322	11.558	1.305	2.954	1.088	
		FA	60.89	0.0237	12.999	0.994	1.395	0.553	
	=======	===	=======	=====	======	=====	====	=====	====
	Moreau	FA	83.35	0.0279	4.5234				3300
	=======	==	======	=====	======	=====	====	=====	====
	S-shaped	FA	41.67	0.0558	0.00352				3300

the closest fit, are compared in Figure 3.1a. At first glance, the adsorption isotherm with 2.5% ACN appears to be convex upward (*i.e.,* langmuirian), the isotherm with 5% ACN exhibits a similar behavior, while with 7.5% ACN, the isotherm exhibits a clear S- shape profile. However, a more careful look at these isotherms shows that all of them exhibit langmuirian behavior at low concentrations, anti-langmuirian behavior at intermediate concentrations, and langmuirian behavior again, at high concentrations. The existence of inflection points in the isotherms is demonstrated by the shift of the shape of the front of the breakthrough curves at the corresponding concentrations. When isotherms are convex upward, the front is self-sharpening; when it is convex downward, this front is a diffuse boundary. The transitions are clear in Figures 3.2a, 3.2f, and 3.2h, and 3.2i, and in Figures 3.3a-d and 3.4a-d. The main difference between the three isotherms in Figure1a, besides the general decrease with increasing ACN concentration of the amount of tryptophan adsorbed at equilibrium with a given mobile phase concentration, is the concentrations at which the two inflection points are observed. These concentrations increase with increasing ACN concentration in the mobile phase. These results are confirmed by the shape of the Scatchard plots (plots of q/C versus q, Figure 3.1b). These plots exhibit an horizontal inflection point (2.5% ACN) or one minimum and one maximum (5 and 7.5% ACN). These features suggest a heterogeneous adsorbent surface and adsorbate-adsorbate interactions.

There are three isotherm models that might fit these experimental data, the Moreau, the bi-Moreau, and the S-shaped (or quadratic) models. The FA adsorption data of tryptophan fitted very well to the Moreau and the S-shaped models. The

nonlinear regression program converges quickly and gives the the isotherm data to the more complex six-parameter bi-Moreau model was not always successful, convergence was slow and, the low concentration data being less accurate, the precision of the parameters of the second term of the model, the one that corresponds to the high-energy adsorption sites, sites that are populated at low concentrations is modest. Therefore, we tried to estimate these parameters by using the inverse method of isotherm determination that derives the isotherm parameters from overloaded band profiles. The best calculated profiles (solid lines) are shown in Figures 3.3a-d and Figures 3.4a-d overlaid with the corresponding experimental profiles (dotted lines). The best values of the parameters of this third model are also listed in Table3.1 that reports also the values of the Fisher numbers for the three models. These numbers are of the same order of magnitude, although higher for the bi-Moreau model than for the other two models. The solid lines in Figure 3.1a show the best bi-Moreau isotherms. The overlaid experimental and calculated overloaded band profiles obtained with the inverse method (Figures 3.3a-d, Figures3.4a-d) demonstrate an excellent agreement, particularly for 5% ACN, for which also the Fisher number is highest.

In general there is a good agreement between the values of the parameters obtained by the FA and the IM method (Table 3.1). However, this agreement is much better for the parameters of the low-energy sites than for the high-energy sites (those that are populated first, at low concentrations). This is because there are much fewer high-energy than low-energy sites. The saturation capacity of the former is only 1 to 6 % of the total saturation capacity of the adsorbent. Therefore,

the errors made in the determination of the parameters of the high- energy sites are larger than those made on the corresponding parameters of the low-energy adsorption sites.

Note that, in principle, the results of the IM method are less sensitive than those of the FA method to fluctuations of the column experimental parameters, notably the temperature, the flow rate and the mobile phase composition, because the acquisition of the data needed is much faster. Each FA breakthrough curve takes 30 to 60 minutes and 40 such measurements are needed for each mobile phase composition (Figures 3.2a-l). The IM method requires recording three band profiles, which can be done in less than two hours. In contrast, the band profile may dilute considerably during its elution, so the IM isotherm may be less accurate than the FA one at high concentrations. These different sources and magnitude of the errors made explain the slight differences found between the parameters calculated by the two methods.

The influence of the ACN concentration in the mobile phase on the values of the isotherm parameters is illustrated in Figures 3.5a-d, which show plots of the variations of the different parameters. These figures illustrate also the degree of agreement between the parameters derived by IM and by FA. They use the data reported in Table 3.1. They suggest that the properties of the aqueous solution of ACN vary significantly around a concentration of 5% ACN, an effect illustrated also by the important changes in the band profiles (Figures 3.3, and Figures 3.4) and in the isotherms (Figure 3.1a). The influence of the ACN concentration in the mobile phase on the parameters of the adsorption isotherm are illustrated by the data in

Table 3.1 and by the plots in Figures 3.5a-d. These plots show also that there is good agreement between the values of the parameters derived from the FA and the IM methods. The saturation capacities of the low-energy adsorption sites, $q_{s,1}$, decrease from 100 - 130 (2.5% ACN) to 97 - 122 (5% ACN) and to 60 - 84g/L (7.5% ACN) and so do the adsorption constants b_1, from 0.096 to 0.10 (2.5% ACN) to 0.04 - 0.05 (5% ACN) and to 0.02 - 0.03 (7.5% ACN) (Figure 3.5a). In contrast, the strength of the adsorbate-adsorbate interactions increases from 2.5 - 3 (2.5% ACN) to 8 -10 (5% ACN) and to 11 - 13 (7.5% ACN) (Figure 3.5b). This result correlates well with the fact that, for 2.5% ACN, the isotherm is convex upward and the adsorbate-adsorbate interactions are the weakest. The saturation capacity of the high-energy adsorption sites is a small fraction of the total saturation capacity of the adsorbent. It decreases from 8.0 - 10 (2.5% ACN) to 3.5 - 4.0 (5% ACN) and to 1 - 1.5 (7.5% ACN), nearly a factor 10 (Figure 3.5a). The numerical values of the adsorption constants on the high-energy sites calculated by the IM method and derived from the FA data are quite different and this is related to the importance of the errors made by both methods in the low concentration range (Figure 3.5b). In general, increasing the ACN concentration affects more strongly the properties of the high-energy sites than those of the low-energy sites. A plot of the difference between the adsorption energies on the low- and the high-energy sites versus the ACN concentration in the mobile phase shows that this difference increases by approximately 2RT when the ACN concentration increases from 2.5 to 7.5% (Figure 3.5d).

The adsorbate-adsorbate interaction parameters on the high- and the low-

energy sites behave quite differently (Figure 3.5c). On the high-energy sites, this parameter increases rapidly with increasing ACN concentration and becomes very large while on the low-energy sites, it decreases slightly and becomes small. The finite value of the energy of the adsorbate-adsorbate interactions explains the behavior of the equilibrium isotherm. Since these interactions on sites of type 1 increase with increasing ACN concentration, the distance between the inflection points increases and the intermediate part of the isotherm becomes increasingly convex downward (see Figures 3.1a-b). The isotherm in 2.5% ACN is initially convex upward and the front of the low-concentration breakthrough curves is a steep shock layer (Figure 3.2a). At higher concentrations, the front of the breakthrough curve becomes a diffuse boundary because the curvature of the isotherm becomes nearly infinite (see Figure 3.1b). At high concentrations, the front is again a steep shock layer. Similar evolutions are observed at higher ACN concentrations, for the same reasons, except that the adsorbate-adsorbate interactions becoming stronger, the isotherm curvature becomes negative in an intermediate range of concentrations.

3.1.2 Adsorption Behavior in Methanol/Water mobile phases

The adsorption isotherms of L-tryptophan were determined for mobile phases containing 5, 7.5, 10, and 20% MeOH. The adsorption isotherms of tryptophan using these four mobile phases, the breakthrough curves, and the overloaded band profiles at low and high concentration are shown in Figures 3.6, 3.7, 3.8, and 3.9 respectively. Figure 3.10 and Table 3.2 show the effect of the concentration of methanol in the mobile phase on the parameters of the adsorption isotherm of tryptophan. The experimental adsorption data (symbols) and the curves

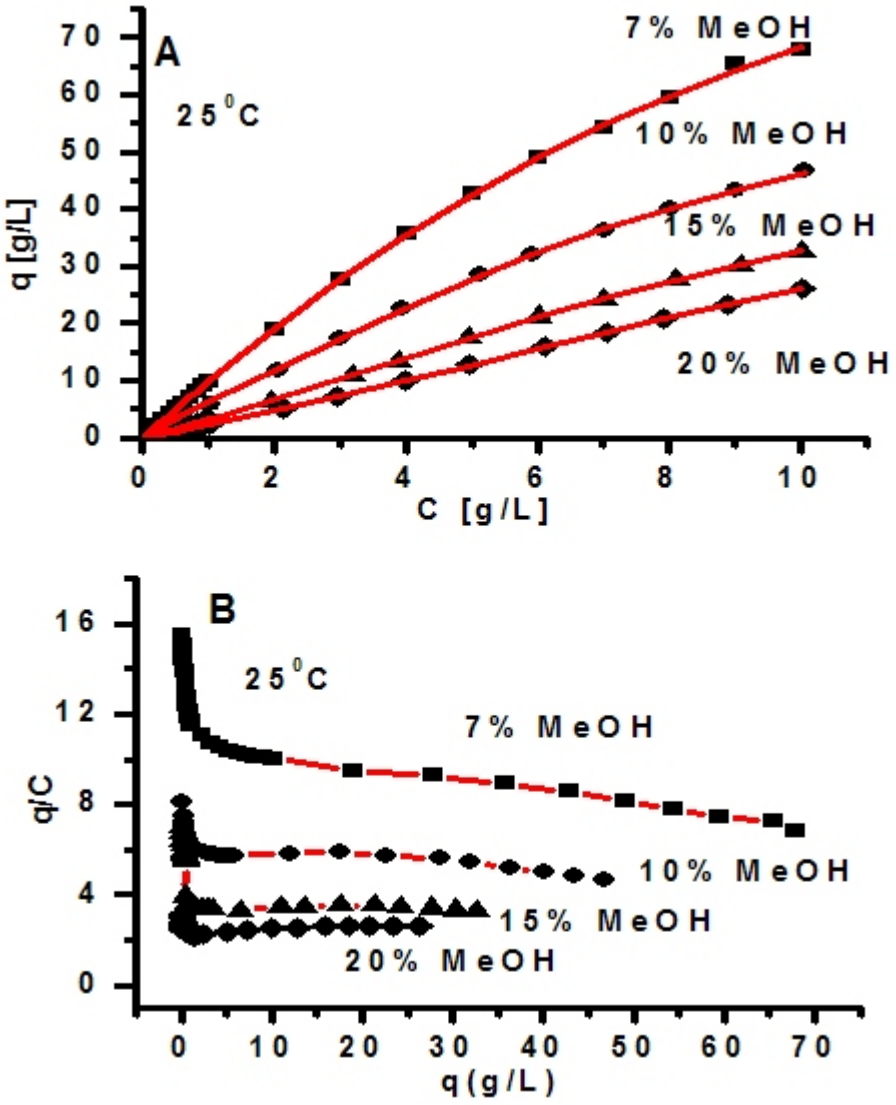

Figure 3.6 A) Experimental isotherm data (symbols) of L-tryptophan on the C_{18} -Kromasil column obtained with four different MeOH-water-acetic acid mixtures as the mobile phases. The solid line is the best fitting of the bi-Moreau model at T=296 K. Note that the curvature of the isotherm decreases from low to high concentrations of MeOH. Top to bottom, 7, 10, 15, and 20% MeOH; B) Scatchard plots for the adsorption of L-tryptophan on C_{18}- Kromasil with four different MeOH-water-acetic acid mixtures as the mobile phases. Left to right (A-D), 7, 10, 15, and 20% MeOH.

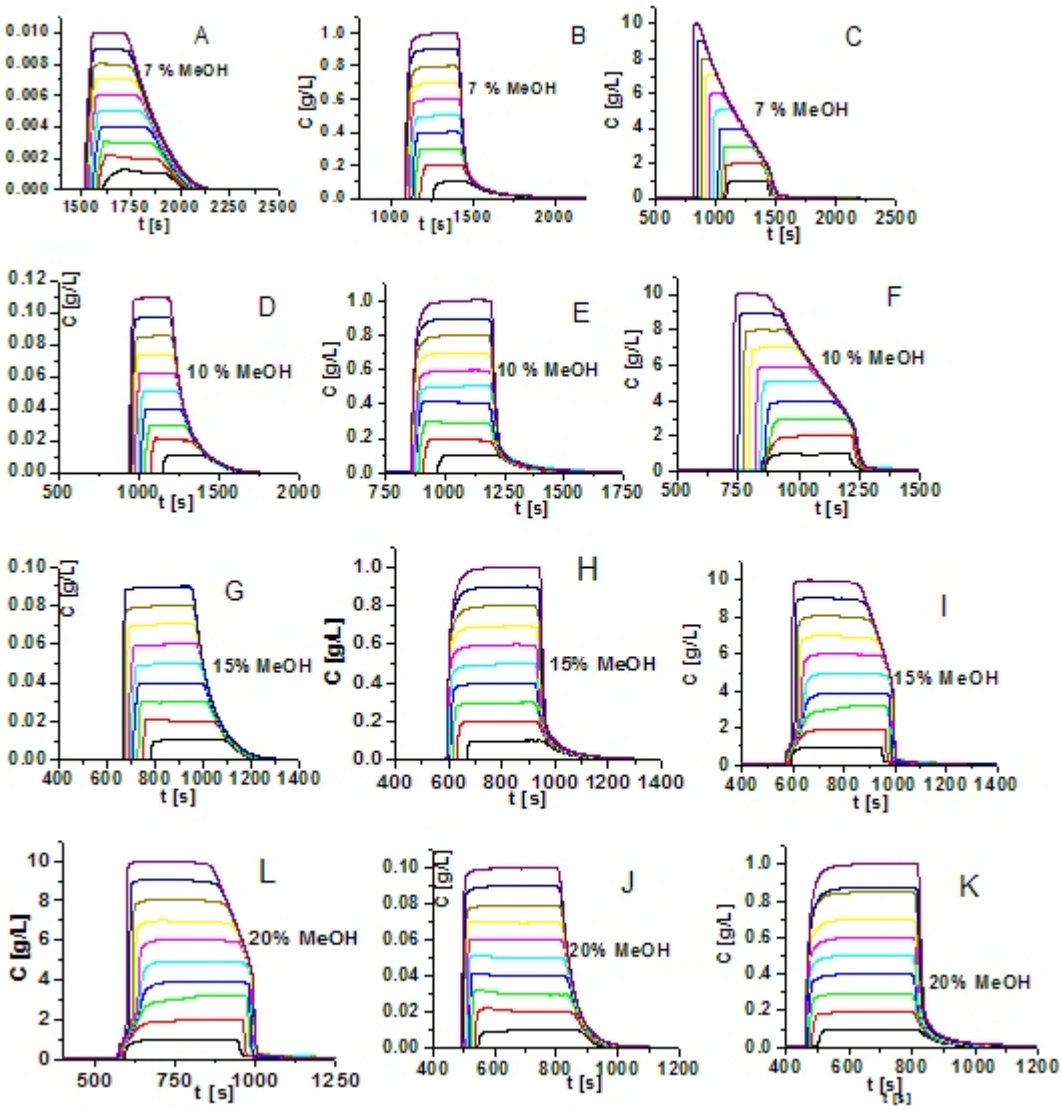

Figure 3.7 Overlaid selected breakthrough curves of tryptophan on C_{18} - Kromasil column, at 1 ml/min, T = 296 K, 1% acetic acid. (A-D) 7 % MeOH and 0.5 g/L at 305 nm; 1g/Lat 305 nm; 10g/L at 310 nm of tryptophan; (E-H) 10% MeOH and 0.1 g/L at 305 nm; 1g/L at 305 nm; 10g/L at 310 nm; (I-L) 15% MeOH; 0.1 g/L at 305 nm; 1g/L at 305 nm; 10g/L at 310 nm; (M-P) 20 % MeOH, 0.1 g/L at 305 nm; 1g/L at 305 nm; 10g/L at 310 nm.

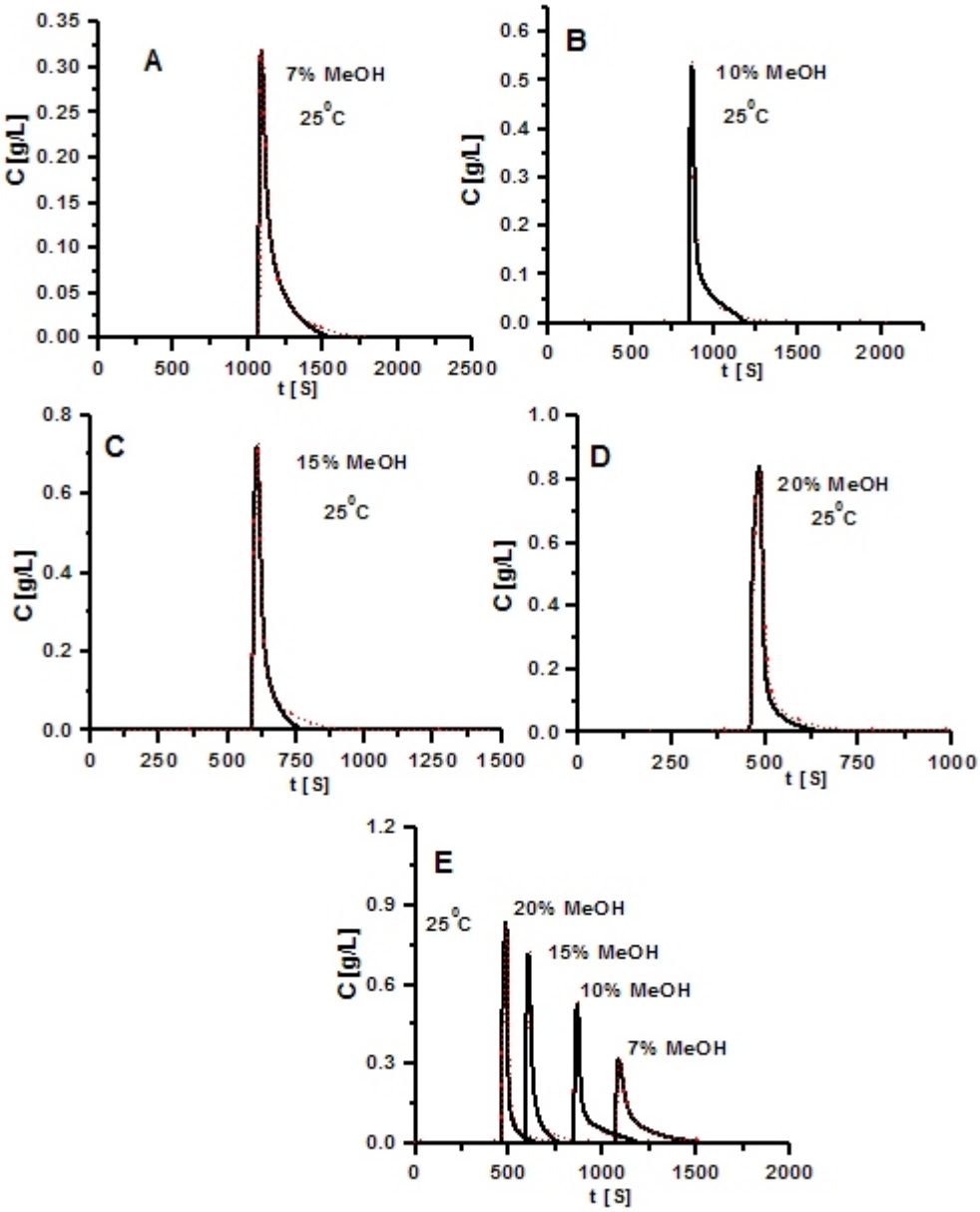

Figure 3.8 Comparison between calculated (solid lines) and experimental (short dots) band profiles on the C_{18}-Kromasil column with the four MeOH-water-acetic acid mixtures with tryptophan concentration in the sample equals to 2 g/L. Injection of a solution of L-tryptophan during 30 s. MeOH concentrations (A) 7 (B)10 (C)15 and (D) 20% (E) Overlay of all profiles with different MeOH concentrations.

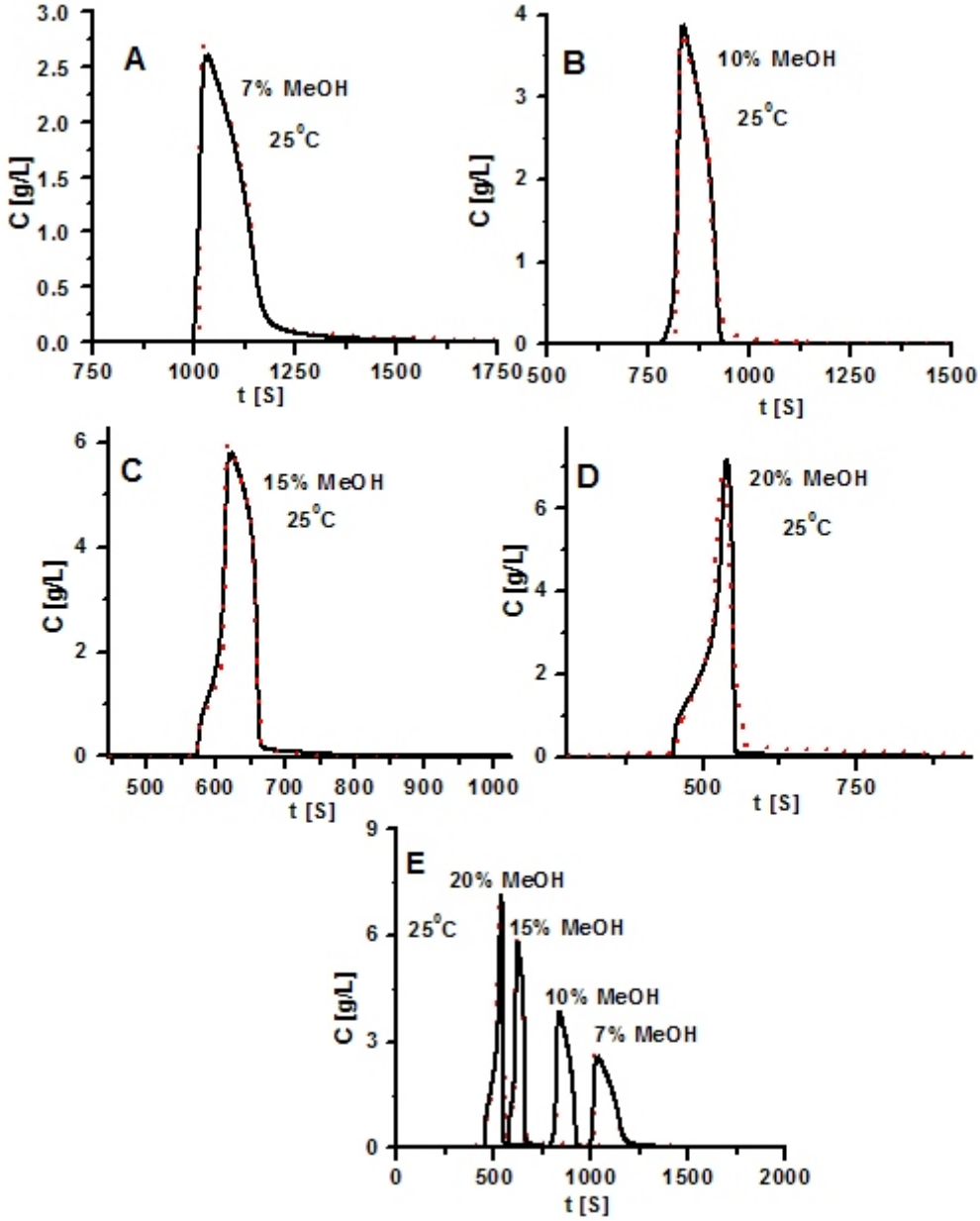

Figure 3.9 Comparison between calculated (solid lines) and experimental (short dots) band profiles on the C_{18}-Kromasil column with the four MeOH-water -acetic acid mixtures with tryptophan concentration in the sample equals to 11 g/L . Injection of a solution of L-tryptophan during 30 s, MeOH concentrations (A) 7, (B)10,(C)15, and (D)20%; wavelength 310nm.

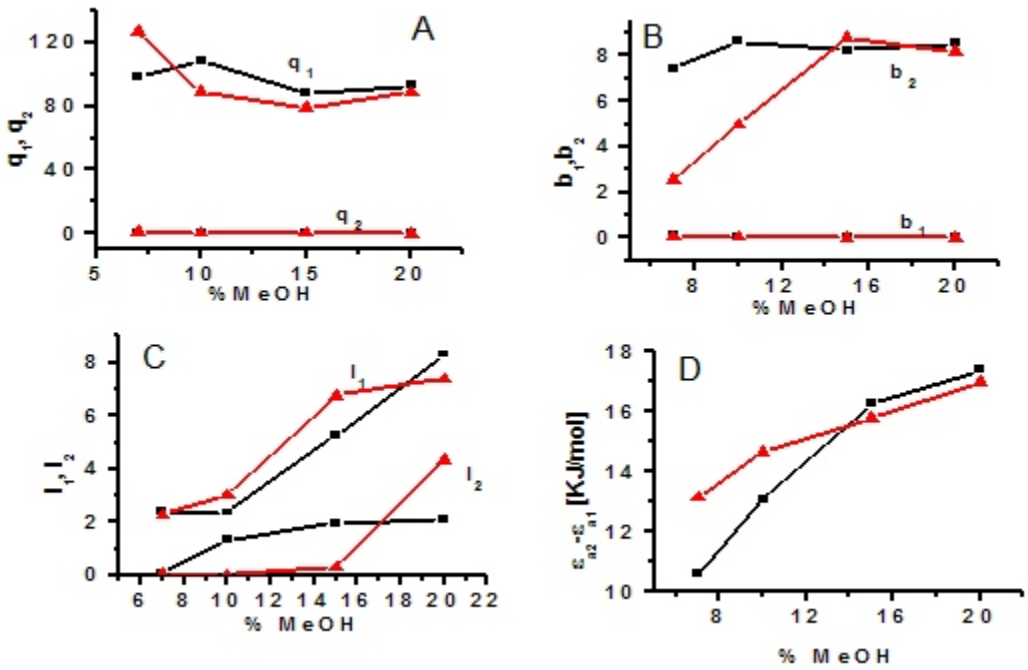

Figure 3.10 Influence of the MeOH concentration on (A) the saturation capacities of the low- (q_1), and the high-energy sites (q_2). (B) the adsorption constants of the low- (b_1) and the high-energy sites (b_2). (C) the adsorbate-adsorbate constant of the low- (I_1) and the high-energy sites (I_2). Each subfigure shows the corresponding isotherm parameter calculated by either non-linear fitting of the isotherm data to the bi-Moreau model (▲) or and by the inverse method (■), using overloaded band profiles of tryptophan (IM averaged for all concentrations, see Table 2). (D) the difference between the adsorption energies of the high- and the low-energy sites versus the MeOH concentration in the mobile phase.

Table 3.2 Best isotherm parameters and Fisher numbers for L-tryptophan on C_{18}-Kromasil with different aqueous solutions of MeOH as the mobile phase

MeOH	Model	Method	q_1 (q_s)*	b_1 (a_1)*	I_1	q_2 (a_2)*	b_2	I_2	F
	bi-Moreau								
	a 10g/L	IM	102.8	0.08691	3.041	0.9687	6.105	0.0695	3700
	b 1g/L	IM	95.55	0.08946	4.086	1.13	5.283	0.0074	
	c 0.5g/L	IM	97	0.088	9.8e-07	0.7	11	0.204	
	Avg a,b,c	IM	98.45	0.08812	2.3757	0.9329	7.433	0.0936	
		FA	127.210	0.0728	2.2850	1.4063	2.5737	0.0783	
	=======	===	======	=======	======	=====	=====	=====	====
7 %	Moreau	FA	139.4069	0.07382	1.7194				3400
	=======	===	======	=======	======		=====	=====	====
	S-shaped		69.7008	0.14765	0.00937				3400
	bi-Moreau								
	a 10 G/L	IM	120.9	0.058	3.059	0.4725	6.967	3.476	6400
	b 1g/L	IM	98	0.0657	4.00	0.600	7.00	0.500	
10 %	c 0.5g/l	IM	105.3	0.0615	0.0422	0.6103	11.93	0.0328	
	Avg a,b,c	IM	108.07	0.06173	2.3671	0.5548	8.632	1.3362	
		FA	89.2902	0.06066	3.0228	0.4283	5.00	0.0274	
	=======	===	=======	=======	======	=====	=====	=====	====
	Moreau	FA	89.71105	0.06274	2.8206				2000
	=======	===	=======	=======	======	=====	=====	=====	====
	S-shaped		70.3972	0.09703		0.0025			2000
	bi-Moreau								
15 %	10 g/L	IM	90.61	0.03998	5.443	0.41	5.136	2.936	39000
	1g/L	IM	94.44	0.04267	5.252	0.2899	9.62	1.819	
	0.5g/L	IM	76.24	0.03872	5.142	0.3699	9.98	1.201	
	Avg a,b,c	IM	87.97	0.04046	5.279	0.3566	8.245	1.9853	
		FA	65.2664	0.03675	6.7738	0.6211	8.7902	0.3063	
	=======	===	=======	=======	======	=====	=====	=====	====
	Moreau	FA	79.1383	0.03933	3.8008				7200
	=======	===	=======	=======	======	=====	=====	=====	====
	S-shaped	FA	128.1167	0.03021		0.0002			7200
	bi-Moreau								
	a 10 g/L	IM	98.00	0.026	7	0.3	8.5	5.214	214000
	b 1g/L	IM	92.87	0.02869	7.213	0.244	8.555	0.7242	
	c 0.5g/L	IM	87.51	0.0286	10.74	0.2312	8.547	0.2743	
	Avg a,b,c	IM	92.793	0.02776	8.318	0.258	8.534	2.0798	
		FA	88.7509	0.02346	7.4	0.0312	8.2046	4.326	
	=======	===	=======	=======	======	=====	=====	=====	=====
20 %	Moreau	FA	92.4839	0.0230	4.8554				12000
	=======	===	=======	=======	======	=====	=====	=====	=====
	S-shaped	FA	46.2417	0.04598		0.0026			

(solid lines) showing the results of the best fits of the four sets of experimental data to the bi-Moreau model are compared in Figure 3.6a, the Scatchard plots are compared in Figure 3.6b. The bi-Moreau model accounts best for these adsorption data. Besides the results of the statistical analyses (Fischer numbers, Table3.2) this choice is justified by the similarity of the behavior of the isotherms, the Scatchard plots, the breakthrough curves (see Figures 3.7a-l), and the overloaded band profiles of L-tryptophan in aqueous solutions of MeOH and ACN (Figures 3.1 to Figures 3.5,and Figures 3.6 to Figures 3.10). The isotherm behavior in 7 and 10% MeOH solutions is similar to that observed in 2.5% ACN in three respects. First, the shapes of the breakthrough curves are similar, all having a definite sharp shock layer at their fronts for all concentrations of the solutions as low as 0.005 g/L (although the behavior becomes linear in this rage), and up to the highest concentration 10 g/L. Second, the shape of the isotherms (convex downward at moderate to high solute concentrations are the same. Third, the breakthrough curves and the overloaded band profiles have similar shapes. The main difference observed between the solute behavior in 2.5% ACN and in 7 or 10% MeOH is that the retention is longer and the maximum amount adsorbed is stronger in the first case. The behavior with 15 and 20% MeOH are similar to those with 5 and 7.5% ACN, respectively, in terms of the shape of the isotherm and those of the breakthrough curves and the overloaded band profiles. All of the isotherms exhibit a langmuirian behavior at low and at high concentrations and an anti-langmuirian behavior in the intermediate concentration range. The best values of the isotherm parameters for the four MeOH concentrations and the Fisher numbers for the three

isotherm models considered are listed in Table3.2. The Fisher numbers are highest for the bi-Moreau model in all of the mobile phases. For the low-energy sites, increasing the MeOH concentration decreases slightly the saturation capacity, $q_{s,2}$, of the low energy sites, from 102 to 92 (IM data) or 127 to 88 (FA data),decreases the adsorption constant, b_2, of the low energy sites, from 0.08 to 0.02 (both IM and FA data), and increase the adsorbate-adsorbate interaction parameter, I_2, from ~ 3 to 7. For the high-energy sites, increasing the MeOH concentration decreases slightly the saturation capacity, from ~ 1.1 to 0.3, increases the adsorption constant, from ~ 6 to 8, and increases the adsorbate-adsorbate interaction constant, I_2, from 0.07 to 5. These effects are illustrated in Figures 3.8a-c. Comparing the results obtained for the adsorption of L-tryptophan from ACN and MeOH solutions shows that the saturation capacity and the adsorption constant of the low energy sites are lower with 7.5% ACN (60-84 and 0.02-0.03, respectively) than with 7% MeOH (95-127 and 0.07-0.08, respectively), while the saturation capacity of the high energy sites is higher but its adsorption constant lower for 7.5% ACN than for 7% MeOH which suggests that the high-energy sites are more accessible or more available in the presence of ACN than of MeOH. The adsorbate-adsorbate interactions on the low- and on the high-energy sites are higher with 7.5% ACN than with 7% MeOH. The higher availability or accessibility of the second types of sites in the presence of ACN may be explained by the results of McCormick and Karger [103] and those of Kazakevich *et al* [104]. While the first group concluded that MeOH forms a relatively dense monolayer and ACN forms two such layers on a C_8 bonded phase, the second group concluded that MeOH forms an adsorbed monolayer but ACN

gives an adsorbed multilayer system, containing about four layers. The data for 2.5 and 5% ACN (Table3.1) and for 10, 15, and 20% MeOH (Table 3.2) show that the saturation capacities of the high energy sites are higher, the adsorption constants lower, and the adsorbate-adsorbate interaction parameters higher with ACN than with MeOH.

These results show how the adsorption behavior of tryptophan depends on the nature and concentration of the organic modifier. The strong influence of this nature is illustrated by the contrast between the isotherms with 7% MeOH and 7.5% ACN, the former being convex upward, the latter downward. This observation is consistent with previous results obtained also with aqueous solutions of ACN and MeOH, for phenol and caffeine [105]. The isotherms with MeOH were also convex upward and those with ACN convex downward for both compounds and for mobile phase compositions similar to those used in our work. This result is not surprising because, under the experimental conditions used in this work, the molecules of tryptophane are zwitterions, hence neutral. So, it is too early to generalize since our work dealt with a quasi-neutral compound and theirs with two neutral compounds. Although previous studies measured the dependence of the isotherm parameters on the MeOH concentration between 30 and 60% and found these isotherms to be always convex upward, there was no similar studies on the influence of the ACN concentration on the adsorption isotherms of phenol or caffeine.

3.2 The Effect of Temperature on the Adsorption Behavior of L-Tryptophan

The influence of temperature on each of the hold-up volume, the breakthrough curves obtained at three different concentrations of the tryptophan solution are shown in Figures 3.11 a-b, 3.12, 3.13, and 3.14. The adsorption isotherms and the overloaded band profiles are shown in Figures 3.15, 3.16, and 3.17. Figure 3.18 and Table 3.3 show the effect of the temperature on the parameters of the adsorption isotherm of tryptophan.

3.2.1 Influence of the Temperature on the Hold-up Volume

Figure 3.11a shows the evolution of the chromatograms of thiourea with increasing temperature and Figure 3.11b a plot of the retention volume of thiourea versus temperature. The retention of thiourea decreases significantly and the efficiency of the thiourea peak increases slightly with increasing temperature. The retention volume of thiourea seems to decrease linearly with increasing temperature (Figure 3.11b). The phenomenon observed is due to the combination of (1) the decrease of the density of the eluent with increasing temperature; (2) the expansion of the bonded alkyl layer; and (3) the decrease of the retention volume of thiourea. In practice, the mass flow rate of the eluent is kept constant. Since liquids expand with increasing temperature, the volume flow rate increases with increasing column temperature, hence the retention time decreases. It has already been reported that the volume of the bonded layer increases with increasing concentration of the organic modifier [106]. The effect is the same here, the mobile phase becomes a better solvent with increasing temperature. Finally, although it is small (2.60 minutes as shown in Figure 3.11a), the retention of thiourea is finite but the linear thermal

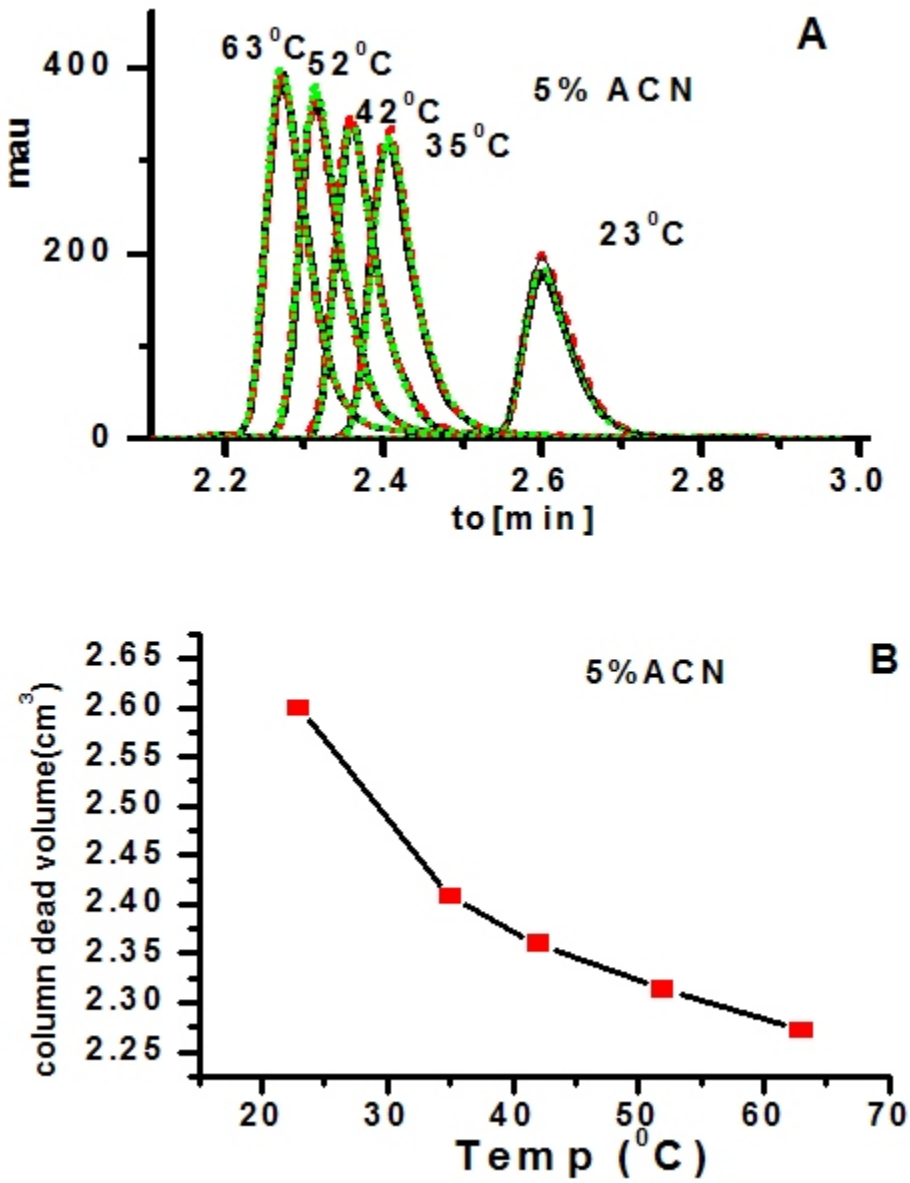

Figure 3.11 A) Overlay of the chromatograms of thiourea at different temperatures. The dotted, solid, and short-dotted lines represent three different injections made at each temperature, during the set of frontal analysis experiments. B) Plot of the retention volume of thiourea versus the temperature. Each point is the average of three trials.

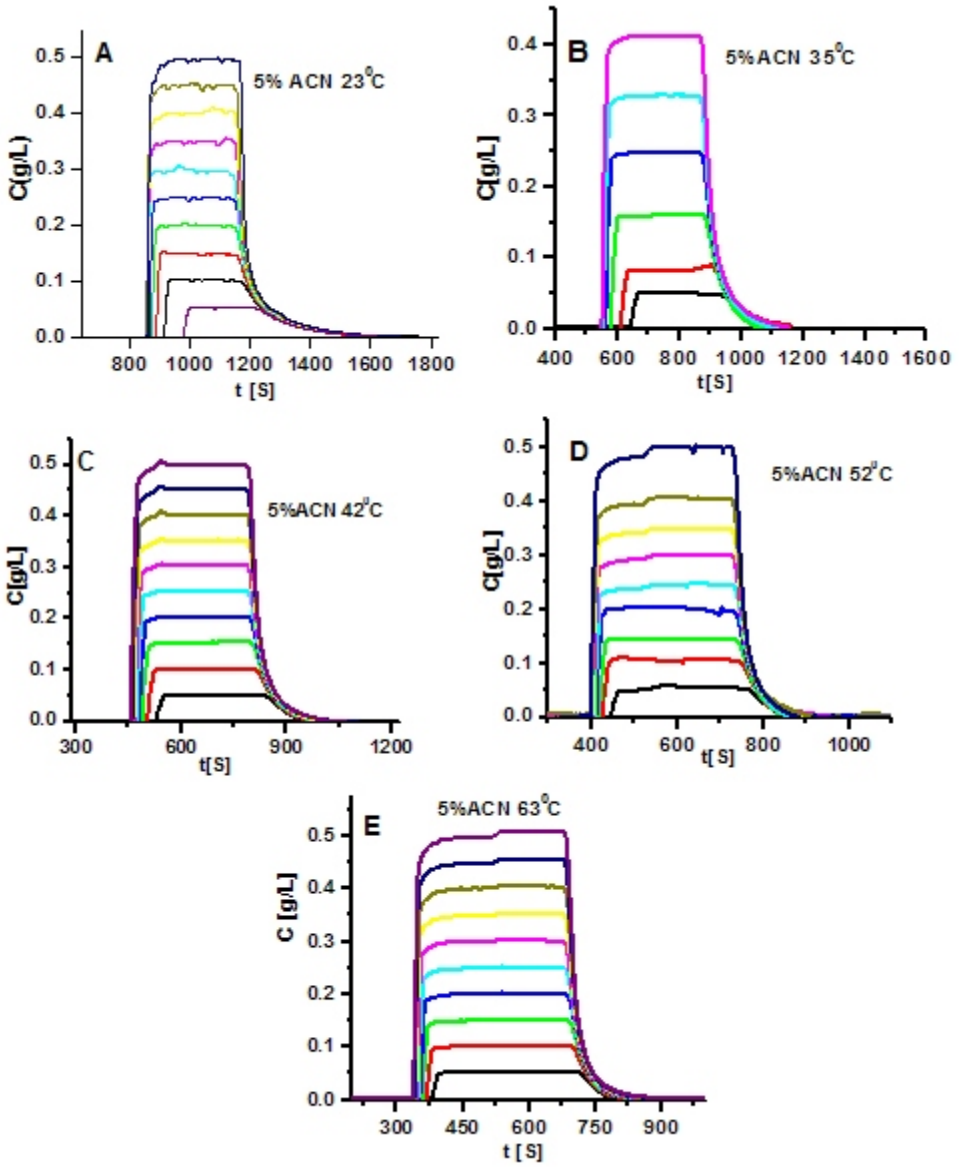

Figure 3.12 Breakthrough curves for the adsorption of tryptophan on C_{18}-Kromsil, using aqueous mobile phase containing 5% acetonitrile and 1% acetic acid. The concentration of tryptophan in the mother solution is 0.5 g/L. The curves are reported in concentration units, the original curves (UV absorbance versus time) were recorded at 280 nm. A) at 23; B) at 35; C) at 42; D) at 52; and E) at 63 °C.

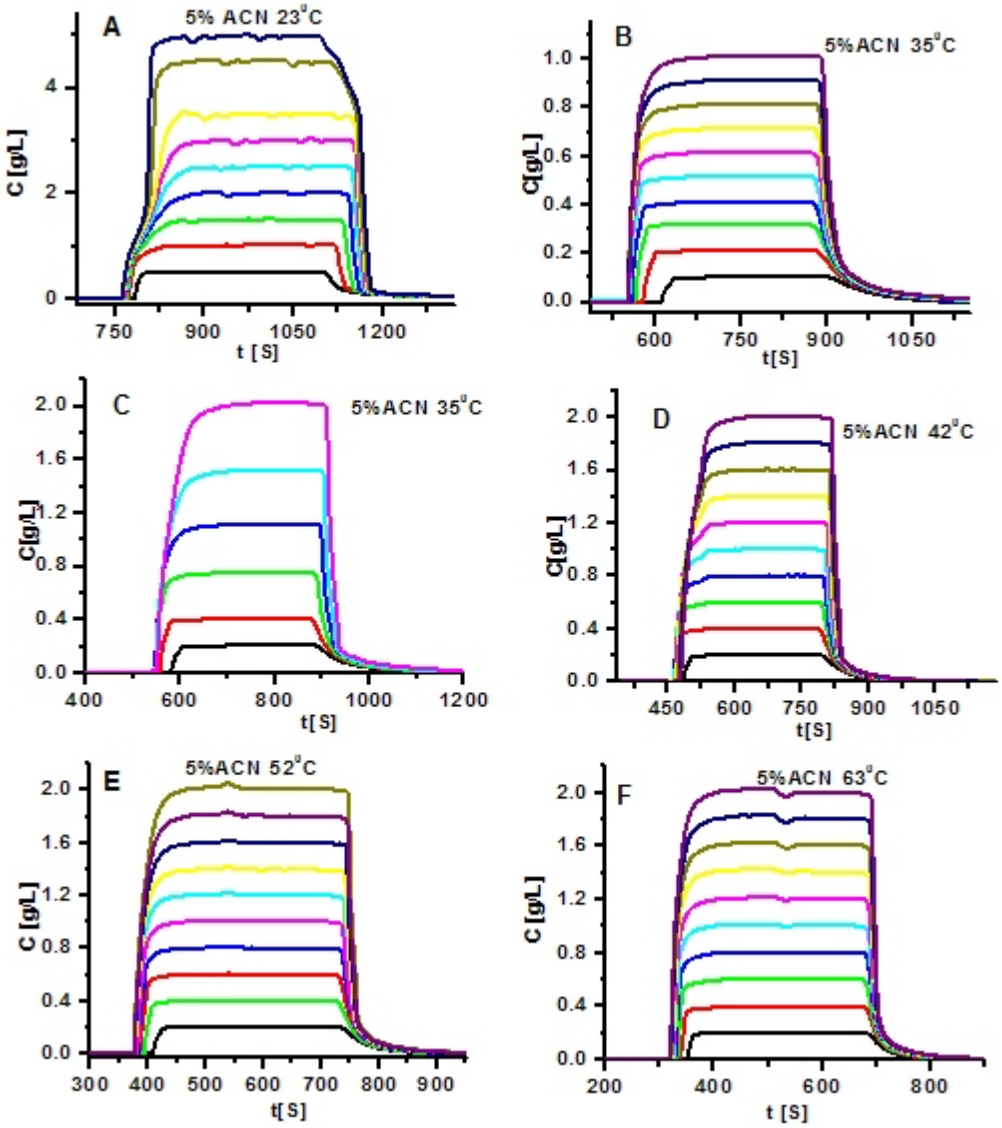

Figure 3.13 Breakthrough curves for the adsorption of tryptophan on C_{18} - Kromsil, using aqueous mobile phase containing 5% acetonitrile and 1% acetic acid. The concentration of tryptophan in the mother solution is 1-5 g/L. The curves are reported in concentration units, the original curves (UV absorbance versus time) were recorded at 305 nm. A) at 23; B, C) at 35; C) at 42; D) at 52; and E) at 63 °C.

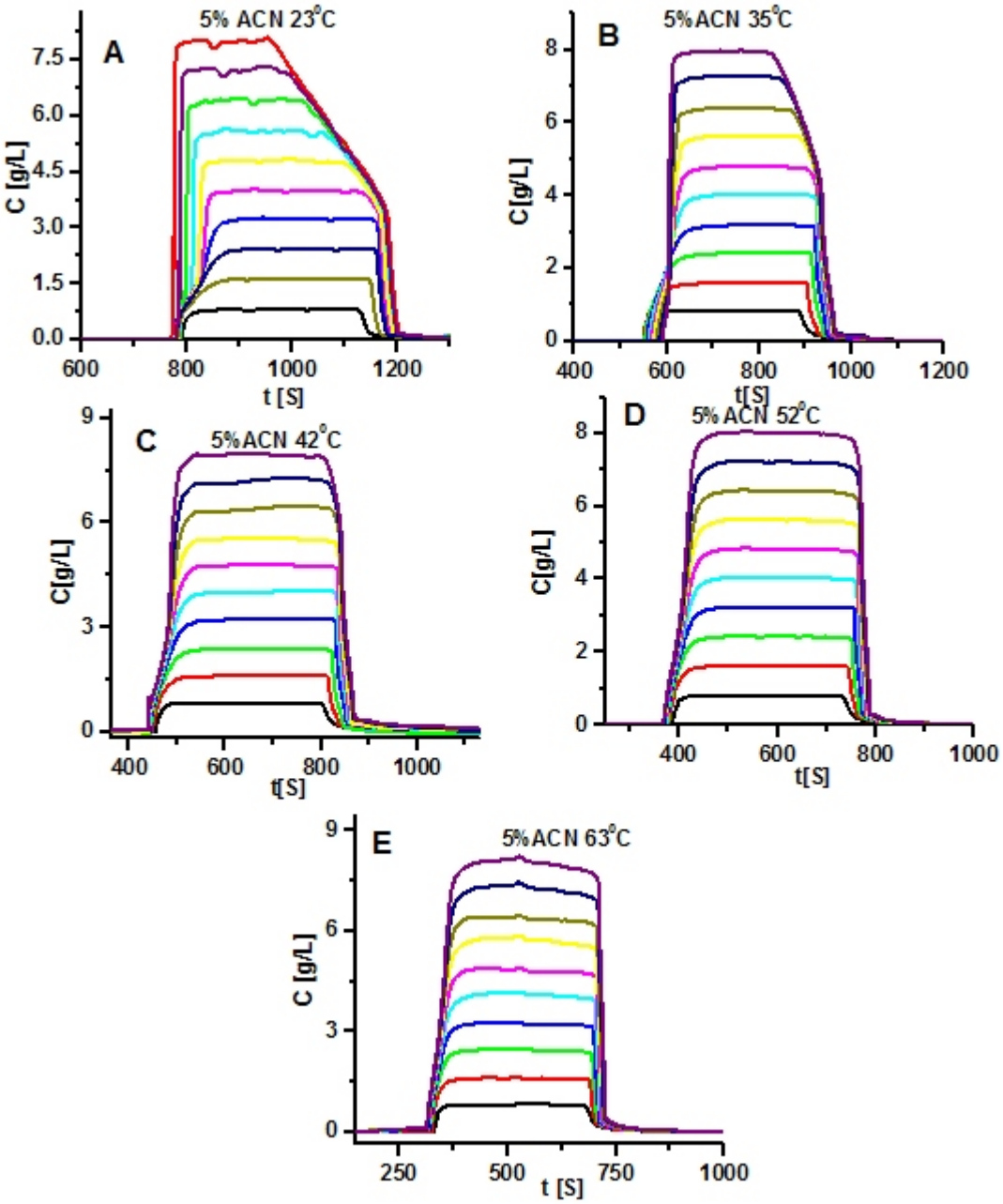

Figure 3.14 Breakthrough curves for the adsorption of tryptophan on C_{18} - Kromsil, using aqueous mobile phase containing 5% acetonitrile and 1% acetic acid. The concentration of tryptophan in the mother solution is 8 g/L. The curves are reported in concentration units, the original curves (UV absorbance versus time) were recorded at 305 nm. A) at 23; B) at 35; C) at 42; D) at 52; and E) at 63 °C.

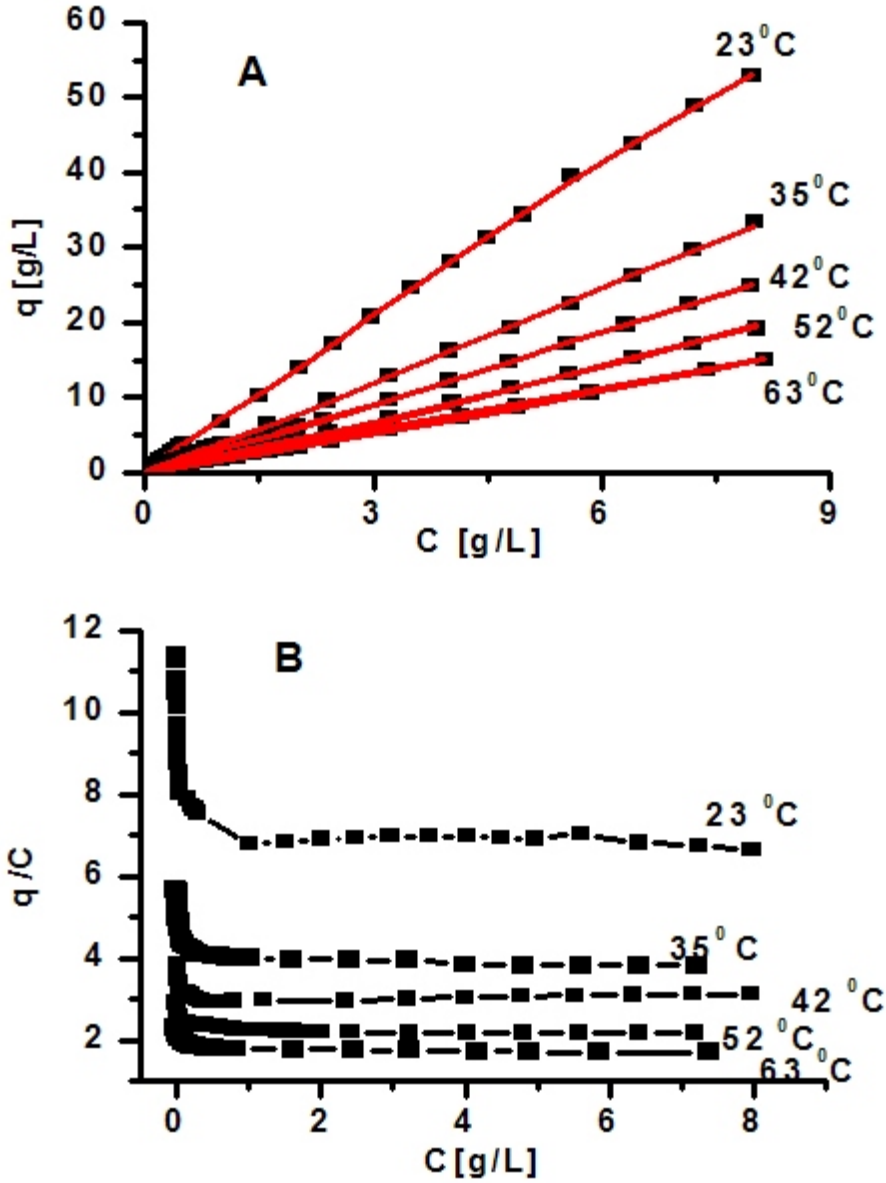

Figure 3.15 A) Experimental isotherm data (FA, symbols) of tryptophan on the C_{18} -Kromasil column obtained with an aqueous mobile phase containing 5% acetonitrile and 1% acetic acid. The solid line is the best fit of the data to a bi-Moreau model at different temperatures. Top to bottom; 23; 35; 42; 52; and 63°C. B) Plot of q/C versus C. Top to bottom; 23; 35; 42; 52; and 63°C.

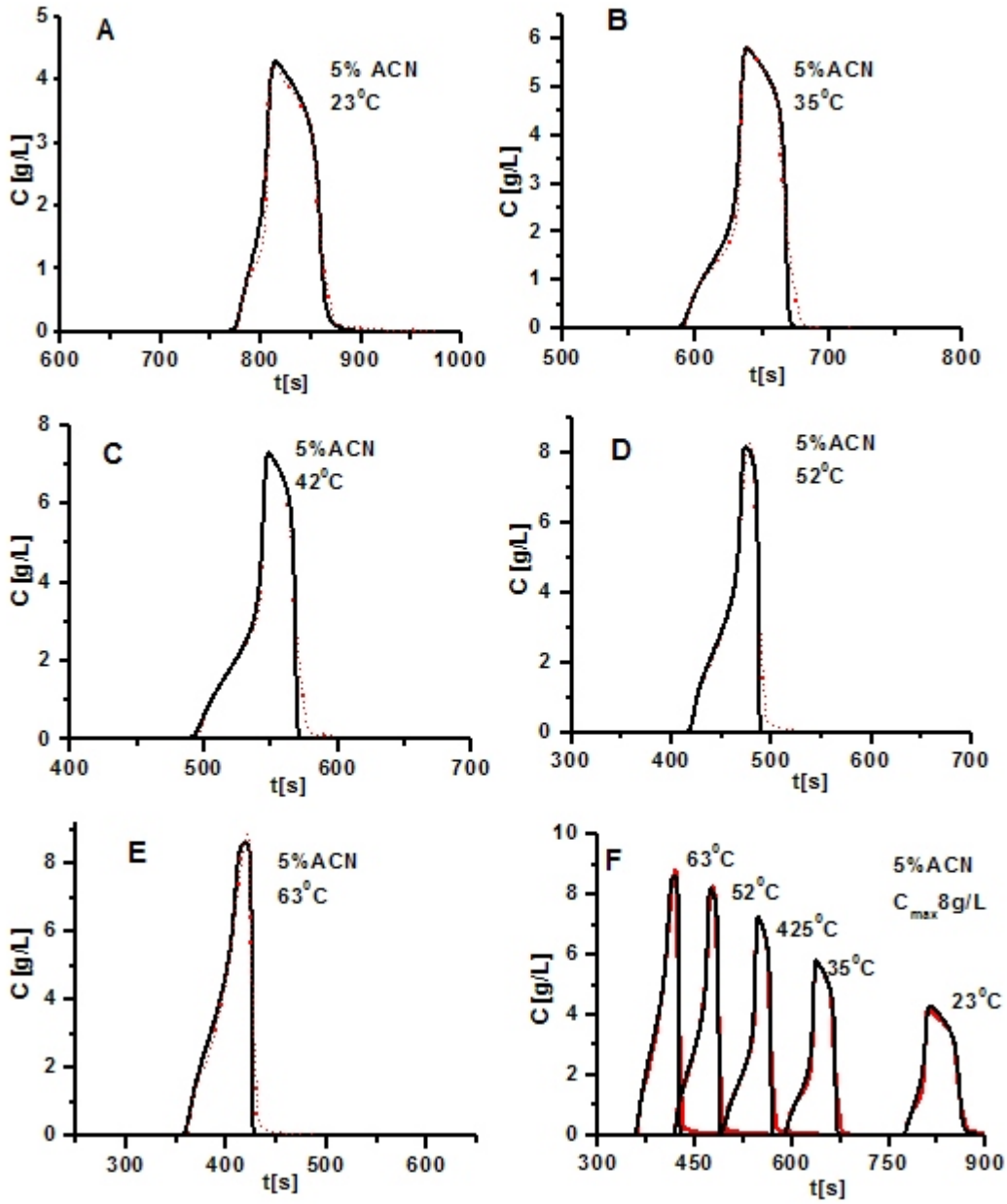

Figure 3.16 Comparison between calculated (solid lines in black) and experimental (dotted lines in red) band profiles overlaid, on C_{18} -Kromasil with a mobile phase containing 5% acetonitrile and 1% acetic acid at different temperatures. Injection of a solution of 8g/L tryptophan during 30 s; A) at 23; B) at 35; C) at 42; D) at 52; and E) at 63°C. F) Overlay of the band profiles calculated and recorded at all the temperatures.

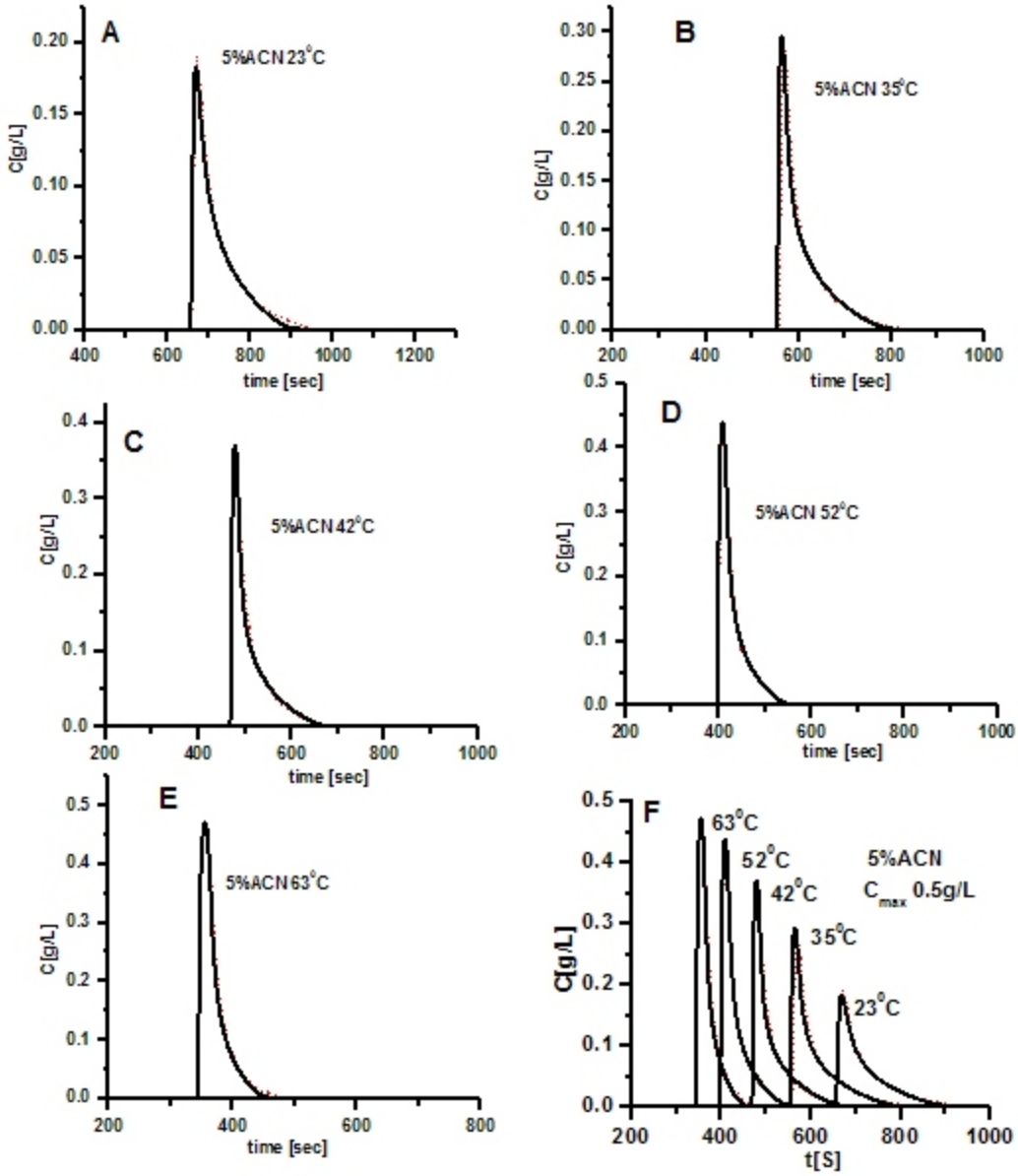

Figure 3.17 Comparison between the calculated (solid lines in black) and the experimental (dotted lines in red) band profiles overlaid, on C_{18} -Kromasil with a mobile phase containing 5% acetonitrile and 1% acetic acid at different temperatures. Injection of a solution of 0.5 g/L tryptophan during 30 s; A) at 23; B) at 35; C) at 42; D) at 52; and E) at 63°C. F) Overlay of the band profiles calculated and recorded at all the temperatures

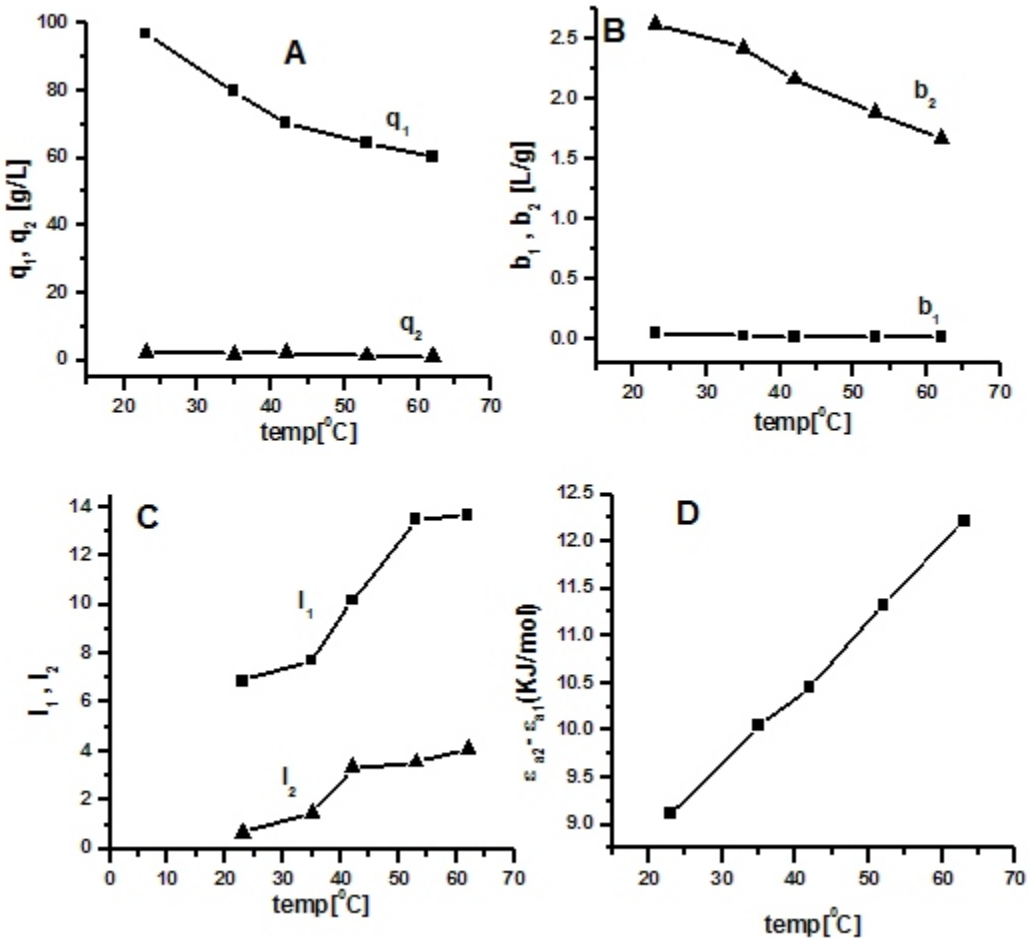

Figure 3.18 Evolution of the best values of the isotherm parameters obtained from IM, squares for low energy sites, and triangles for high energy sites. A) Saturation capacity of the low energy sites $q_{s,1}$, and saturation capacity of the high energy sites $q_{s,2}$. B) adsorption constant of the low energy sites b_1 and the high energy sites b_2, C)

Table 3.3 Best isotherm parameters and Fisher numbers for L-tryptophan on C_{18}-Kromasil with aqueous solutions of 5% ACN and 1% acetic acid as the mobile phase at different temperatures.

Temp °C	method	$q_{s,1}$	b_1	I_1	$q_{s,2}$	b_2	I_2	Fischer #
25	FA IM	123.16 96.87	0.03787 0.05200	6.42 6.89	4.08 2.60	1.0146 2.6300	0.31 0.67	14000
35	FA IM	98.21 79.82	0.02608 0.02823	8.19 7.72	1.65 2.00	0.9044 1.8364	2.11 1.49	18000
45	FA IM	71.01 70.27	0.02281 0.02304	11.84 10.18	1.85 2.15	0.6804 1.7996	4.05 3.35	14000
55	FA IM	66.57 64.38	0.01685 0.01686	14.62 13.49	1.68 1.53	0.5251 1.7048	2.19 3.10	21000
65	FA IM	64.42 60.55	0.0136 0.01405	16.34 13.67	1.01 1.174	0.5053 1.6841	2.26 2.98	13000

dependence observed is not inconsistent with a small retention factor. In the following, we considered that the hold-up volume decreases as shown in Figure 3.11b and used these values in isotherm calculations as estimates of the hold-up volume (see Eq 1.1). It should be noted that thiourea is not an ideal tracer, due to its small but finite adsorption. Alternative methods are available, like those suggested by Wells and Clark [107] and by Kazakevich and McNair [108] The first one is based on the measurement of the retention volume of a dilute solution of sodium nitrate. It was used by Miyabe et al. [109], Dorsey [110], and Gritti et al. [111 The second one consists in integrating the plot of the retention times of the perturbations obtained over the whole concentration range (from pure water to pure acetonitrile) and determining its average. The sodium nitrate method and the pycnometric method agree to give a column hold-up volume of 2.55 minutes. Therefore k` of thiourea is 0.02, which is negligible.

3.2.2. Frontal Analysis and Breakthrough Curves

Forty breakthrough curves were recorded for tryptophan at each of the five different temperatures studied. These curves were divided into four groups corresponding to concentrations of the mother solution used in the FA measurements below 0.05 g/L; between 0.05 and 0.5 g/L; between 0.5 and 2 g/L; and above 2 g/L. Figures 3.12 to 3.14 reports the curves obtained with mother solutions of concentrations 0.5 g/L (Figure 3.12), 2 g/L (Figure 3.13), and 8 g/L (Figure 3.14). For the sake of simplicity, no breakthrough curve of the first group is shown because these curves exhibit the same behavior as those in the second group. In each set of breakthrough curves, there are 10 curves corresponding to

dilution between 10 and 100% of the mother solution (see Section 2.5 in the experimental). This division is explained mainly by the large differences between their qualitative behavior. Note that the breakthrough curves are all given in concentration units. All the curves of the first group (Figures 3.12a-e, concentration 0.5 g/L) exhibit a sharp front shock and a diffuse rear. They all correspond to langmuirian behavior under overloading conditions. The increase of temperature from 23 to 63°C has no effect on the shape of these curves but it has a clear effect on the time at which the front of the breakthrough curve elutes. This time is approximately 850 sec at 23°C and 350 sec at 63°C, an effect which corresponds to the decreasing retention of tryptophan with increasing temperature. For each set of curves, the elution time decreases also with increasing concentration, a characteristic property of nonlinear chromatography. Increasing the temperature affects also the time difference between the curves obtained for the highest and the lowest concentrations. A rough estimates of the time difference between the highest and lowest concentration curves are 129, 97, 73, 53, and 49 sec for the temperatures of 23, 35, 42, 52, and 63°C, respectively. This result indicates that increasing the temperature not only reduces the retention of each set of curves but also compresses the curves so that the high and low concentration curves become closer to each other.

Two distinct effects control the shapes of the breakthrough curves of the second group (Figures 3.13a-e, concentration 1 to 5 g/L). The first is the increase of the solute concentration, the second that of the temperature. The effect of increasing concentration is illustrated by a systematic comparison of each subfigure

of Figure 3.13 with the corresponding subfigure of Figure 3.12 at the same temperature. The ratio of the concentrations of these curves is ten. The fronts of the high concentration curves in Figures 3.13a-f have an antilangmuirian behavior. Some of the curves, mostly the last three breakthrough curves in each of the Figures 3.13a, b, c, d, and e have a diffuse front and a diffuse rear boundaries. The low concentration curves (the first seven curves of each series) do exhibit this effect to some extent but it is not as distinct as for the three upper curves. However, the phenomenon is nearly the same at all temperatures.

The second effect that can be observed in this second group of breakthrough curves is that of temperature. The first (lowest concentration) breakthrough curves are well separated from each other in Figure 3.12a at 23 C°, the high concentration curves eluting faster than the low concentration ones, the characteristic property of nonlinear chromatography with a langmuirian isotherm, as seen above. This effect, however, can no longer be seen in Figures 3.13b or 3.13c where the fronts of the different curves are mixed up, some of the higher concentration curves having fronts that overlap the fronts of lower concentration curves while the plateaus of all these are separate. This phenomenon disappears at the higher temperatures of 52 and 63°C where the sets of curves are again separated in the normal manner; i.e, the higher concentration curves eluting faster than the lower concentration ones. If we estimate roughly the time distance between the highest and the lowest concentration curves at each temperature we find 21, 38, 22, 37, and 32 sec at 23, 35, 42, 52, and 63°C, respectively, values that are lower than the corresponding ones in Figures 3.12a-e. Both the temperature and the concentration contribute to compress the

breakthrough curves but it seems that the effect of the concentration is somewhat stronger than that of temperature in the present case since at 23°C the distance between the front of the highest and the lowest curves is 129 sec for a maximum concentration of 0.5 g/L while it is 97 sec at 35°C at this concentration and only approximately 21 sec for a maximum concentration of 2 g/L.

The breakthrough curves of the third group (Figures 3.14a-e, concentration 8 g/L) exhibit the most pronounced antilangmuirian effect of all. At all temperatures, these curves exhibit a diffuse front and a rear shock. This effect is due to adsorbate–adsorbate interactions that increase with increasing concentration. At 23°C, the first three breakthrough curves in Figure 3.14a exhibit this antilangmuirian behavior. When the plateau concentration exceeds *ca* 2.5 g/L, a front shock appears while the rear shock seems to grow up to *ca* 3.5 g/L. Then, the situation reverses, the front shock grows and moves toward shorter retentions while the rear boundary becomes increasingly diffuse (Figure 3.14a) down to the rear shock that remains stable, with a constant height and a constant retention time. At 35°C (Figure 3.14b), the fronts of the curves are mixed up, as observed previously, in the case of the 2g/L breakthrough curves (Figures 3.13b and 3.13c). In addition, the first five low concentration bands have diffuse fronts and rears while shocks appear at higher concentrations in the front and the rear. The front shock persists at high concentrations while the rear shock has a finite maximum amplitude. This is suggestive of several inflection points on the isotherms in the corresponding concentrations [9]. At higher temperatures, Figures 3.13c to 4e, all the fronts become diffuse boundaries and the rear of each profiles exhibits a concentration

shock. The curves are again well separated from each other. The interval between the elution of the highest and lowest concentration curves are estimated to be approximately 21, 41, 17,18, and 18 sec for temperatures of 23, 35, 42, 52, and 63°C, respectively. This means that increasing the temperature, has little effect on the separation between the lowest and the highest breakthrough curves.

3.2.3. Adsorption Isotherms

In section 3.1.1, we showed that the adsorption isotherm of tryptophan at 23°C, in mobile phases of different compositions exhibit up to three different regions in which the concavity is different. The isotherm was convex downward (i.e., langmuirian) at low concentrations, convex upward at intermediate concentrations, and convex downward at high concentrations. According to the shape of the isotherm and its curvature, the breakthrough curves may exhibit langmuirian or have a sharp shock on their fronts at low concentrations, exhibiting a langmuirian antilangmuirian shapes and may change shape, depending on the concentration of the solute. We found that the bi-Moreau model was the best model that accounts for the adsorption data and that it gives the best agreement between calculated and experimental band profiles. Although the adsorption data could be fitted as well to other models than the bi-Moreau model (e.g., the S-shape or quadratic model and the simpler Moreau model, two models with only three parameters) these model were disregarded because the bi-Moreau model gave the highest value for the Fisher number and for other reasons detailed in the earlier sections. The bi-Moreau model was the best model for all mobile phase compositions used. We now investigate the applicability of the same bi-Moreau model to the isotherm data

acquired at different temperature with one of the mobile phase composition previously studied, 5% of acetonitrile in water.

Figure 3.15a shows the adsorption data (symbols) and their best fit to the bi-Moreau model (solid lines) at the five different temperatures. The amount of tryptophan adsorbed on the C_{18} -bonded silica at equilibrium decreases with increasing temperature. All five isotherms have an inflection point, the isotherms being convex upward at low concentrations and downward at intermediate concentrations. The inflection points are not seen easily on the isotherms, but are obvious on plots of *q/C* versus *C* (Figure 3.15b). These plots exhibit a minimum at some intermediate concentration that correspond to the inflection point. The presence of inflection points in the isotherms is confirmed by the change observed in the shapes of the fronts of the breakthrough curves upon changing the concentration of the solution. As seen in Figure 3.12, all the breakthrough curves behavior. At higher concentrations, they exhibit an antilangmuirian behavior, with a diffuse front boundary and a rear shock. The isotherm at 23°C has a third, langmuirian part where it is convex upward at still higher concentrations. This is seen very clearly in the high concentration breakthrough curves in Figure 3.14a for which we observe the reappearance of a front shock. The *q/C* versus *C* plot for 23°C in Figure 3.15b shows another maximum at high concentrations.

The isotherms at higher temperatures do not exhibit this behavior, do not seem to have a second inflection point and a langmuirian part at high concentrations, consistent with the shape of the breakthrough curves in Figures 3.13b to 3.13e and 3.14b to 3.14e which do not exhibit a return of the sharp shocks to their fronts as

happens in Figure 3.14a at 23°C. This effect may be explained in part by the decreasing amount of acetonitrile adsorbed on the surface when the temperature increases. However, since the amount of acetonitrile adsorbed at room temperature is small [112] , its decrease with increasing temperature can have only limited consequences. The nonlinear fitting of the experimental data to the bi-Moreau model (six parameters) converged slowly and with difficulties, as mentioned earlier (section 3.1.1). These difficulties were alleviated by using the inverse method (IM) of isotherm determination with the series of overloaded band profiles recorded at the model. The best values of the parameters obtained by the IM method and derived five different temperatures. The parameters obtained by the IM method were used to initiate the nonlinear regression of the frontal analysis data to the bi-Moreau from the fit of the FA data are listed in Table 3.3 which reports also the values of the Fisher numbers. The bi-Moreau model gave higher values of the Fisher parameters than all other models. The solid lines in Figure 3.15a show the best bi-Moreau-isotherms calculated with the parameters derived from the FA data.

3.2.4. Overloaded Band Profiles

The experimental band profiles (dotted lines) are overlaid in Figures 3.16a to 3.16e (low concentrations, 0.5 g/l) and Figures 3.17a to 3.17e (high concentrations, 8g/L) on those calculated (solid lines) with the isotherm provided by the inverse method. Both Figures demonstrate an excellent agreement between the experimental and the calculated band profiles, at all temperatures used, and at both high and low concentrations. The whole sets of experimental and calculated profiles, for all temperatures studied are overlaid in Figures 3.16f (sample solution,

0.5 g/L) and Figure 3.17f (sample solution, 8 g/L). These figures show that increasing the temperature from 23 to 63°C decreases the elution time of tryptophan by approximately 350 seconds.

Temperature has another effect on the shape of the profiles. Figures 3.17 show that all the high concentration profiles have an antilangmuirian behavior, with a diffuse front and a rear shock. This behavior is indicative of significant solute-solute interactions. These interactions increase with increasing temperature as shown by the evolution of the profiles with increasing temperature, the steepness of the shocks increasing gradually. The two figures also show that the heights of the overloaded band profiles increase and their widths decrease with increasing temperature.

3.2.5. Parameters of the Isotherm

The parameters obtained by IM for the three profiles recorded at each temperature were averaged. The values obtained are reported in Table3.3 and plotted in Figures 3.18a to 3.18c. The profiles (solid lines) calculated by the ED model from the isotherms obtained by the IM method are shown in Figures 3.16 and 3.17 overlaid to the experimental profiles (dotted lines). As already mentioned above, there is an excellent

agreement between these experimental and calculated band profiles.

The results in Table 3.3 and Figures 3.18a to 3.18c illustrate the dependence of the isotherm parameters on the temperature. The saturation capacities $q_{s,1}$ and $q_{s,2}$ and the adsorption constants b_1 and b_2 of the low and the high energy types of sites decrease with increasing the temperature (Figure 3.18a-b). In contrast, the

coefficient of the adsorbate-adsorbate interactions, I_1 and I_2, for the low and the high energy types of sites increase with increasing temperature.

The decrease of the saturation capacity of the low energy type of sites with increasing temperature is consistent with previous results obtained for phenol on a C_{18}-bonded silica at different temperatures [51]. In contrast to our results, however, no effect of the temperature on the saturation capacity of the high energy type of sites for phenol was reported. The case of phenol is unusual because of its small molecular size. It has been suggested that the solubility of compounds in the mobile phase increases with increasing temperature [113-114]], and that the mobility of the alkyl chains bonded to the silica surface increases in the same time, on the basis of the adsorption isotherms of caffeine and phenol on C_{18} stationary phases [115-117]. These last results showed also that caffeine is less retained than the phenol, in contrast to what is expected, due to phenol being more polar and less bulky than caffeine. This unusual behavior was explained by the differences between the saturation capacities of the low and high energy types of sites of both compounds. Phenol has saturation capacities that are twice and fifteen times larger than those of caffeine on its low and high energy types of sites, respectively. The surprisingly large difference of the latter capacity, together with the rather small difference (ca 3.13 kJ/mole) between the adsorption energies on the high and the low energy sites for both compounds, leads to the conclusion that the high energy sites are probably buried deeply inside the C_{18}-bonded layers and cannot be silanols or dissociated silanophilic groups found on the exposed bare silica surface [115-116]. The access to these sites is controlled by the molecular size of the solute, small solute

molecules being able to penetrate deep inside cavities in the C-$_{18}$ bonded layer that are not accessible to large ones. The size and number of these cavities is less affected by a change in temperature than the structure of the alkyl layer/mobile phase interface.

In the present study, tryptophan has a molar mass (204.2) twice as large as phenol (94.1). Due to its larger size, it has access to fewer high energy sites than phenol. There are different possible reasons why the number of high energy sites available to tryptophan is low. First, these sites being deeply buried inside the bonded layer, tryptophan can access only those sites that are close to the interface. Second, tryptophan being flat, this reduces further the proportion of cavities accessible to it compared to those accessible to phenol. Third, binding to the high energy sites may take place via some kind of weak polar interactions between the amine or the carboxyl group and residual silanol groups on the silica surface. The difference between the adsorption energies on the low and the high energy sites increases with increasing temperature, reaching up to 11.8 KJ/mol. This energy is still too small, however, to correspond to interactions between hypothetical silanol groups of the high energy sites and tryptophan molecules, ruling out this assumption and leaving only the first two ones. Tryptophan molecules may probably access only those high energy sites that are close to the surface and can accommodate its shape.

These conclusions are consistent with a comparison with the saturation capacities of phenol reported previously [51] for the low and the high energy types of sites. The capacity $q_{s,2}$ (~60-65)) at 23°C is approximately one third the capacity

$q_{s,1}$ (~180-190). For L-tryptophan (see Table 3.3) $q_{s,2}$ (~1-4) is small compared to $q_{s,1}$ (96-123), showing the high energy sites to be less accessible to the bulkier L-tryptophan. However, the organic modifier used in the study of phenol adsorption [51] and in this work, methanol and acetonitrile, are different. The former solvent is less strongly adsorbed than the latter, which can form multilayers on the surface [117]. Solvent adsorption, even light [112] , has an impact on the adsorption equilibrium of tryptophane, which prevents from making a close comparison between the results of these two studies.

The adsorption constants on the low and high energy sites decreasing and the adsorbate-adsorbate interactions increasing with increasing temperature may be due to the simultaneous increases in solubility and in mobility of the chains, resulting in the decrease of adsorption entropy. At increasing temperature, the high energy sites close to the surface may be more easily accessible, making the binding easier and explaining the decrease of the adsorption constants while their availability, hence their saturation capacities, decreases due to the increase in the entropy of the adsorbed system which lowers the probability of tryptophan molecules occupying these sites.

The results in Table 3.3 show excellent agreement between the isotherms obtained by frontal analysis and the inverse method. They also show that increasing temperature affects the high energy sites more than the low energy sites. The saturation capacity of the latter decreases by ~ 36%, that of the former by ~54% when temperature increases from 23 to 63°C. The adsorption constants on both types of sites decrease by 72 and 36% for the low and the high energy sites,

respectively. In contrast, in the same time, the adsorbate-adsorbate interactions more than double.

3.3. The Effect of Temperature at Different Mobile Phase Compositions

Figures 3.19 a-b show the effect of mobile phase composition and temperature on the detector calobration and on the column dead volume respectively. The effects of both mobile phase composition and temperature on the breakthrough curves at low 0.5 g/L , intermediate 1-2 g/L and at high 11g/L concentration of tryptophan are shown in Figiures 3.20, 3.21, and 3.22 respectively. For each of these Figures, movement horizontally along the Figure shows the effect of solvent, and movement vertically shows the effect of temperature. The effect of temperature on the adsorption isotherms and on the scatchard curves for each of the mobile phases is shown in Figures 3.23, 3.34, and 3.25. The effect on the overloaded band profiles is shown by Figure 3.26, while the effect on the parameters of the adsorption isotherm is illustrated by Figures 3.27 and by Tables 3.4, and 3.5 respectively. These effects will be explained in details in the next sections.

3.3.1. Effect of the Temperature and the Mobile Phase Composition on the Detector Calibration

Figure 3.19a shows the isotherm data obtained for three mobile phase compositions at room temperature. Figure 3.19b shows the data obtained for one mobile phase composition (7.5% ACN) at five different temperatures. The data for the other mobile phase compositions and the other temperatures are not shown. These Figures show that the detector signal is affected by both the mobile phase

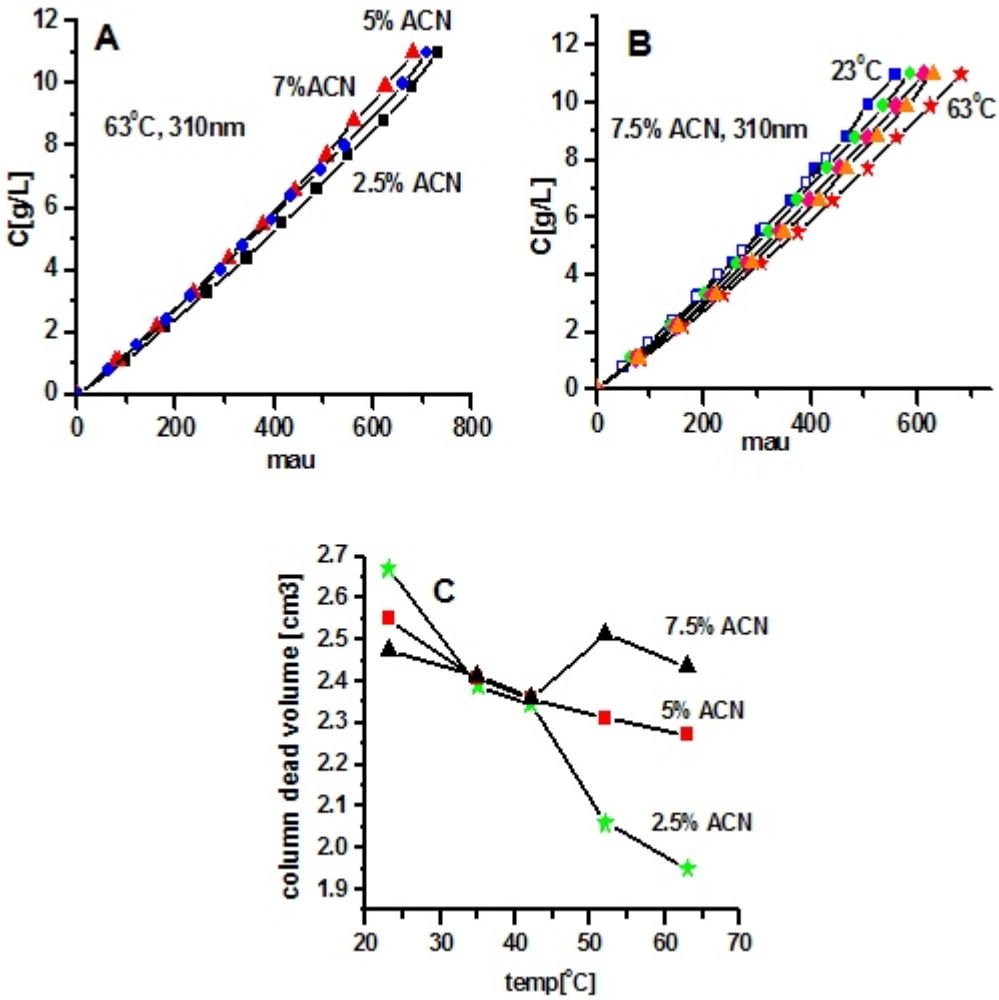

Figure 3.19 Calibration of the detector. A) At 63°C, for three different mobile phase compositions; B) At five different temperatures, for one mobile phase composition.(C) Effect of the temperature and mobile phase composition on the column hold-up volume measured as the retention time of thiourea.

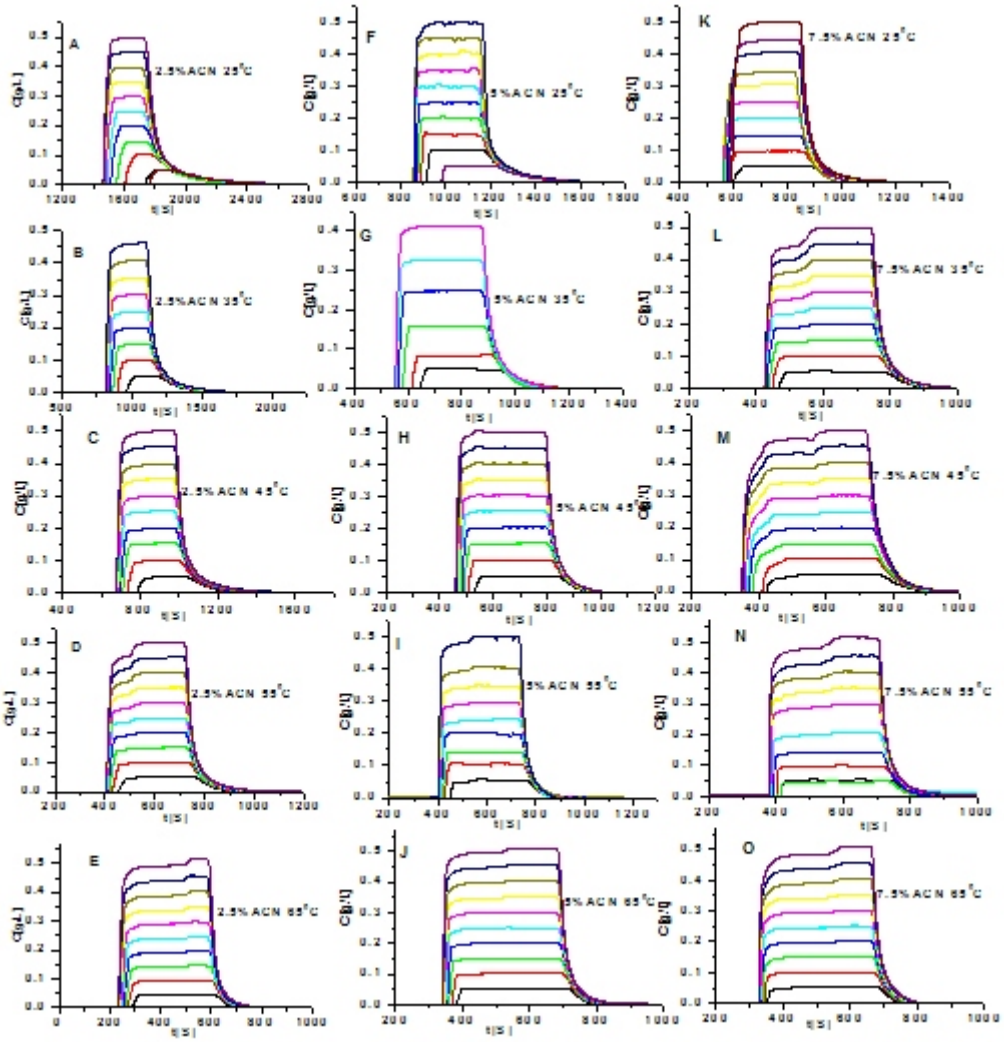

Figure 3.20 Breakthrough curves for the adsorption of tryptophan on C_{18}-Kromasil. All the aqueous mobile phases contain 1% acetic acid with the concentration of tryptophan in the mother solution is 0.5 g/L. A-E) 2.5% ACN at 23, 35, 42, 52, and 63°C; F-J) 5%ACN at 23, 35, 42, 52, and 63°C; and K-O) 7.5%ACN at 23, 35, 42, 52, and 63°C. The curves are reported in concentration units, the original curves (UV absorbance versus time) were recorded at 305 nm.

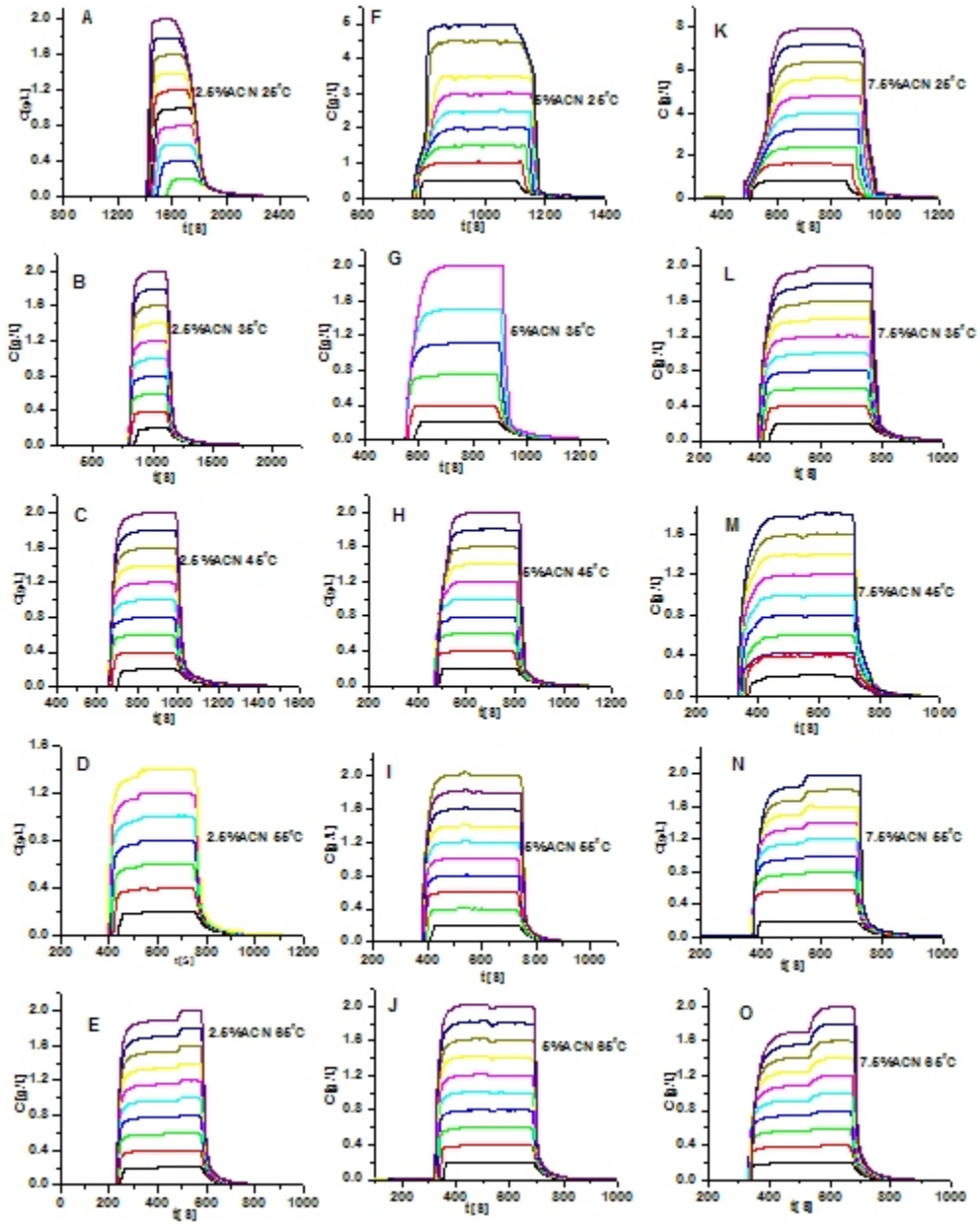

Figure 3.21 Breakthrough curves for the adsorption of tryptophan on C_{18} -Kromasil. All the aqueous mobile phases contain 1% acetic acid with the concentration of tryptophan in the mother solution is 2-5 g/L. A-E) 2.5% ACN at 23, 35, 42, 52, and 63°C; F-J) 5% ACN at 23, 35, 42, 52, and 63°C; and K-O) 7.5%ACN at 23, 35, 42, 52, and 63°C. The curves are reported in concentration units, the original curves (UV absorbance versus time) were recorded at 305 nm.

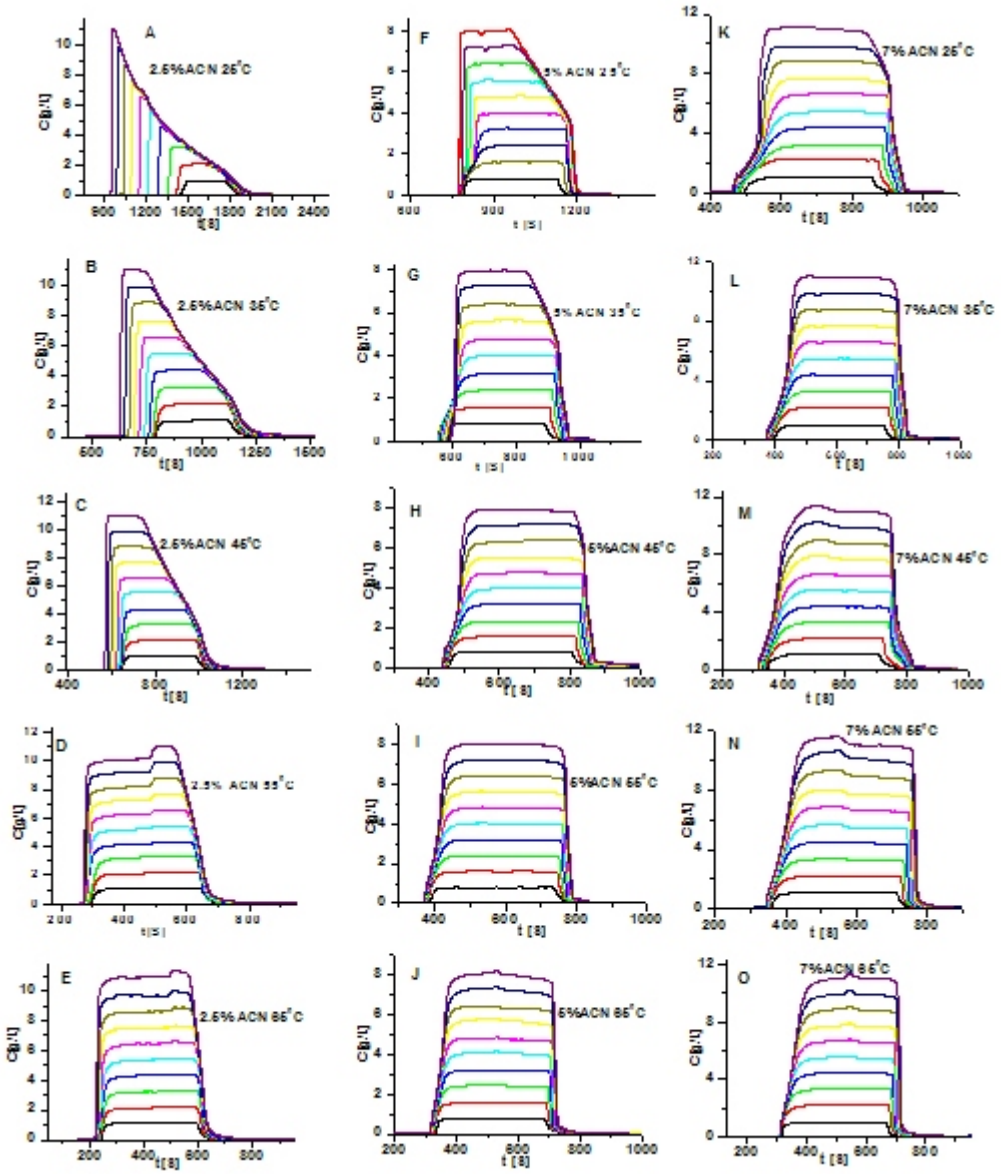

Figure 3.22 Breakthrough curves for the adsorption of tryptophan on C_{18}-Kromasil. All the aqueous mobile phase contain 1% acetic acid with the concentration of tryptophan in the mother solution is 8-11 g/L. A-E) 2.5% ACN at 23, 35, 42, 52, and 63°C; F-J) 5% ACN at 23, 35, 42, 52, and 63°C; and K-O) 7.5% ACN at 23, 35, 42, 52, and 63°C. The curves are reported in concentration units, the original curves (UV absorbance versus time) were recorded at 310 nm.

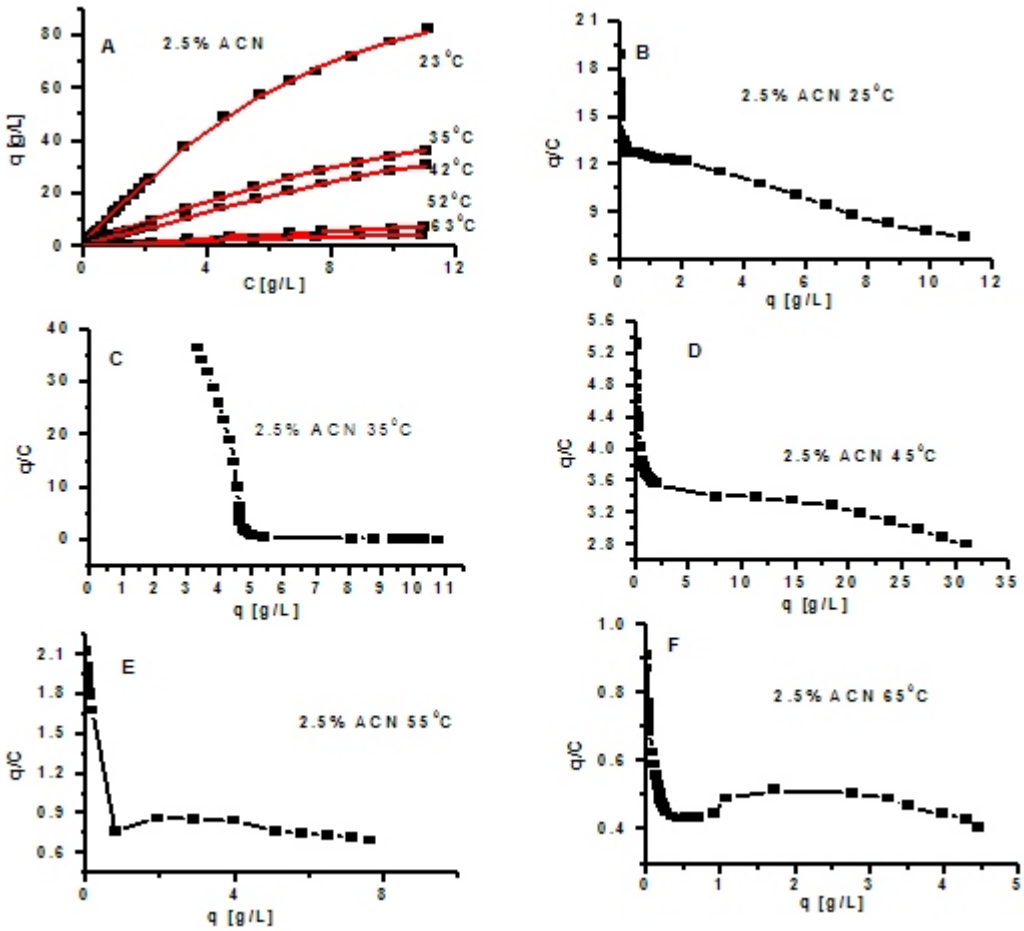

Figure 3.23 A) Experimental isotherm data (FA, symbols) of tryptophan on C_{18} -Kromasil with an aqueous mobile phase containing 2.5% acetonitrile and 1% acetic acid. The solid line is the best fit of the data to a bi-Moreau model at different temperatures. Top to bottom; 23; 35; 42; 52; and 63°C. B-F) Scatchard, plots of q/C versus q, at 23; 35; 42; 52; and 63°C respectively.

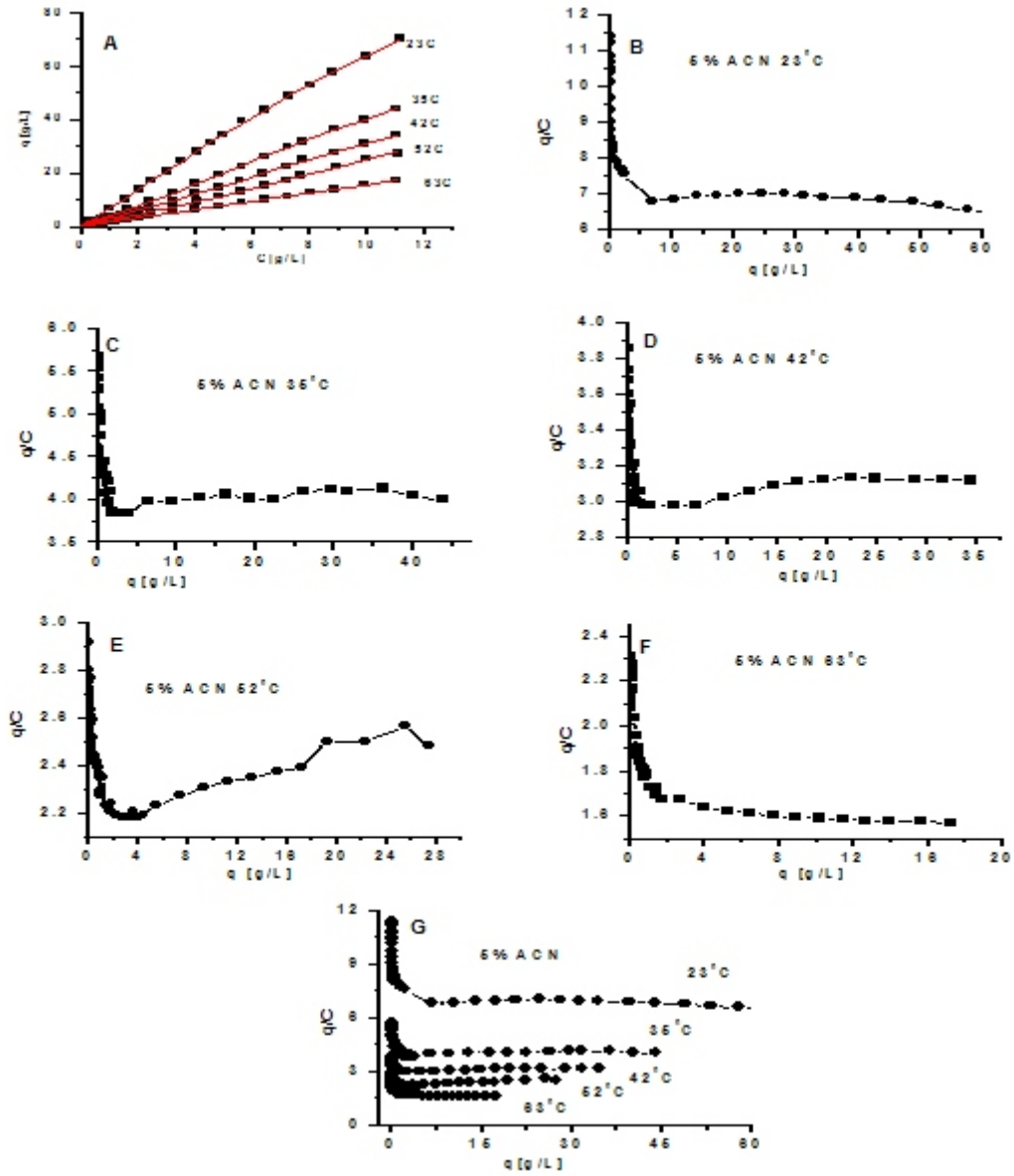

Figure 3.24 Experimental isotherm data (FA, symbols) of tryptophan on C_{18} -Kromasil with an aqueous mobile phase containing 5% acetonitrile and 1% acetic acid. The solid line is the best fit of the data to a bi-Moreau model at different temperatures. Top to bottom; 23; 35; 42; 52; and 63°C. B-F) scatchard plots of q/C versus q, at 23; 35; 42; 52; and 63°C respectively, G) Scatchard for all temperatures.

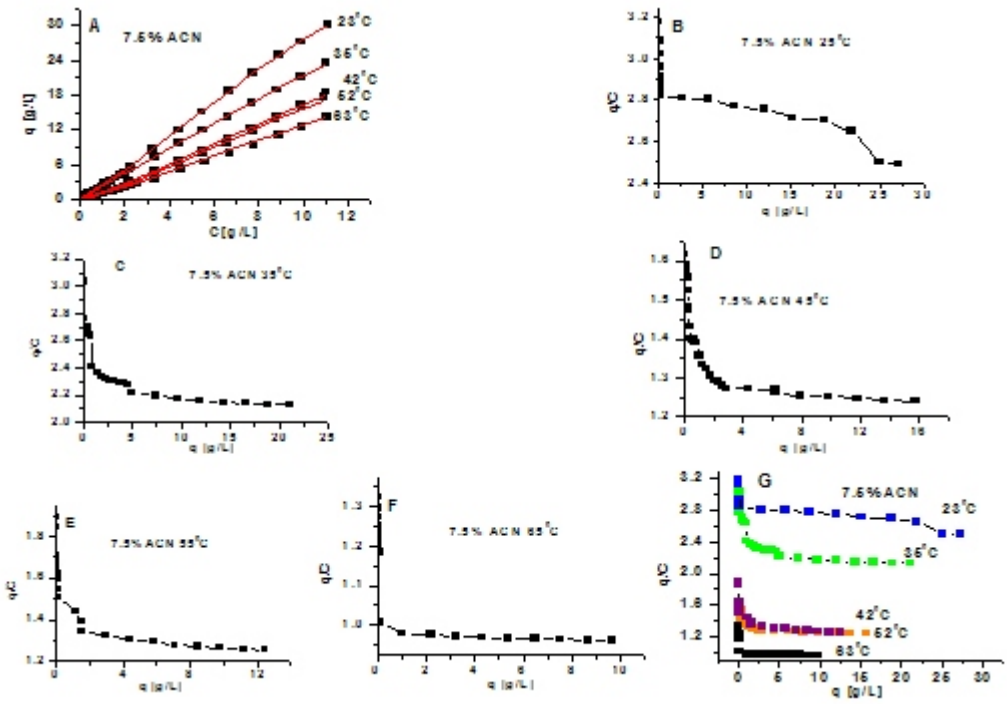

Figure 3.25 Experimental isotherm data (FA, symbols) of tryptophan on C_{18} -Kromasil with an aqueous mobile phase containing 7.5% acetonitrile and 1% acetic acid. The solid line is the best fit of the data to a bi-Moreau model at different temperatures. Top to bottom; 23; 35; 42; 52; and 63°C. B-F) Scatchard plots of q/C versus q, at 23; 35; 42; 52; and 63°C respectively, G) Scatchard plots at all temperatures

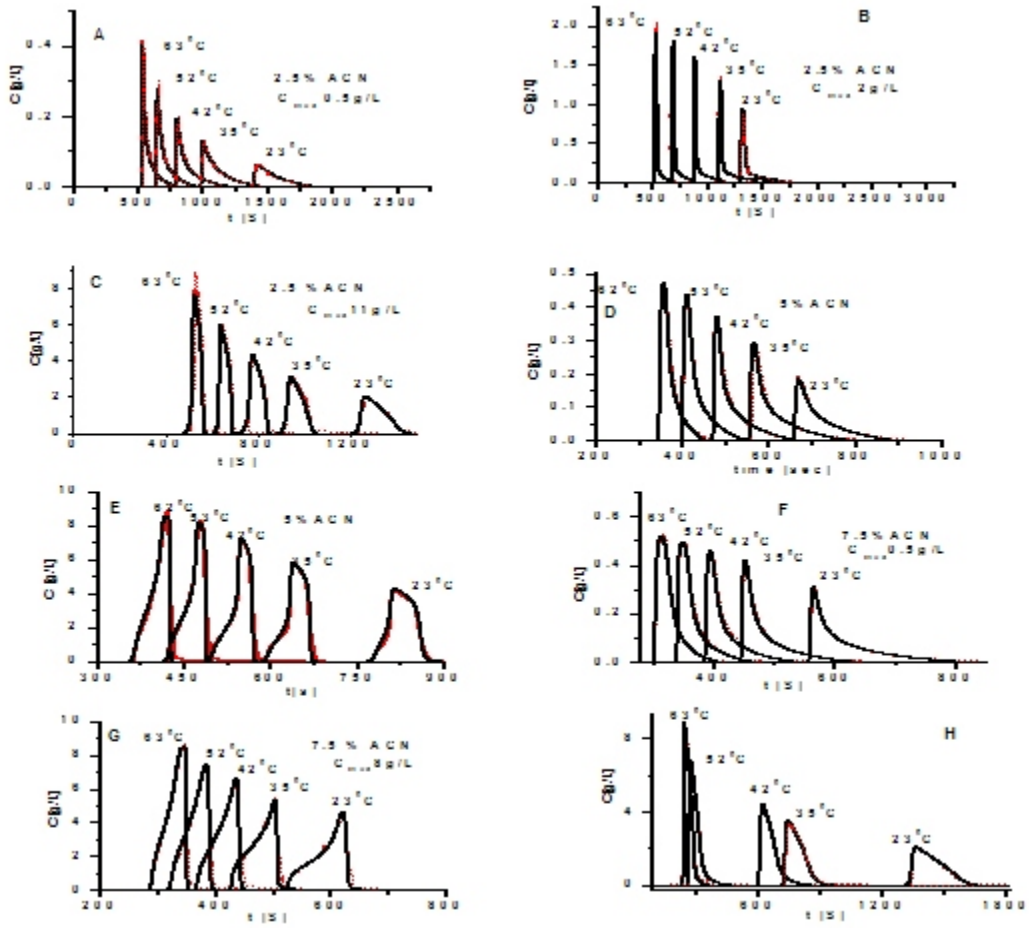

Figure3.26 Comparison between calculated (solid lines in black) and experimental(dotted lines in red) band profiles overlaid. Conditions: C_{18} - Kromasil with a mobile phase containing 1% acetic acid. Data at 5 different temperatures overlaid. The composition of the mother solution of tryptophan is A-C) 2.5% ACN at 0.5, 2, and 8g/L. D-E) 5%ACN at 0, 5 and 8 g/L; and F-G) 7.5%ACN at 0.5, and 8 g/L. The injection of the tryptophan solution lasted 30 s. H) Same as C except the that profiles were recorded in long period.

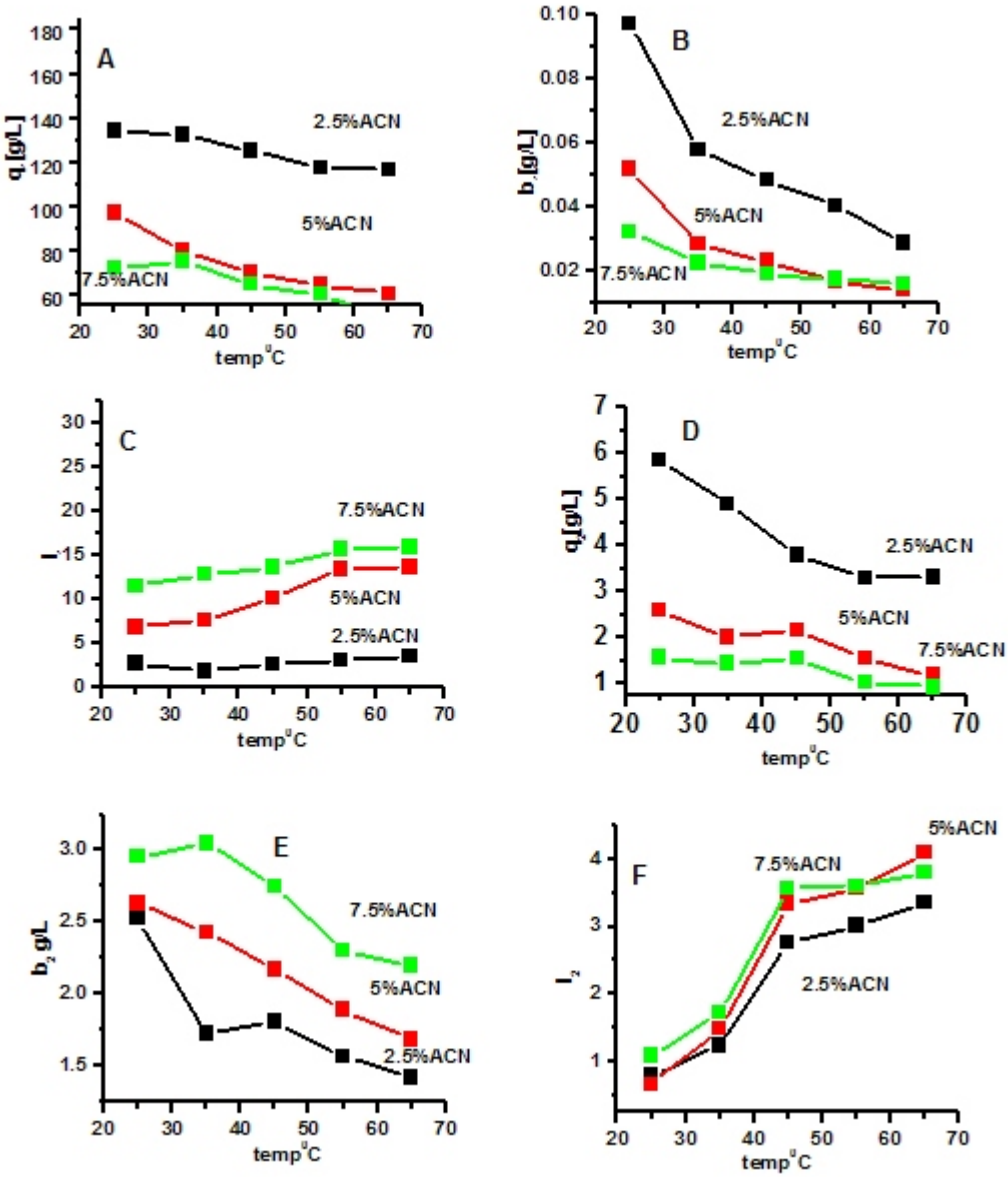

Figure 3.27 Effect of temperature on the parameters of the isotherm obtained by the IM method for three mobile phase compositions. A) Saturation capacity of the low energy sites; B) Saturation capacity of the high energy sites; C) Adsorption constant of the low energy sites; D) Adsorption constant of the high energy sites; E) Adsorption-Adsorbate parameter of the low energy sites; and F) Adsorption-Adsorbate parameter of the high energy sites. Black squares :2.5% ACN, red triangles: 5% ACN; and green circles: 7.5% acetonitrile.

Table 3.4 Best isotherm parameters obtained by frontal analysis method(FA) and by the inverse method(IM) for the low energy sites for L-tryptophan on C_{18}-Kromasil with aqueous solutions of 2.5%, 5%, 7.5% ACN and 1% acetic acid as the mobile phase at different temperatures

%ACN	Tem	q_1(IM)	q_1(FA)	b_1(IM)	b_1(FA)	l_1(IM)	l_1(FA)
2.5%ACN	25	134.2	167.9	0.0976	0.0764	2.83	1.04
	35	132.4	141.2	0.0579	0.0581	1.92	1.37
	45	125.2	134.1	0.0485	0.0452	2.77	2.69
	55	117.5	121.9	0.0405	0.0382	3.17	3.26
	65	116.5	115.8	0.0288	0.0299	3.63	3.54
5%ACN	25	96.87	123.2	0.0520	0.0379	6.89	6.41
	35	79.82	98.2	0.0282	0.0261	7.72	8.19
	45	70.27	71.0	0.0230	0.0228	10.18	11.84
	55	64.375	66.6	0.0169	0.0169	13.49	14.62
	65	60.55	64.4	0.0141	0.0137	13.67	16.34
7.5%ACN	25	72.21	93.9	0.0322	0.0283	11.56	12.85
	35	75.41	86.1	0.0224	0.0224	12.85	11.71
	45	64.55	78.5	3	3	13.73	12.74
	55	60.19	71.6	0.0191	0.0191	15.74	11.18
	65	49.73	61.4	2	2	15.99	11.82
				0.0174	0.0174		
				9	2		
				0.016	0.016		

Table 3.5 Best isotherm parameters obtained by frontal analysis method(FA) and by the inverse method(IM) for the high energy sites for L-tryptophan on C_{18}-Kromasil with aqueous solutions of 2.5%, 5%, 7.5% ACN and 1% acetic acid as the mobile phase at different temperatures.

%ACN	**Temp**	**q_2(IM)**	**q_2(FA)**	**b_2(IM)**	**b_2(FA)**	**l_2(IM)**	**l_2(FA)**
2.5%ACN	25	5.87	7.77	2.5234	7.0399	0.79	1.83
	35	4.90	7.12	2.0011	6.3703	1.24	1.66
	45	3.79	5.49	1.8102	5.8945	2.77	2.87
	55	3.30	4.82	1.5645	3.9408	3.01	0.38
	65	3.31	6.47	1.4168	3.4918	3.36	0.86
5%ACN	25	2.60	4.08	2.6301	1.0146	0.67	0.31
	35	2.00	1.65	2.4334	0.9044	1.49	2.11
	45	2.15	1.85	2.1718	0.6804	3.35	4.05
	55	1.53	1.68	1.8927	0.5251	3.56	2.19
	65	1.17	1.00	1.6841	0.5053	4.09	2.26
7.5%ACN	25	1.30	1.71	2.9542	3.0505	1.09	0.29
	35	1.57	1.64	2.8735	2.7475	1.72	0.26
	45	1.43	1.51	2.5475	2.6124	3.57	0.48
	55	1.54	0.96	2.3003	2.2983	3.60	0.68
	65	1.01	0.82	2.1975	1.9917	3.80	0.88

composition and the temperature. To correct for these effects, the calibration curves were fitted to a third order polynomial. The equations obtained were used to convert the overloaded profiles and the breakthrough curves from absorbance units into concentration units.

3.3.2. Effect of the Temperature and the Mobile Phase Composition on the Column Hold-up Volume

The hold-up volume decreases with increasing temperature and organic modifier concentration in the mobile phase. However the variations are not linear, are complex (Figure 3.19), and for some temperatures and compositions, the curves intersect. The reason for this behavior are discussed later.

3.3. 3 Effect of the Temperature on the Breakthrough Curves

3.3.3.1. Breakthrough Curves with 2.5% Acetonitrile in the Mobile Phase

Figures 3.20a-e, 3.21a-e, and 3.22a-e show the effect of the temperature on the breakthrough curves obtained with 2.5% ACN in the mobile phase and tryptophan concentrations of 0.5, 2, and 11g/L, respectively. The data at the lower concentration of 0.05 g/L are not shown because of their strong similarity with those at 0.5 g/L. All the Figures 3.20a-e and 3.21a-e exhibit a sharp front shock layer and a diffuse rear boundary. Almost all these breakthrough curves exhibit a plateau. A careful glance at the rear of the curves in Figure 3.21a shows S-shaped isotherm behavior, notable especially at concentrations between 1.2 and 2.0 g/L, where the plateau begins to decay at 23°C. The curves are normal again at 35°C and higher temperatures for the same concentration range. The same behavior takes place for

the breakthrough curves recorded with a tryptophan concentration of 11 g/L. Most curves in Figure 3.22a do not exhibit a plateau at 23°C, which indicates a strong adsorption of the tryptophan onto the stationary phase. However, the width of the plateau increases with increasing temperature. The comparison of each successive set of breakthrough curves at 23°C with the similar curves at 63°C, both run with the same concentration of tryptophan leads to the following conclusions: The elution time of the front of the highest concentration breakthrough curve in Figure 3.20a (23°C) is at ~1450 sec. while that of the smallest concentration curve is at 1750 sec, a difference of 300 sec. Both tails end at the same time, approximately 2400 sec. At 63°C, Figure 3.20e, the difference between the retention times of the highest (230 sec.) and the lowest breakthrough curves (280sec.) is about 50 sec., with both tails ending at ~800 sec. This illustrates how increasing the temperature At 63°C, Figure 3.20e, the difference between the retention times of the highest (230 sec.) and the lowest breakthrough curves (280sec.) is about 50 sec., with both tails ending at ~800 sec. This illustrates how increasing the temperature compresses the .curves At high concentrations of tryptophan, the fronts of the first and the last breakthrough curves at 23°C (Figure 3.22a) elute at 830 and1450 sec., respectively, both ending at 2100 sec, nearly the same as in Figure 3a when one takes into account that the end of the tail is not easy to locate at the small scale used in the Figure. At 63°C (Figure 3.22e) the corresponding fronts elute at 220 and 240 sec., respectively, and both tails end at 800 sec. This illustrates how much increasing the temperature decreases the difference between the elution times of two fronts, from ~620 sec. at 23°C to about 20 sec. at 63°C and decreases the retention time, by

300 sec.

3.3.3.2. Breakthrough Curves with 5% Acetonitrile in the Mobile Phase

Figures 3.20f-j, 3.21f-j, and 3.22f-j show the effect of increasing the temperature on the breakthrough curves recorded with 5% acetonitrile in the mobile phase, with the same three concentration ranges of tryptophan as studied in the Section above. All the curves of the first group (Figures 3.20f-j, concentration 0.5 g/L) exhibit a sharp front shock layer and a diffuse rear boundary. They all correspond to langmuirian behavior under overloading conditions. The increase of temperature from 23 to 63°C has no effect on the shape of these curves, it merely causes a strong decrease of the elution times of the fronts of the breakthrough curves. This time is approximately 850 sec. at 23°C (Figure 3.20f) and 350 sec at 63°C (Figure 3.20j). This is due the decrease of retention of tryptophan with increasing temperature. For each set of curves, the elution time decreases also with increasing concentration, a characteristic property of nonlinear chromatography with langmuirian isotherms. Increasing the temperature affects also the time difference between the curves obtained for the highest and the lowest concentrations (the first and the last shock layers). Rough estimates of this time difference are 129 seconds at 23°C and 49 sec at 63°C. This result illustrates the compression of the breakthrough curves.

Two distinct effects control the shapes of the breakthrough curves of the second group (Figures 3.21f-j, concentrations between 1 and 5 g/L). The first results from the increase of the solute concentration, the second from that of the temperature. The effect of increasing concentration is illustrated by a systematic

comparison of each subfigure of Figure 3.21 with the corresponding subfigure of Figure 3.22 at the same temperature. The ratio of the concentrations corresponding to all these curves is ten. The fronts of the high concentration curves in Figures 3.21f-j have an antilangmuirian behavior. Some of these curves, mostly the last three breakthrough curves in each of the Figures 3.21f, g, h, I, and j have diffuse parts in their front and rear boundaries. The low concentration curves (the first seven curves of each series) do exhibit this effect to some extent but it is not as distinct as for the three upper curves. However, the phenomenon is nearly the same at all temperatures.

The second effect observed is that of temperature. The low concentration breakthrough curves are well separated from each other in Figure 3.20f (23C°), the higher the concentration the shorter the elution time of the front, a characteristic property of nonlinear chromatography in the case of a langmuirian isotherm. This neat separation of the fronts of the breakthrough curves is no longer seen in Figures 3.20h and 3.20i. The fronts of the different curves become mixed up, some of the higher concentration curves having fronts that overlap the fronts of lower concentration curves while the plateaus of all these curves are obviously well separated. This phenomenon disappears at the highest temperature (Figure 3.20j, at 63°C).

In Figures 3.21i-j, the sets of curves are again separated in the normal manner; i.e, the higher concentration curves eluting faster than the lower concentration ones. The time distance between the fronts of the highest and the lowest concentration curves are approximately 21 sec. at 23°C and 32 sec. at 63°C.

These values are lower than those observed in Figures 3.20a-e. Both temperature and concentration contribute to compress the breakthrough curves but it seems that the effect of concentration is somewhat stronger than that of temperature in the present case, since this distance is 129 sec. at 23°C for a concentration of 0.5 g/L while it is 97 sec. at 35°C and at this concentration and only approximately 21 sec. for a maximum concentration of 2 g/L.

The breakthrough curves of the higher concentration group (Figures 3.22f-j, concentration 8 g/L) exhibit a still more pronounced antilangmuirian effect. At low temperatures, these curves exhibit a diffuse front and a rear shock layer. This effect is explained by the adsorbate–adsorbate interactions that increase with increasing concentration. At 23°C, the first three breakthrough curves in Figure 5a exhibit this antilangmuirian behavior. When the plateau concentration exceeds *ca* 2.5 g/L, a front shock layer appears while the rear shock seems to grow up to *ca* 3.5 g/L. Then, the situation reverses, the front shock grows and moves toward shorter retentions while the rear boundary becomes increasingly diffuse (Figure 3.22f), down to the rear shock that remains stable, with a constant height and a constant retention time. At 35°C (Figure 3.22g), the fronts of the curves are mixed up, as observed previously, in the case

of the 2g/L breakthrough curves (Figures 3.22g and 3.22h). In addition, the first five low concentration bands have diffuse fronts and diffuse rear boundaries while shock layers appear at higher concentrations in the front and the rear. The front shock persists at high concentrations while the rear shock has a finite maximum amplitude. This suggests that the isotherm has several inflection points at the corresponding

concentrations.

At higher temperatures, Figures 3.22h to 3.22j, the fronts become diffuse boundaries and the rear of each profile exhibits a concentration shock. The curves are again well separated from each other. The interval between the elution of the highest and the lowest concentration curves (the first and last shock) is approximately 21 sec. at 23°C, and 18 sec at 63°C. This means that increasing the temperature has little effect on the separation between the lowest and the highest breakthrough curves.

3.3.3.3. Breakthrough Curves With 7.5% Acetonitrile in the Mobile Phase

Figure 3.20k shows that at 25 °C and at low concentrations (0.5g/L) the breakthrough curves have a different behavior than those observed at the same temperature with only 5 or 2.5% ACN (Figures 3.20a to 3.20f). The anti-Langmuirian behavior is already seen at 0.5 g/L (Figure 3.20k) and is also observed at higher temperatures (see Figures 3.20m-o). The shocks of the low and high concentrations curves in Figure 3k are mixed, the curve corresponding to 70% of the maximum concentration of 0.5g/L elutes first, before the highest concentration curve (100% of the 0.5 g/L). Figure 3.20k shows also that there is a difference of 50 sec. between the elution of the first and last shock and that the band tails end at 1100 sec.

At 63 °C (Figure 3.20o), the elution times of the first and last fronts are 330 and 360 sec. respectively, the tails ending at 800 sec. The curves are compressed but they are well separated from each other, the highest concentration curve elutes first, the lowest concentration one elutes last.

Increasing the concentration to 2 (Figures 3.21k-o) and 11 (Figure 3.22k-o) g/L enhances the consequences of the anti-Langmuirian behavior, which causes the fronts to become almost completely diffuse while the band exhibit rear shock layers. This effect is due to the adsorbate–adsorbate interactions that increase with increasing concentration and also with increasing temperature. Accordingly, the fronts of the breakthrough curves of the high concentrations bands in Figures 3.22k-o become quite diffuse at 63 °C.

In summary, increasing the temperature and the acetonitrile concentration decreases the difference between the elution times of the highest and lowest concentration shock layers. Comparing the Figures 3.20a,f,k, 3.21a,f,k, or 3.22a,f,k or other rows of figures shows that the influence on the band profiles of the solvent concentration is much stronger than the effect of the temperature.

3.3.4. Effect of the Temperature on the Adsorption Isotherms

Figures 3.23a shows the five sets of adsorption isotherm data obtained for tryptophan with a mobile phase containing 2.5% ACN at the five different temperatures studied. Figures 3.24a and 3.25a show the same results obtained with 5 and 7.5% ACN in the mobile phase. These frontal analysis data were fitted to the bi-Moreau model because this model was found earlier (Sections 3.1.1, and 3.2.3) to be the model that accounts best for these data, Although the nonlinear fitting of the FA data to the bi-Moreau model was difficult The solid lines in Figures 3.23a, 3.24a, and 3.25a show the best bi-Moreau isotherms obtained by regression of the FA data to this model. The isotherms obtained with 2.5% ACN (Figure 3.23a) look all convex downward, with the isotherm at 23°C having the highest curvature. The

Scatchard plots of the isotherms in Figure 3.23a are given in Figures 3.23b-f. These plots show that the different isotherms have at least one inflection point, most having more than one. The presence of these inflection points is confirmed by the profiles of the breakthrough curves in Figures 3.20, 3.21, and 3.22 and by the overloaded band profiles in Figure 3.26. The isotherms show that the amount of tryptophan adsorbed at equilibrium with a given mobile phase concentration decreases with increasing temperature. However, this amount is not simply related to the temperature. For example, the gap between the isotherms at 23 and 35°C is much larger than the one between the isotherms at 35 and 42°C, itself much smaller than the gap between the isotherms at 42 and 52°C. It would be expected that this gap decreases regularly with increasing temperature. A partial explanation for this result is that the actual temperature of the oven is not that was set in the controller. When the temperature was set at 25, 35, 45, 55, and 65°C, the actual temperature of the column was 23, 35, 42, 52, and 63°C, respectively. This explanation does not suffice to explain the differences seen between the different isotherms. The hold-up volume of the column was measured as the retention volume of thiourea. The measurements were repeated regularly during the FA measurements. It was found that the hold-up volume decreases with increasing temperature. When the temperature was reset to 23°C without changing the mobile phase composition,

the hold-up volume for the influences of the mobile phase composition and the temperature on these data, and has a higher Fisher number than other possible models. measured was different from the one measured previously at that temperature, even if the column was equilibrated overnight at 23°C. The only way

to restore the initial value of the column hold-up volume was to wash it with a solution rich in ACN (20 to 50%) for an hour, then to equilibrate it again with the chosen mobile phase, for several hours. This treatment restored the previous value of the hold-up volume. For example, the holdup time for thiourea using 5%ACN in the mobile phase at 23°C is 2.55 min. After heating the column at 63°C, carrying out for 2 days a series of frontal analysis experiments at this temperature, and cooling the column to 23°C, this holdup time was 2.11 min. The original value of 2.55 min. was restored, however, after the treatment just described. It seems as if a layer of ACN covers the stationary phase, to vanish progressively when the column temperature is raised. A similar phenomenon takes place when breakthrough curves or overloaded band profiles are recorded. After the completion of each series of frontal analysis experiment at a certain temperature, the column should be cooled to room temperature, treated with an acetonitrile-rich solution and equilibrated with the mobile phase at the new desired temperature. The overloaded profiles shown in Figure 3.26h (next section) illustrate the problem that results when overloaded profiles are acquired during 5 consecutive series of frontal analysis experiments (for a relatively long period of time ~10 days) to measure isotherms at 23, 35, 42, 52 and 63°C. These experiments were done without following the washing and equilibration steps between each successive temperature. It is important to note that as long as the mobile phase stream is not interrupted, the holdup time measured during successive experiments is highly reproducible. So, during the collection of the breakthrough curves needed for the four concentration ranges of each isotherm, at each temperature, we kept the instrument running, even

when washing the pump that delivers the sample solution.

The isotherm data measured at 5 and 7.5% ACN are similarly shown in Figures3.24a-f and 3.25a-f, respectively. Figures 3.24a and 3.25a shown the adsorption data, Figures 3.24b-f and 3.25b-f the Scatchard plots. The isotherm curvatures at a given temperature are different for different ACN concentrations. The isotherms at 5 and 7.5% ACN are antilangmuirian at high concentrations and langmuirian at low concentrations. The evolution of the isotherm curvature shows that the adsorbate-adsorbate interactions increase with increasing ACN concentration.

There is no clear effect of temperature on the isotherm plots but most Scatchard plots show a minimum that moves toward lower concentrations with increasing temperature. This means that the corresponding inflection point moves toward lower concentrations. The same is true for the other inflection point, that exists at a higher concentration and which does not appear clearly on all Scatchard plots, but is obvious in Figures 3.24b,d.

3.3.5. Effect of the Temperature on the Overloaded Band Profiles

Overloaded band profiles were recorded at all the combinations of temperature and mobile phase composition as described earlier. These profiles were used to apply the inverse method and derive best estimates of the isotherm model parameter, the bi-Moreau model being selected. Further advantages of the method is the rapidity with which the profiles can be acquired compared to the time needed to acquire the FA data. This method has the further advantages of requiring much smaller amounts of solvents and chemicals.

The recorded overloaded profiles are shown in Figures 3.26a-g. In these figures, the recorded profiles (dotted lines) and the best calculated profiles (solid lines) are overlaid. There is an excellent agreement between the experimental and calculated profiles in all cases. For all the mobile phase compositions used and at all the temperatures, the profiles recorded at low concentrations have a classical langmuirian shape, with a sharp front shock layer and a diffuse rear boundary. However, the shapes of the profiles are different at higher concentrations. Some have a diffuse front boundary and a rear shock layer. Others have both a front and a rear shock layer. Yet, the inverse method employing the bi-Moreau model was successful in accounting for all these profiles and in affording complete sets of isotherm parameters for all profiles. Figure 3.26h illustrates the problem mentioned in the previous section. It shows the overlay of profiles recorded during frontal analysis experiments made with 2.5%ACN, at five different temperatures. The profiles at 35 and 42°C overlap in part and so do the profiles at 52 and 63°C. In contrast, Figure 3.26c shows that the corresponding profiles, recorded successively in a short period of time, do not overlap. So, it is difficult to know which factor contributes more to cause this problem, not washing and re-equilibrating the column using the method mentioned previously, acquiring the profiles over a long period of time, or a combination of both factors. Similar experiments made with other mobile phases, when overloaded profiles were acquired one temperature at a time, did not show any differences between profiles acquired separately and profiles acquired between successive frontal analysis experiments. This suggests that the washing and equilibrating sequence is the most important factor to achieve reproducible

results.

3.3.6. Effect of the Temperature and the Mobile Phase Composition on the Parameters of the Isotherms

The parameters of the isotherms obtained by the FA and IM are listed in Tables 3.4 (low energy sites) and 3.5 (high energy sites). In general there is a good agreement (except for the value of b_2) between the values of the parameters obtained by the two . methods. However, this agreement is much better for the parameters of the low-energy sites than for those of the high-energy sites, sites that are populated first, at low concentrations. This is due to the much smaller density of the high-energy sites which have a saturation capacity only 1 to 6 % of the total saturation capacity of the adsorbent. Therefore, the errors made in the determination of the parameters of the high-energy sites are larger than those made on that of the corresponding parameters of the low-energy adsorption sites. Note that, in principle, the results of the IM method are less sensitive than those of the FA method to fluctuations of the column experimental parameters, notably the temperature, the flow rate, and the mobile phase composition, because the data acquisition is much faster. Each FA breakthrough curve takes 30 to 60 minutes and 40 such measurements are needed for each mobile phase composition (Figure 3.20). The IM method requires the recording of three band profiles only, which can be done in less than two hours. In contrast, however, injected profiles dilute considerably during their elution, making the IM isotherm less accurate than the FA one at high concentrations. The different sources and magnitudes of the errors made explain the slight differences found between the parameters derived by the

two methods. In the next two sections, we elaborate on the effects of the temperature and the mobile phase composition on the parameters of the IM isotherm. The two sets of values are similar. However, due to the experimental errors and uncertainties indicated in section 3.3.4, we believe that the parameters derived by the IM method are the more accurate.

3.3.6.1. Effect of the Mobile Phase Composition on the Isotherm Parameters

The effect of increasing the ACN concentration from 2.5 to 7.5% on the parameters of the adsorption isotherms of tryptophan is as follows:

1- The saturation capacity of the low energy sites, q_1, decreases from 134 to 72 (i.e., by 46%) at 23°C. An effect of similar importance (ca. 50%) takes place at the other temperatures.

2- The saturation capacity of the high energy sites, q_2 , decreases from 5.9 to 2.6 (i.e., 56%) at 23°C. An effect of similar importance is observed at the other temperatures.

These two results show that the effect of the solvent strength on both saturation capacities is almost the same at all temperatures.

3- The adsorption constant on the low energy sites, b_1, decreases from 0.098 to 0.03 (i.e., 70%) at 23°C. Similar effects but of a somewhat decreasing importance take place at higher temperatures, the decrease in the equilibrium constant being of 62, 61, 58, and 45% at 35, 42, 52, and 63°C, respectively.

4- The adsorption constant on the high energy sites, b_2, increases from 2.5 to 3.0 (i.e., 20%) at 23°C, and by 45, 39, 47, and 55% at 35, 42, 52, and 63°C, respectively. 5- The coefficient of adsorbate–adsorbate interactions on the low

energy sites, I_1, increases from 2.8 to 11.6 (i.e., four-fold) at 23°C and by comparable amounts at 35, 42, 52, and 63°C.

6- The coefficient of adsorbate–adsorbate interactions on the high energy sites, I_2, increases from 0.8 to 1.1 (i.e., 40%) at 23°C and by similar amounts at 35, 42, 52, and 63°C.

These increases in the solute-solute interaction coefficients are confirmed by the change in shapes of the breakthrough curves in Figures 3.22a,f,k when the ACN concentration in the mobile phase increases from 2.5 to 7.5%. The change in the breakthrough curves shows that there is a strong change in the sign of the isotherm curvature.

3.3.6.2. Effect of the Temperature on the Isotherm Parameters

Figures 3.27a-f illustrate the effect of the temperature on the six parameters of the isotherm model for the three mobile phases used. Increasing the column temperature from 23

to 63°C has the following effects on the parameters of the adsorption isotherms of tryptophan at constant mobile phase composition.

1- The saturation capacity of the low energy sites, q_1, at 2.5% ACN drops from 134 to 116 (i.e., 13%); at 5% ACN it drops from 96 to 60 (i.e., 38%); and at 7.5% ACN it drops

with the corresponding changes in the bands recorded in FA. In Figures 3.20a-o, 3.21a-o, and 3.22a-o, the elution times of the fronts of the breakthrough curves with 2.5% ACN are more strongly affected by a change in temperature than those with the other mobile phases. For example, in Figures 3.20a and 3.20e (2.5% ACN) the

front elutes at 1460 sec at 23°C and at 230 sec. at 63°C (a difference of ca. 1200 sec.). In Figures 3.20k and 3.20o (7.5% ACN) the fronts elute at 570 and 340 sec.at 23°C and 63°C, respectively, (a difference of only 230 s ec.). These results indicates that the high energy sites contribute as much to the retention as the low energy sites and that their effect is more pronounced at the lowest ACN concentration. This confirms an earlier observation that the homogeneity of the adsorbent surface increases with increasing concentration of the organic modifier [118-121]. Because the order of increasing importance of the equilibrium constant at any given temperature is 2.5% ACN > 5% ACN > 7.5 %ACN on the low energy sites and 7.5% ACN > 5% ACN > 2.5% ACN on the high energy sites (see Figures 3.27c and 3.27d), the variations of the equilibrium constant with temperature are markedly different for the two types of sites. The effect of an increase of the temperature from 25 to 65°C on the adsorption constants is as follows:

2- The adsorption constant on the low energy sites decreases from 0.098 to 0.029 (i.e., 70%) with 2.5% ACN; from 0.052 to 0.014 (i.e., 73%) with 5% ACN; and from 0.032 to 0.016 (i.e., 50%) with 7.5% ACN.

4- The adsorption constant on the high energy sites decreases from 2.52 to 1.4 (i.e., 44%) with 2.5% ACN; from 2.63 to 1.68 (i.e., 36%) with 5% ACN; and from 2.95 to 2.20(i.e., 34%) with7.5%ACN

5- The coefficient of adsorbate -adsorbate interactions on the low energy sites, I_1, increases from 2.8 to 3.6 with 2.5% ACN; from 6.9 to 13.6 for 5% ACN; and from 11.6 to 16.0 with 7.5% ACN.

6- The coefficient of adsorbate -adsorbate interactions on the low energy sites, I_2,

increases from 0.8 to 3.3 with 2.5% ACN; from 0.7 to 4.1 with 5% ACN; and from 1.1 to 3.8 with 7.5% ACN.

The increase of the adsorabte-adsorbate interaction parameters is consistent with the profiles of the breakthrough curves in Figures 3.22k-o, the fronts of which becomes diffuse at 63°C while a rear shock forms at the rear, indicating that strong adsorbate-adsorbate interactions have resulted into an anti-langmuirian shape of the isotherm.

The results obtained regarding the effects of the temperature and the mobile phase composition on the parameters of the adsorption isotherm of tryptophan show that the saturation capacities decrease and the adsorbate-adsorbate parameters increase with increasing temperature and ACN concentration in the mobile phase. The effects of increasing the temperature and the ACN concentration on the adsorption constants on the low energy sites are the same. In contrast, the adsorption constant on the high energy sites decreases with increasing temperature but increases by increasing the ACN concentration.

CHAPTER 4

CONCLUSION

Our results demonstrate that the adsorption isotherm behavior of L-tryptophan depends strongly on the composition of the mobile phase and particularly on the nature and concentration or the organic modifier. The thermodynamics of the adsorption of tryptophan is unusually complex, with the isotherms in aqueous solutions of either ACN or MeOH having two inflection points and changing from convex upward to convex downward in the moderate to high concentration range, depending on the organic modifier concentration. The bi-Moreau model accounts for the adsorption behavior of L-tryptophan on C_{18} RPLC with both modifiers, in the whole concentration range studied. This model suggests that the adsorbent surface is heterogeneous and is covered with two different types of sites. The adsorption energy is low on the first type, high on the second type.

All the parameters of the adsorption isotherm depend on the modifier concentration but the dependance of the parameters of the high energy sites is larger than that of the low energy sites. Increasing the modifier concentration decreases the saturation capacities of both types of sites. The adsorption constant of the low energy sites are almost independent of the modifier concentration Those of the high energy sites increase with increasing modifier concentration. The adsorbate-adsorbate interaction parameter of the low and high energy sites increase for both solvents. The saturation capacities of the high energy sites are higher for

ACN than for MeOH.

The previous results show also that the bi-Moreau isotherm model accounts best for the adsorption behavior of L-tryptophan on Kromasil C_{18} in a wide range of temperature. This means that the adsorption mechanism remains the same at all temperatures and for all mobile phase compositions. This result suggests that the adsorbent surface is heterogeneous and covered with two different types of sites. The isotherm is initially convex upward and it has zero (weak adsorbate-adsorbate interactions) or two inflection points, but the second one may not be observed if it takes place at high concentrations. This result is confirmed by the shape of the breakthrough curves and by the *q/C* versus *C* plots. Increasing the temperature affects the isotherm in two ways. First, the amount adsorbed on the stationary phase at equilibrium decreases with increasing temperature while all the parameters of the isotherm change. The saturation capacities of the low and the high energy types of sites decrease, the adsorption constants of both types decrease, and the adsorbate-adsorbate interaction parameter increases. The difference between the saturation capacities of the low and high energy sites is much larger for tryptophan than for phenol, indicating that high energy sites are much less accessible for tryptophan than for phenol and that their access depends on the molecular size of the compound.

Our results support previous findings [122-123] that both temperature and the mobile phase composition solvent affect the parameters of the adsorption isotherms of many compounds but not the model itself. In all cases, increasing the amount of organic modifier or the temperature causes decreases of the saturation capacities

of the low and high energy types of sites and a decrease of the adsorption constant of the low energy sites. The effect of these parameters on the adsorption constant of the high energy sites is more complex. These results were explained by an increased mobility of the alkyl chains bonded to the silica.

The results also confirm the validity of a general scheme of isotherm data acquisition in a wide range of experimental parameters (e.g., temperature, mobile phase composition). The acquisition of a single set of frontal analysis data at a certain composition and temperature, followed by the recording of overloaded band profiles in conditions covering the whole range of parameters of interest permits the determination of the isotherm parameters at any intermediate value, by interpolation. This means that huge savings of time, effort, and chemicals in the measurement of isotherms is now possible.

The inverse method is a quick method of determination of isotherms under various experimental conditions that uses only small amounts of sample and solvent. This approach has important advantages over FA for the determination of the tryptophan isotherms because the latter method suffers from various difficulties at low acetonitrile concentrations and at high temperatures. These difficulties include the long times needed to equilibrate the column with the mobile phase and the loss of the acetonitrile layers formed on the adsorbent surface during the long periods of time required to acquire the FA data, resulting in a loss of the accuracy of the data. Additional problems were caused by the need to calibrate the detector at each temperature, at several wavelengths, at different temperatures, and at different mobile phase compositions. Although similar calibrations are needed for

the inverse method, the work is less important because it is not necessary to acquire overloaded profiles at each concentration used in the frontal analysis experiments. Only one or two overloaded profiles and one low concentration profile are needed to obtain the isotherm parameters at different experimental conditions. Also, the non-linear fitting of the frontal analysis data to a six-parameter model was difficult in some cases and the set of parameters obtained by IM was a useful initial guess to smoothen the process or to set certain restrictions to the values of the parameters.

Using IM with the bi-Moreau model gives calculated profiles that are in excellent agreement with the experimental ones at the whole range of concentrations used and at all temperatures and mobile phase compositions used. The saturation capacities q_1 and q_2 of the low and high energy sites decrease with increasing ACN concentration and temperature while the adsorbate-adsorbate interaction parameters, I_1 and I_2 increase. However, the adsorption constant b_1 of the low energy sites decreases with increasing temperature and/or acetonitrile concentration while the adsorption constant b_2 of the high energy sites decreases with increasing temperature and increases with increasing acetronitrile concentration. The 2.5%ACN mobile phase is the most affected by a temperature increase. It gives isotherm parameters that differ significantly from those of the 5% and 7.5% ACN mobile phases that have values close to each other. The shapes of the breakthrough curves exhibit also different behavior, the 5% and7.5% ACN solutions giving similar profiles at low and high concentrations, except at 23°C (Figure 3.21b,c). Therefore, we conclude that the effects of temperature and of the

mobile phase composition are not independent [124]. It could be useful to study the influence of the temperatures above 63°C in preparative liquid chromatography, but stationary phases stable at high temperatures would be needed.

REFERENCES

[1] J. C. Giddings “ Unified Separation Science “ , Wiley Interscience, New York, 1991.

[2] M. Martin, G. Blue, G. Guiochon, J. Chromatogr. Sci., **11** (1973) 641.

[3] R. Rouchon, M. Schonauer, P. Valentine, G. Guiochon, Separat. Sci. Technol., **22** (1987) 1793.

[4] J. Coner, J. Yong, “Physico Chemical Measurements by gas chromatography” ,Wiley, New York, NY, 1979.

[5] D. Skoog, F. Holler, T. Nieman, “Principles of instrumental analysis” Harcourt brace college, 1998.

[6] J. C. Giddings “Unified Separation Science”, Wiley Interscience, New York, 1991.

(7) Bingchang Lin and Georges Guiochon, *Modeling for preparative chromatography*, Elsevier, Amsterdam, The Netherlands, 1st edition 2003.

[8] D. Harris, “Quantititive Chemical Analysis”, W. H. Freeman and company, New York, 1999.

[9] G. Guiochon, A. Felinger, A. M. Katti, D. Shirazi, *Fundamentals of preparative and nonlinear chromatography*, Elsevier, Amsterdam, 2nd edition, 2006.

[10] E. Wicke, Kolloid Z., **86** (1939) 295.

[11] J. N. Wilson, J. Am. Chem. Soc., **62** (1940) 1583.

[12] D. DeVault, J. Am .Chem. Soc., **65** (1943) 532.

[13] E. Kováts, “The Science of chromatography, ” F. Bruner, Ed, Elsevier, Amsterdam, the Netherlands, 1985.

[14] L. Lapidus and N. R. Amundson, J. Phys. Chem., **56** (1952) 505.

[15] J. C. Giddings, “ Dynamics of Chromatography’ “ M. Dekker, New York, N. Y, 1965.

[16] J. J. Van Deemter, F. J. Zuiderweg , A. Klinkenberg, Chem. Eng. Sci., **5** (1956) 271.

[17] P.C. Haarhoff, H. J. Van der Linde,Anal. Chem. , **38** (1966) 573.

[18] S. Golshan-Shirazi, G. Guiochon, J. Cchromatogr., **506** (1980) 495.

[19] B. Lin, Z. Ma, S. Golshan-Shirazi, G. Guiochon, J. Chromatogr.,500 (1990)185.

[20] G. H. Houghton, J. Phys. Chem., **67** (1963) 84.

[21] P. Rouchon, P. Valntine, M. Schönauer, C. Vidal-Madjar, G. Giochon, J. Phys. Chem., **88** (1985) 2709.

[22] P. Rouchon, M. Schönauer, P. Valntine, G. Guiochon, Separat. Sci. Technol., **22** (1987) 1793.

[23] G. Guiochon, S. Golshan-Shirazi, A. Jaulmes, Ana. Chem 60 (1988) 1856.

[24 M. Czok, G. Guiochon, Anal. Chem., **62**, (1990) 189.

[25] A. M. Katti, E. V. Dose, G. Guiochon, J. Chromatogr., **540** (1991) 1.

[26] A. M. Katti, M. Diack, M. Z. El-Fallah, S. Golshan-Shirazi, S. C. Jacobson, A. Seidel-Morgenstern, G. Guiochon, Acc. Chem. Res., **25** (1992)366.

[27] S. Golshan-Shirazi, G. Guiochon, ana. Chem. **60** (1988) 2364.

[28] G. Guiochon, A. Felinger, A. M. Katti, D. Shirazi, *Fundamentals of preparative and nonlinear chromatography*, Elsevier, Amsterdam, 2nd edition, 2006.

[29] D.M. Ruthven, *Principles of adsorption and adsorption processes*, Wiley, New york,1984.

[30] G. Zong, P. Sajonz, G. Guiochon, *Ind. Eng. Chem.* (*Res.*) **36** (1997) 506.

[31] M. Moreau, P. Valentin, C. Vidal-Madjar, B.C. Lin, G. Guiochon, *J. Colloid Interface Sci.* **141** (1991) 127.

[32] H. Poppe, *J. Chromatogr. A* **656** (1993) 19.

[33] M. Jaroniec, R. Madey, *Physical Adsorption on Heterogeneous Solids*, Elsevier, Amsterdam, The Netherlands, 1988.

[34] V. Svoboda, *J. Chromatogr. A* **518** (1990) 77.

[35] J. Zhu, A. M. Katti, G. Guiochon, *J. Chromatogr. A* **552** (1991) 71.

[36] M. Diack, G. Guiochon, *Langmuir,* **8** (1992) 1587.

[37] I. Quinones, G. Guiochon, *J. Chromatogr. A* **796** (1998) 15.

[38] M. Suzuki, *Adsorption Engineering*, Elsevier, Amsterdam 1990.

[39] E. V. Dose, S. Jacobson, G. Guiochon, *Anal. Chem.* **63** (1991) 833.

[40] G. Guiochon, F. James, M. Sepulveda, *Inverse Problems* **10** (1994) 1299.

[41] G. Guiochon, F. James, M. Sepulveda, *Int. Ser. Numer. Math.* **129** (1999) 423.

[42] A. Felinger, A. Cavazzini, G. Guiochon, *J. Chromatogr. A.* **986** (2003) 207.

[43] P.W. Danckwerts, *Chem. Eng. Sci.* **2** (1953)1.

[44] P. Rouchon, P. Valentin, M. Schonauer, C. Vidal-Madjar, G. Guiochon, *J. Phys. Chem* **88** (1985) 2709.

[45] P. Rouchon, M. Shonauer, P. Valentin, G. Guiochon, *Sep. Sci. Technol.* **22** (1987) 1793.

[46] G. Guiochon, S. Golshan-Shirazi, A. Jaulmes, *Anal. Chem.* **60** (1988) 1856.

[47] X. Liu, D. Zhou, P. Szabelski, G. Guiochon, *Anal. Chem.* ***75*** (2003) 3999.

[48] D. Zhou, X. Liu, K. Kaczmarski, A. Felinger, G. Guiochon, *Biotechnol. Progr*. **19** (2003) 945.

[49] X. Liu, D. Zhou, P. Szabelski, G. Guiochon, *J. Chromatogr. A* ***988*** *(*2003) 205.

[50] P. Szabelski, A. Cavazzini, K. Kaczmarski, X. Liu, J. Van Horn, G. Guiochon, *J. Chromatogr. A* **950** (2002) 41.

[51] H. Kim, F. Gritti, G. Guiochon, *J. Chromatogr. A* **1049** *(*2004) 25.

[52] F. Gritti, G. Guiochon, *J. Chromatogr. A* **1043** (2004) 159.

[53] F. Gritti, G. Guiochon, *J. Chromatogr. A* **1033** (2004) 43

[54] F. Gritti, G. Guiochon, *J. Chromatogr. A* **1033** (2004) 57.

[55] F. Gritti, G. Guiochon, *J. Chromatogr. A* **1047** (2004) 33.

[56] F. Gritti, G. Guiochon, *Anal.Chem.* **76** (2004) 4779.

[57] F. Gritti, G. Guiochon, *J. Chromatogr*. *A* **1028** (2004) 197.

[58] F. Gritti, G. Guiochon, *J. Chromatogr*. *A* **1041**(2004) 63.

[59] F. Gritti, G. Guiochon, *J. Chromatogr. A* **1038** (2004) 53.

[60] F. Gritti, G. Guiochon, *J. Chromatogr. A* **995** (2003) 37.

[61] F. Gritti, G. Guiochon, *Anal. Chem.* **77** (2005) 4257

[62] F. Gritti, G. Guiochon, *J. Chromatogr. A* **1010** (2003) 153.

[63] G. Zong, P. Sajonz, G. Guiochon, *Ind. Eng. Chem.* (Res.) **36** (1997) 506.

[64] K. D. Nugent, W.G. Burton, T. K. Slattery, B.F. Jhonson, L. R. Snyder, *J. Chromatogr*. **443** (1988) 381.

[65] H. Colin, J. C. Diez-masa, G. Guiochon, T. Czajkowska, I. Miedziak, *J. Chromatogr*. **167** (1978) 41.

[66] E. J. Kikta, E. Grushka, *Anal. Chem*. **48** (1976) 1098.

[67] C.G. Horváth, B.A. Preiss, S. R. Lipsky, *Anal. Chem*. **39** (1967)1422.

[68] C.G. Horváth, S. R. Lipsky, *J. Chromatogr. Sci*. **7** (1969) 109.

[69] H. Chen, C. Horváth, *Anal. Methods Instrum*. **1** (1994) 213.

[70] P. L. Zhu, L. R. Snyder, J. W. Dolan, N.M. Djordjevic, D. W. Hill, L.C. Sander, T. J. Waeghe, *J. Chromatogr. A* **756** (1996) 21.

[71] B. Yang, J. Zhao, J. S. Brown, J. Blackwell, P.W. Carr, *Anal. Chem*. **72** (2000) 1253.

[72] N.S. Wilson, M.D. Nelson, J. W. Dolan, L. R. Snyder, P. W. Carr, *J. Chromatogr. A* **961** (2002) 195.

[73] J. W. Dolan, L. R. Snyder, N.M. Djordjevic, D. W. Hill, T. J. Waeghe *J. Chromatogr. A* **857** (1999) 1.

[74] J. J. Kirkland, C.H. Dilkes, J. E. Hendeson, *LC-GC* **11** (1993) 290.

[75] H. Chen, C. G. Horváth, *Anal. Meth. Instr*. **1** (1993) 213.

[76] H. Chen, C. G. Horváth, *J. Chromatogr. A* **705** (1995) 3.

[77] F. D Antia, C. J. Horváth, *J. Chromatogr*. **435** (1988) 1.

[78] J. W. Li, P. W. Carr, *Anal. Chem*. **69** (1997) 837.

[79] J. W. Li, P. W. Carr, *Anal. Chem*. **69** (1997) 2193.

[80] J. W. Li, Y. Hu, P. W. Carr, *Anal. Chem*. **69** (1997)3884.

[81] J. Zhao, P. W. Carr, *Anal. Chem*. **71** (1999) 5217.

[82] J. D. Thompson, P. W. Carr, *Anal. Chem*. **74** (2002) 4150.

[83] B. Yan, J. Zhao, J. S. Brown, J. Blackwell, P. W. Carr, *Anal. Chem*. **72** (2000)

1253.

[84] R. M. Smith, R. J. Burgess, *J. Chromatogr. A*, **785** (1997) 49.

[85] R. M. Smith, R. J. Burgess, *Anal. Chem*. **33** (1996) 327.

[86] B. A. Ingelse, H. G. Janssen, C. A. Cramers, *J. High Resol. Chromatogr*. 21 (1998) 613.

[87] X. Yang, L. Ma, P. W. Carr, *J. Chromatogr. A*, **1079** (2005) 213.

[88] F. Gritti, G. Guiochon, *J. Chromatogr. A*, **995** (2003) 37.

[89] H. Kim, F. Gritti, G. Guiochon, *J. Chromatogr. A*, **1049** (2004) 25.

[90] F. Gritti, G. Guiochon, *Anal. Chem*., **77** (2005) 4257.

[91] L.A. Cole, J. G. Dorsey, *Anal. Chem*. **70** (1992) 1317.

[92] K. Miyabe, G. Guiochon, *Anal. Chem*. **74** (2002) 5982.

[93] C. A. Doyle, T. J. Vickers, C. K. Mann, J. G. Dorsey, *J. Chromatogr. A* **877** (2000) 41.

[94] K. B. Sentell J. Chromatogr. A 656 (1993) 231.

[95] M. W. Ducey, C. J. O rendroff, J. E. Pemberton, L.C. Sander, *Anal. Chem*. **74** (2002) 41.

[96] A. Felinger, A. Cavazzini , G. Guiochon, J. Chromatogr. A **986** (2003) 207.

[97] A. Cavazzini, A. Felinger, G. Guiochon, J. Chromatogr. A **1012** (2003) 139.

[98] G. Guiochon, A. Felinger, A. M. Katti, D. Shirazi, *Fundamentals of prepa-rative and nonlinear chromatography*, Elsevier, Amsterdam, 2nd edition, 2006.

[99] M. Kele, G. Guiochon, J. Chromatogr. A **855** (1999) 423.

[100] F. Gritti, G. Guiochon, J. Chromatogr. A **1003**, (2003) 43.

[101] A. Felinger, F. Gritti, G. Guiochon, J. Chromatogr. A **1024** (2004) 21.

[102] Agilent Technologies HP1090 manual.

[103] R.M. McCormick, B.L Karger, *Anal. Chem.* **52** (1980) 2249.

[104] Y.V. Kazakevich, R. LoBrutto, F. Chan, T. Patel, *J. Chromatogr. A* **913** (2001) 49.

[105] G. Zong, P. Sajonz, G. Guiochon, *Ind. Eng. Chem.* (Res.) **36** (1997) 506.

[106] F. Gritti, G. Guiochon, *J. Chromatogr. A* **1010** (2003) 153.

[107] M. J. M. Wells, C. R. Clark, *Anal. Chem*., **53** (1981) 1341.

[108] Y. V. Kazakevich , H. M. McNair, *J. Chromatogr. Sci.* **31** (1993) 317.

[109] K. Miyabe, g. Guiochon, *Anal. Chem*., 74 (2002) 5754.

[110] J. Dorsey, Presentation 820-5, *Pittsburg conference*, Orlando, FL, March, 2006.

[111] F. Gritti, G. Guiochon, *J. Chromatogr. A* **- 06- 871**.

[112] M. Z. ElFallah, G. Guiochon, *Anal. Chem*. 63 (1991) 2244.

[113] W. Melander, Cs. Horvath in: Cs. Horvath (Ed.), High performance of liquid chromatography: Advances and Perspectives, vol. 2, Academic press, New York, 1980.

[114] J. G. Dorsey, K. A. Dill, *Chem. Rev*. **89** (1989) 331.

[115] F. Gritti, G. Guiochon, *J. Chromatogr. A* **1028** (2004) 105.

[116] F. Gritti, G. Guiochon, *Anal Chem* **75** (2003) 726.

[117] F. Gritti, A. Felinger, G. Guiochon, *Chromatographia*, **60** (2004) S3.

[118] F. Gritti, W. Piatkowski, G. Guiochon, J. Chromatogr. A **978**,(2002) 81.

[119] F. Gritti, G. Guiochon, J. Chromatogr. A **1008** (2003) 13.

[120] F. Gritti, G. Guiochon, J. Chromatogr. A **1008** (2003) 23.

[121] F. Gritti, G. Guiochon, J. Chromatogr. A **1028**(2004) 121.

[122] T. Ahmad, G. Guiochon, J. Chromatogr. A **1114** (2006) 111.

[123] T. Ahmad, G. Guiochon, J. Chromatogr. A **1129** (2006) 174.

[124] T. Ahmad, G. Guiochon, J. Chromatogr. A submitted.

VITA

Tarab Jamil Ahmad was born on April 26, 1965 in Jerusalem, Palestine. She is married and have three boys (Tariq, Tahir, and Yasser) and one girl (Sadiqah Yafah). Tarab graduated form the University of Jordan at Amman- Jordan where she earned her BS and MS degrees in chemistry and analytical chemistry respectively. She worked as chemistry instructor in the Alkwarzmi Community College in Amman- Jordan, and as the head of the medical sciences department in the same college from 1989-1992. After that she worked as a chemistry instructor in the University of Applied Sciences in Amman-Jordan from 1992 to 1999. She immigrated to the United States in September 1999, and became a US citizen on April 2005. She entered the doctoral program in chemistry at the University of Tennessee, Knoxville in December 2002. She earned her Ph.D in December 2006.